

SANDIA REPORT

SAND96-8255 • UC-702

Unlimited Release

Printed September 1996

Transpiring Wall Supercritical Water Oxidation Reactor Salt Deposition Studies

B. L. Haroldsen, D. Y. Ariizumi, B. E. Mills, B. G. Brown, D. Greisen

Prepared by
Sandia National Laboratories
Albuquerque, New Mexico 87185 and Livermore, California 94551
for the United States Department of Energy
under Contract DE-AC04-94AL85000

Approved for public release; distribution is unlimited.

Issued by Sandia National Laboratories, operated for the United States Department of Energy by Sandia Corporation.

NOTICE: This report was prepared as an account of work sponsored by an agency of the United States Government. Neither the United States Government nor any agency thereof, nor any of their employees, nor any of the contractors, subcontractors, or their employees, makes any warranty, express or implied, or assumes any legal liability or responsibility for the accuracy, completeness, or usefulness of any information, apparatus, product, or process disclosed, or represents that its use would not infringe privately owned rights. Reference herein to any specific commercial product, process, or service by trade name, trademark, manufacturer, or otherwise, does not necessarily constitute or imply its endorsement, recommendation, or favoring by the United States Government, any agency thereof or any of their contractors or subcontractors. The views and opinions expressed herein do not necessarily state or reflect those of the United States Government, any agency thereof or any of their contractors or subcontractors.

This report has been reproduced from the best available copy.

Available to DOE and DOE contractors from:

Office of Scientific and Technical Information
P. O. Box 62
Oak Ridge, TN 37831

Prices available from (615) 576-8401, FTS 626-8401

Available to the public from:

National Technical Information Service
U.S. Department of Commerce
5285 Port Royal Rd.
Springfield, VA 22161

SAND96-8255
Unlimited Release
Printed September 1996

TRANSPIRING WALL SUPERCRITICAL WATER OXIDATION REACTOR SALT DEPOSITION STUDIES

B. L. Haroldsen, B. E. Mills, D. Y. Ariizumi, B. G. Brown
Sandia National Laboratories, Livermore, CA

D. Greisen
GenCorp, Aerojet, Sacramento, CA

ABSTRACT

Sandia National Laboratories has teamed with Foster Wheeler Development Corp. and GenCorp, Aerojet to develop and evaluate a new supercritical water oxidation reactor design using a transpiring wall liner*. In the design, pure water is injected through small pores in the liner wall to form a protective boundary layer that inhibits salt deposition and corrosion, effects that interfere with system performance. The concept was tested at Sandia on a laboratory-scale transpiring wall reactor that is a 1/4 scale model of a prototype plant being designed for the Army to destroy colored smoke and dye at Pine Bluff Arsenal in Arkansas. During the tests, a single-phase pressurized solution of sodium sulfate (Na_2SO_4) was heated to supercritical conditions, causing the salt to precipitate out as a fine solid. On-line diagnostics and post-test observation allowed us to characterize reactor performance at different flow and temperature conditions. Tests with and without the protective boundary layer demonstrated that wall transpiration provides significant protection against salt deposition. Confirmation tests were run with one of the dyes that will be processed in the Pine Bluff facility. The experimental techniques, results, and conclusions are discussed.

*This work was supported by the DOE/EM-50 Office of Technology Development, the U.S. Army Armament Research, Development, and Engineering Center, Picatinny Arsenal, NJ, and the DOE-DP-DoD Office of Munitions Memorandum of Understanding.

Contents

Introduction	7
Bench Scale System Design.....	7
1/4 Scale Transpiring Wall Reactor Description.....	7
Effectiveness Ratio.....	10
EER Test Bed Description.....	12
Effects of Thermal Conduction	13
Temperature Profiles Inside the Reactor.....	15
Testing	16
Overview.....	16
Test Procedure	16
Test Without Transpiring Wall Protection	19
Tests with Different Effectiveness Ratios.....	26
Possible Explanations	35
Tests Without Injection Heating Water.....	36
Test With Flow Injector.....	42
Test to Remove Salt Deposits	46
Test with Subcritical Transpiration Water.....	48
Tests with Organic Wastes.....	50
Implication for Prototype Plant.....	62
Summary.....	63
References.....	64

Illustrations

Figure 1	Conceptual Operation of the Transpiring Wall Reactor.....	8
Figure 2	1.4 Scale Transpiring Wall Reactor.....	8
Figure 3	Diffuser	9
Figure 4.	1/4 Scale Reactor Effectivenss Predictions	11
Figure 5.	Prototype Reactor Effectivness.....	11
Figure 6.	Sandia EER Platelet Configuration.....	12
Figure 7.	Effect of Temperature Variation On Platelet.....	14
Figure 8.	Fluid Temperature Measurement Locations.....	15
Figure 9.	Solubility of Sodium Sulfate.....	18
Figure 10.	Temperature Before Transpiration Water Was turned Off.....	20
Figure11.	Temperature With Transpiration Water Off	20
Figure 12.	Flow Rates, Test without Transpiration Flow.....	21
Figure 13.	Temperatures, Test wihtout Transpiration Flow.....	21
Figure 14.	Differential Pressure, Test without Transpiration Flow.....	22
Figure 15.	Electrical Conductivity, Test without Transpiration Flow.....	23
Figure 16.	Electrical Conductivity Calibration Data.....	24
Figure 17.	Salt Deposits, Test without Transpiration Flow.....	25
Figure 18.	Salt Deposits, Test without Transpiration Flow.....	25
Figure19.	Salt Deposits, Test without Transpiration Flow.....	26
Figure 20.	Temperatures for Low Effectiveness Test.....	27
Figure 21.	Electrical Conductivity, Low Effectiveness Test.....	27
Figure 22.	Differential Pressure, Low Effectivness Test	28
Figure 23.	Differential Pressure, Low Effectiveness Test.....	29
Figure 24.	Flow Rates, Low Effectiveness Test.....	29
Figure 25.	Electrical Conductivity, Low Effectiveness Test.....	30
Figure 26.	Salt Deposits, Low Effectiveness Test.....	31
Figure 27.	Salt Deposits, Low Effectiveness Test.....	32
Figure 28.	Temperatures for Medium Effectiveness Test.....	33
Figure 29.	Electrical Conductivity, Medium Effectiveness Test.....	33
Figure 30.	Temperatures for High Effectiveness Test.....	30
Figure 31.	Temperatures, High Effectivness Test.....	35
Figure 32.	Temperatures for First Test Without Heating Water	37
Figure 33.	Flow Rate, First Test Without Heating Water	37
Figure 34.	Electrical Conductivity, First Test Without Heating Water	38
Figure 35.	Salt Deposits, First Test Without Heating Water.....	39
Figure 36.	Salt Deposits, First Test Without Heating Water.....	39
Figure 37.	Temperatures for Second Test Without Heating Water.....	40
Figure 38.	Electrical Conductivity, Second Test Without Heating Water.....	41
Figure 39.	Temperature, Second Test Without Heating Water	41
Figure 40.	Salt Deposits, Second Test Without Heating Water	42
Figure 41.	Injector Test Configuration and Temperatures	43
Figure 42.	Temperature, Injector Test.....	45
Figure 43.	Electrical Conductivity, Injector Test	45

Figure 44. Temperatures During Salt Buildup	46
Figure 45. Temperatures During Rinse	47
Figure 46. Electrical Conductivity, Salt Removal Test	47
Figure 47. Temperatures for 350°C Test.....	48
Figure 48. Electrical Conductivity, 350°C Transpiration Water.....	49
Figure 49. Electrical Conductivity, 365°C Transpiration Water.....	49
Figure 50. Electrical Conductivity, 380°C Transpiration Water.....	51
Figure 51. Internal Temperature, 380°C Transpiration Water.....	51
Figure 52. Temperatures for First Red Dye Test	52
Figure 53. Flow Rate and Pressure, First Red Dye Test.....	53
Figure 54. Electrical Conductivity and pH, First Red Dye Test.....	53
Figure 55. Internal Temperature, First Red Dye Test	55
Figure 56. Salt Deposits, First Red Dye Test.....	55
Figure 57. Salt Deposits, First Red Dye Test.....	56
Figure 58. Flow Rates, First Red Dye Test	56
Figure 59. Differential Pressure, First Red Dye Test	57
Figure 60. Temperatures for Second Red Dye Test.....	59
Figure 61. Reactor Exit Pressure, Second Red Dye Test.....	59
Figure 62. Flow Rates, Second Red Dye Test.....	61
Figure 63. Total Organic Carbon, Second Red Dye Test.....	61
Figure 64. Effect of Temperature on Pressure Fluctuations.....	63

Transpiring Wall Supercritical Water Oxidation Reactor Salt Deposition Studies

Introduction

Sandia National Laboratories is working with Foster Wheeler Development Corp. and GenCorp, Aerojet to design and build a Supercritical Water Oxidation (SCWO) prototype plant for the Army at Pine Bluff Arsenal, Arkansas. The plant, with a capacity of 80 pounds of waste per hour, will be used to destroy hazardous colored smokes and dyes (references 1 and 2). A novel feature of this plant will be the use of a transpiring wall reactor to address two major technical problems with SCWO. These problems are: 1) salts, soluble at ambient conditions, precipitate from the supercritical fluid and plug the reactor; and 2) acids that form during the oxidation process corrode the reactor (reference 3, 4, and 5). The transpiring wall reactor promises to mitigate both salt deposition and corrosion by forming a protective boundary layer of pure water along the wall. The concept is based on Aerojet's platelet technology, which they developed for aerospace applications such as cooling rocket nozzles and nose cones (references 6,7,8).

This report documents the results of a laboratory-scale experimental program to evaluate the utility of a transpiration protected reactor. The focus of the program was to demonstrate the ability of the reactor to resist deposition of sticky salts. Corrosion mitigation has not been evaluated. Salt deposition is the most immediate problem because it prevents continuous operation, making a larger scale plant impracticable. The test reactor, which Aerojet designed and fabricated, is a 1/4 scale version of the prototype plant. The testing was done on Sandia's Engineering Evaluation Reactor (EER). This report describes the reactor configuration, the experimental techniques, and the test results, with explanations, theories, and implications for the prototype plant.

Bench Scale System Design

1/4 Scale Transpiring Wall Reactor Description - The configuration of the 1/4 scale reactor and the EER system for these tests is described in detail in reference 9 and is given only limited treatment here. The transpiring wall reactor concept is illustrated in Figure 1. Figure 2 shows the 1/4 scale design. The reactor has an inside diameter of 2.8 cm (1.1 inch), outside diameter of 6.35 cm (2.5 inches), and total length of 91.4 cm (36 inches). Typical operating pressure is 255 bar (3700 psi). The reactor is mounted vertically with the waste inlet at the top. The outer wall of the reactor is made of Inconel 625. An inner liner, called a platelet, distributes water uniformly to small transpiration pores along the inner surface through a complex system of internal manifolding and metering channels.

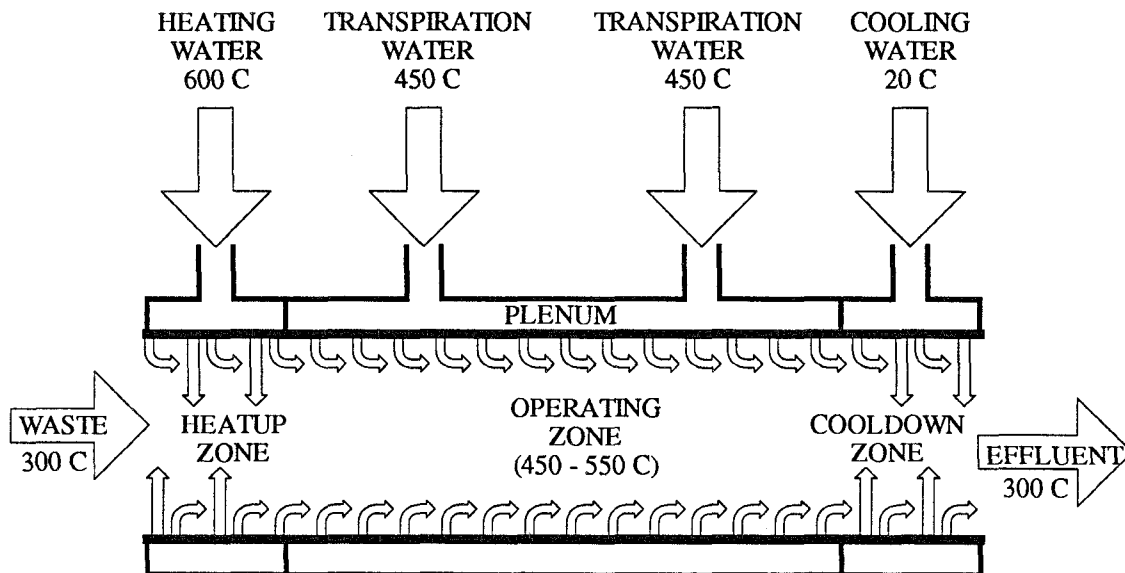


Figure 1 -- Conceptual operation of the bench-scale transpiring wall reactor showing the various fluid streams.

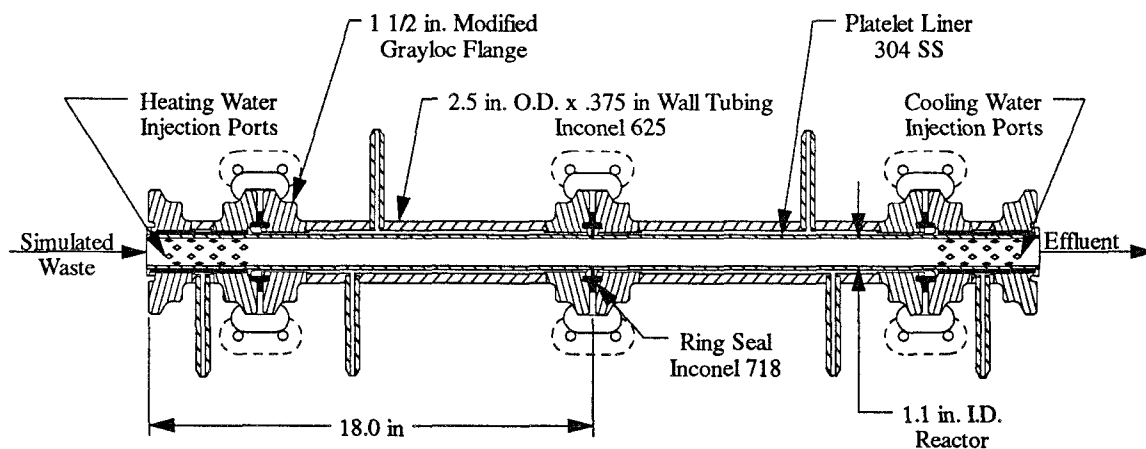


Figure 2 -- The bench-scale reactor is a 1/4 scale version of the prototype plant to be built at Pine Bluff Arsenal.

The volume between the outer wall and the platelet forms a plenum from which water is fed into the platelet. The plenum volume is divided into three parts. The central section, 66 cm (26 inches) in length, supplies the transpiration water. It is fed through two lines, each typically supplying 5.25 grams per second (5 gallons per hour) of water at 450°C (842°F). At this flow rate, the pressure drop through the internal channels of the platelet is about 0.9 bar (130 psi).

The smaller plenum volumes at either end, both 12.7 cm (5 inches) in length, feed several large, diamond-shaped holes that are interspersed among the transpiration pores near the ends of the reactor. Hot and cold water is injected through these diamond-shaped holes at the reactor inlet and outlet, respectively, to heat or cool the waste stream. The transition of the waste stream between subcritical and supercritical temperature must occur inside the transpiring wall reactor to prevent salt deposition in the inlet and outlet lines. Waste entering the reactor at subcritical temperature is heated rapidly as it mixes with the hot water. Similarly, it is cooled back to subcritical temperature before exiting. Injection heating and cooling is convenient for the test reactor but will not be used on the prototype plant because of the large amount of water required. Instead, heating will be done with a small amount of hot water and a supplementary fuel supplied through an injector. Cooling will be accomplished with a recirculating quench tank at the reactor outlet.

The test reactor was fabricated in two sections, each 0.45 meters (18 inches) long. A Grayloc flange joins the Inconel housings of the two sections and a gold-plated copper gasket seals the gap between the two stainless steel platelets. This gasket relies on thermal expansion and does not seal until the system reaches about 320°C (608°F). Below that temperature, the transpiration water can bypass the platelet and flow directly from the plenum to the inside of the reactor.

Because the flow rate of the waste stream on some tests was relatively low, a diffuser plate was placed at the reactor inlet to provide uniform flow. The diffuser, shown in Figure 3, has eighty-nine, 0.13 mm (0.005 inch) diameter holes.

Although the test reactor is basically a 1/4 scale model of the prototype plant, two aspects should be noted. First, because of capacity limitations of the EER, the test reactor does not provide sufficient temperature or residence time to fully oxidize most organic wastes. It was intended only to demonstrate the ability of the transpiring wall to prevent salt deposition. The ability of SCWO to

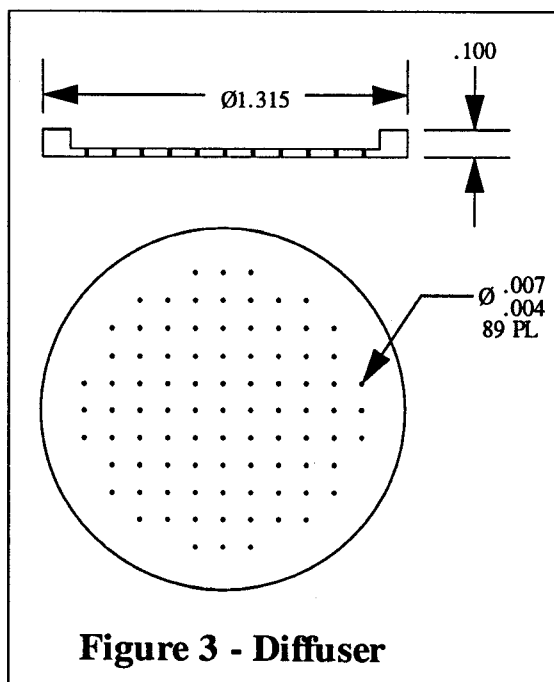


Figure 3 - Diffuser

destroy wastes has been demonstrated on other reactor systems (reference 10). Second, the ratio of waste to transpiration fluid does not scale linearly with reactor diameter and is considerably smaller in the laboratory scale reactor than in the analogous full scale reactor. The reason is apparent from the geometry. The spacing and pattern of the pores in the quarter-scale platelet are the same as in the full-scale platelet, so the flow rate of transpiration fluid scales with the surface area which is proportional to the diameter. The flow of waste, however, scales more closely with cross-sectional area which is proportional to the diameter squared.

Effectiveness Ratio - The scaling is actually more complex than the geometrical effects just discussed. The standard procedure for scale model testing is to use a dimensionless parameter, such as Reynolds number, to determine analogous flow conditions for the full-scale and reduced-scale hardware. For the transpiring wall reactor, we use the platelet wall protection effectiveness ratio, η , as the dimensionless parameter. The wall protection effectiveness ratio is defined as:

$$\eta = \frac{C_{core} - C_{wall}}{C_{core} - C_{transpiration}}$$

where C is the calculated concentration of waste and the subscripts refer to the location in the center of the reactor (core), at the surface of the reactor (wall), and in the transpiration flow. $C_{transpiration}$ in this case is zero because it is pure water. At an effectiveness ratio of one, there would be no salts or acids in contact with the wall.

The effectiveness ratio is not a measurement of how "effective" the platelet is at preventing salt deposition or corrosion. Rather, it is a calculated number that is used to establish similitude between the quarter-scale and full-scale systems. Once appropriate flow conditions are determined, the effectiveness ratio can be used to select analogous operating conditions in the full scale system. Like other dimensionless numbers used in fluid dynamics and heat transfer, the effectiveness ratio is calculated from the geometry, temperature, pressure, flow rates, and thermodynamic properties of the fluids. The calculation, however, is complex and was done with Aerojet's computer design code. Figure 4 shows the average effectiveness ratio for the 1/4 scale reactor with different flow rates. The expected effectiveness ratio for the prototype plant at nominal operating conditions is approximately 0.99 as shown in Figure 5.

In choosing the effectiveness ratio as the scaling parameter, we choose to match the conditions at the wall that lead to corrosion and salt deposition. However, we sacrifice similitude of other fluid dynamic properties such as Reynolds number. This is an inherent problem in scale model testing.

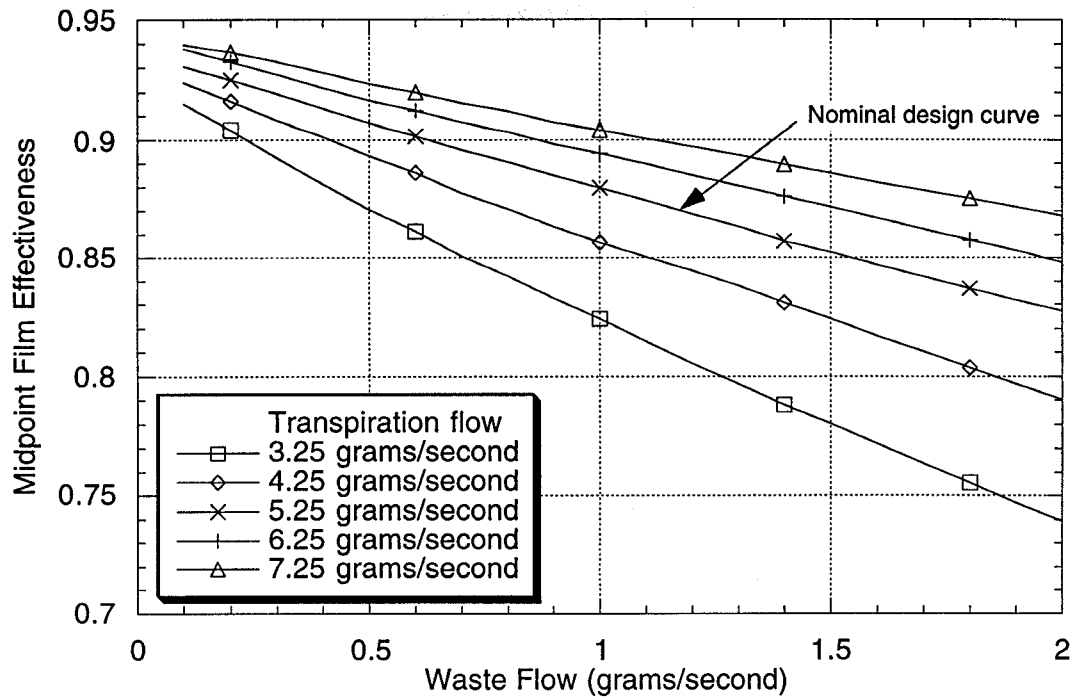


Figure 4 -- The predicted average effectiveness ratio of the bench-scale reactor is varied by changing the flow rates of either the waste or the wall transpiration water.

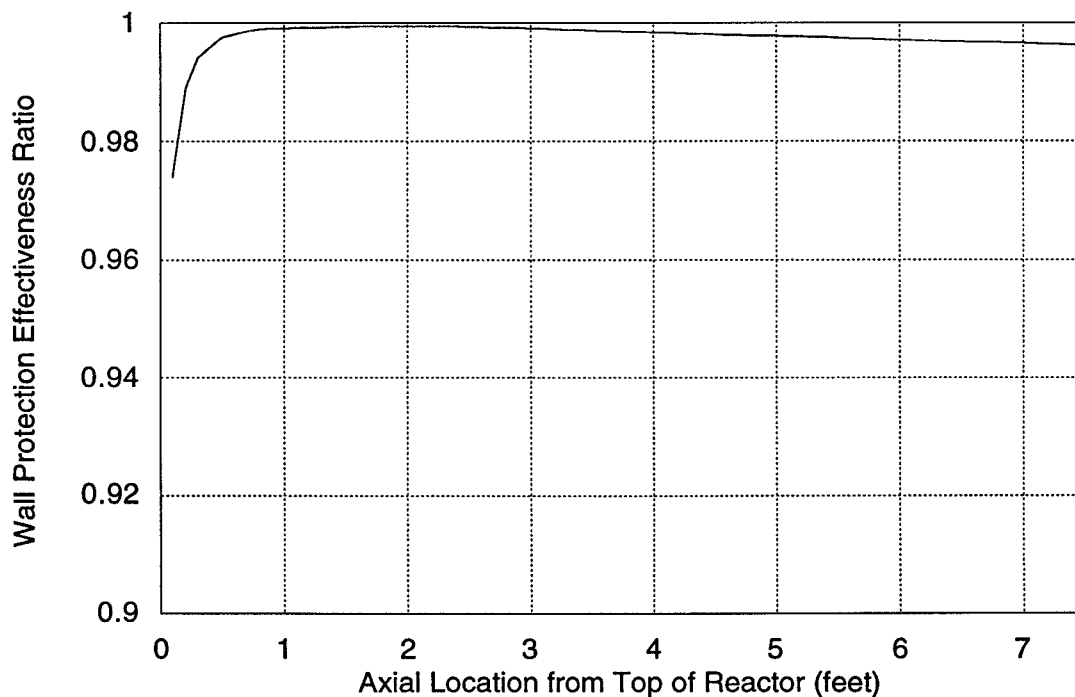


Figure 5 -- The predicted effectiveness ratio along the entire length of the prototype reactor exceeds the highest value that was tested on the bench-scale reactor.

EER Test Bed Description - Figure 6 shows a schematic of the EER with the transpiring wall reactor. The EER is a second generation, laboratory scale reactor system designed specifically for evaluating engineering aspects of SCWO technology. Its modular design facilitates different test configurations and its computer based control system allows maximum flexibility in operating conditions. It has a maximum operating temperature of 650°C (1202°F) at an operating pressure of 345 bar (5000 psi). As mentioned earlier, a detailed description of the EER is given in reference 9.

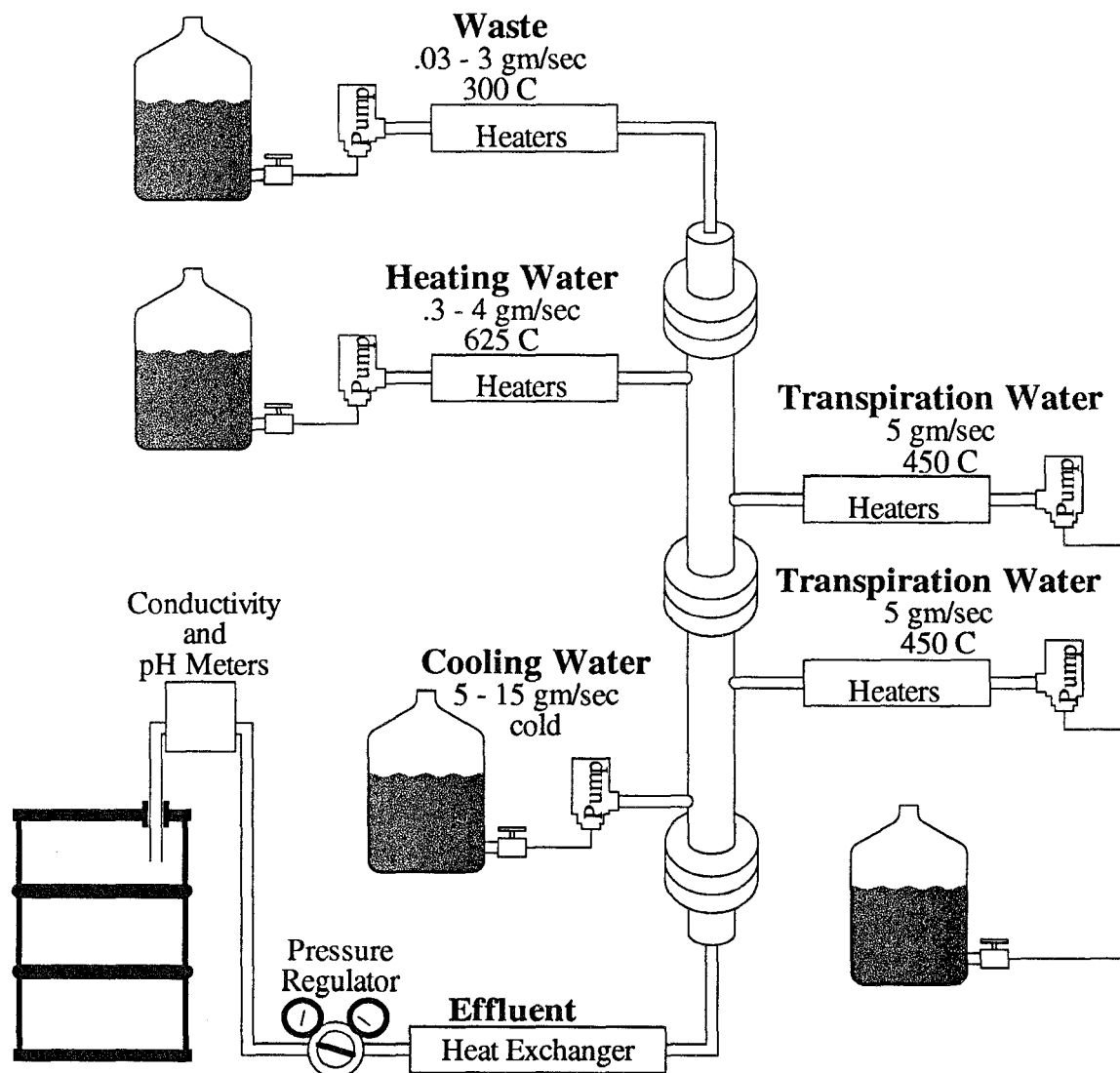


Figure 6 -- Schematic of Sandia's Engineering Evaluation Reactor configured to test the transpiring wall reactor.

Separate pumps supply the waste, the transpiration water, the injection-heating water, and the injection-cooling water at pressures up to 345 bar (5000 psi). All tests were done at about 260 bar (3770 psi). The waste pump supplies water during reactor startup and shutdown and salt solution or other waste solution during operation. This is accomplished by remotely switching the feed to the pump. The lines entering and leaving the reactor are 1.4 cm (9/16-inch) outside diameter (OD), 0.48 cm (3/16-inch) inside diameter (ID) Inconel 625 tubing. Pressure transducers and thermocouples are installed in T-unions to measure fluid pressure and temperature at various locations. Pressure measurements are not possible within the reactor due to the double wall geometry. The fluid streams are heated with cable heaters wrapped around the tubing.

The effluent is cooled in a counterflow heat exchanger and is discharged through a liquid back pressure regulator that controls the pressure in the system. A small fraction of the low pressure effluent stream is diverted to a fraction collector for post-test chemical analysis. The remaining effluent flows through on-line conductivity and pH meters. An on-line spectrometer also collects absorption spectra from which various compounds in the effluent can be detected.

The reactor system is controlled remotely through a graphical user interface to LabVIEW on a Macintosh Quadra 950. The interface also logs the reactor condition throughout the test.

Effects of Thermal Conduction - Although the intent is to heat and cool the fluids in the reactor entirely by mixing, the walls of the reactor and the inlet tubing provide a conduit for conductive heat transfer, which increases the temperature of the waste stream and decreases the temperature of the heating water before they enter the reactor. This effect must be considered in selecting test conditions and in interpreting results because the waste must remain below about 350°C (662°F) to prevent deposition in the inlet tubing. This problem is most severe when the waste flow rate is small. Despite efforts to control the temperature, there were indications on some tests of salt deposition on the diffuser plate at the reactor inlet.

The temperature of the transpiration water in the plenum volume is similarly affected, becoming hotter at the top of the reactor near the heating water and cooler at the bottom near the cooling water. It also becomes cooler as it moves circumferentially around the plenum. Thermocouples in the plenum recorded circumferential temperature variations as large as 40°C (72°F) at the same axial location. Axial variations of the same magnitude were inferred from external skin temperature measurements. This heat transfer between the structure and the fluid presumably continues as the fluid flows through the small channels within the platelet, resulting in even greater temperature variation before the fluid actually enters the reactor.

This gradient in transpiration fluid temperature has an undesirable effect on the platelet performance. The platelet meters the flow by maintaining an equal pressure drop at all locations. Near the bottom of the reactor, the temperature of

the transpiration water flowing through the metering channels is presumably subcritical due to the influence of the cold water that is injected through the lower diamond-shaped holes. The flow rate of subcritical water, for a given pressure drop, is greater than that of supercritical water because of the higher density. Consequently, the temperature gradient in the reactor results in non-uniform transpiration flow with increased flow near the bottom of the reactor and decreased flow near the top.

A side effect of this non-uniformity is that the total pressure drop across the platelet is less than if the flow had all been supercritical. This side effect was used to confirm that the non-uniformity existed. With the system at normal operating condition, the cooling water was turned off. The effect on the effluent exit temperature is seen in the top curve on Figure 7. The lower curve shows the corresponding change in the pressure drop across the platelet, which increased from 7.2 to 9 bar (105 to 130 psi). The cooling water was turned on again, but at a lower flow rate resulting in the partial recovery seen at about 307 minutes. The periodic pressure variation seen in this figure is the result of cycling of the compressor that supplies the air-driven pumps for transpiration, heating, and cooling water. It was present on all tests.

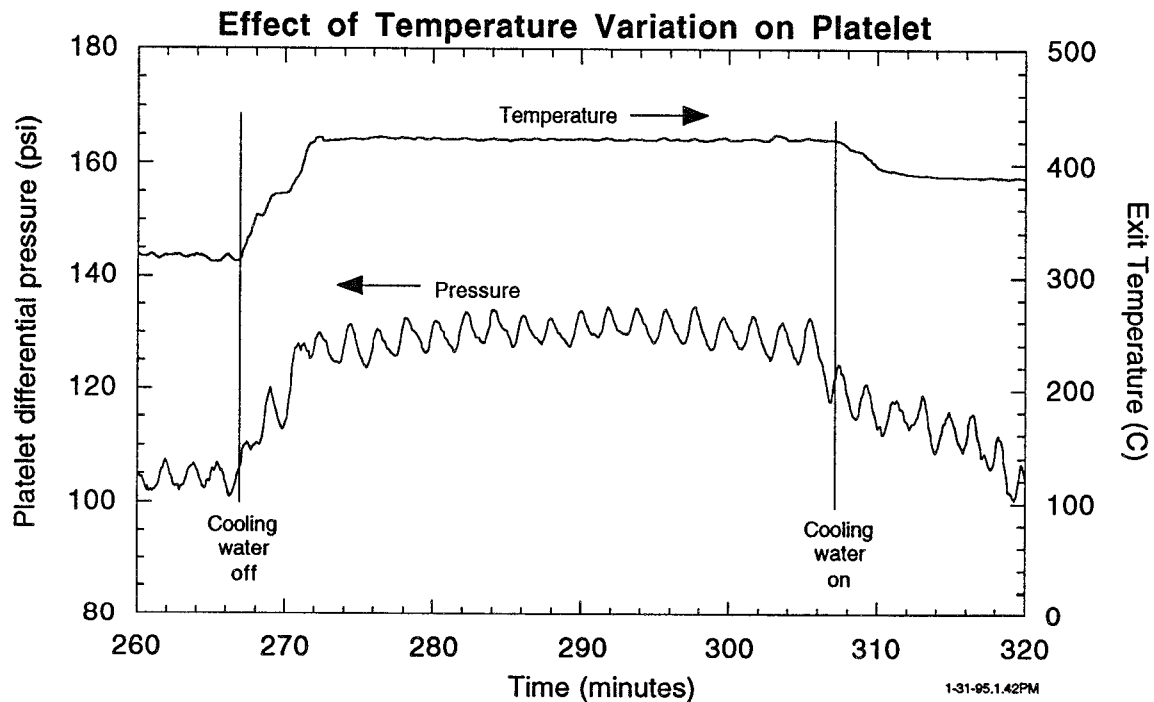


Figure 7 -- With the cooling water off, the pressure drop through the platelet increased, confirming that temperature gradients affected the spatial uniformity of the transpiration flow.

Temperature Profiles Inside the Reactor - Figure 8 shows the location of thermocouples around the reactor. The thermocouples measuring the transpiration fluid in the plenum volume are duplicated on the lower platelet section. Another thermocouple measures the effluent temperature exiting the reactor. Not all thermocouples were present on every test. The internal thermocouple has to extend in from the end of the reactor because it cannot penetrate the platelet. This thermocouple was not used on most tests because it provided an unprotected surface for salt deposition. Consequently, temperatures inside the reactor had to be inferred from inlet and outlet conditions. This was done with a simple uniaxial model that performs mass and energy balances in incremental steps through the reactor using measured inlet temperatures and flow rates. The model assumes complete mixing of all fluids at each step without accounting for the temperature variation and flow non-uniformity described in the previous section. The model first estimates adiabatic conditions then arbitrarily estimates a uniform heat loss to force the calculation to match the measured reactor outlet temperature. Although simple, the model provides useful insights about conditions in the reactor. Calculations based on this model are shown in the detailed discussion of the tests.

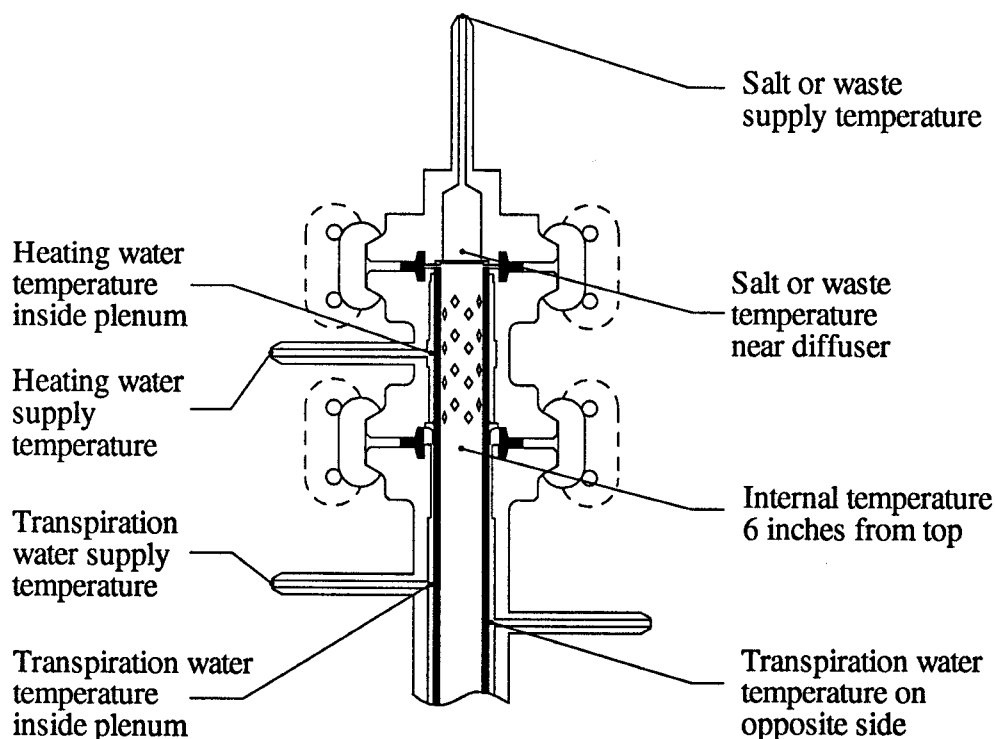


Figure 8 -- Schematic showing the location of thermocouples in the top reactor section to measure fluid temperatures. Thermocouples were located in similar locations in the bottom section. Absolute and differential pressure measurements were made through the same instrumentation ports.

Testing

Overview and Procedure - The waste stream in the majority of these tests was a single-phase, aqueous solution of sodium sulfate (Na_2SO_4). These tests used no organic compounds or oxidizer. Concentration of the salt solution ranged from 1.5 to 3 weight percent, which is equivalent to the salt concentration formed by oxidation of a 5 to 10 weight percent solution of red dye. Two confirmation tests were done with red dye with hydrogen peroxide as the oxidizer.

There were four general categories of test. First was a test with no transpiration flow to provide a baseline for comparison. Next was a series of tests to demonstrate reactor performance and to investigate the influence of the effectiveness ratio. In the third category were tests intended to improve performance or increase understanding. In the last category were the tests with red dye. One other test, already described, investigated the effects of thermal gradients on the pressure drop across the platelet. Table 1 shows a summary of the tests. Table II provides more detailed information including temperatures and flow rates for each test.

Table 1 -- Test Summary

Date 1995	Intent	Waste	Concent ration wt %	Flow Rate gm/sec	Duration min.	Category
3/16	Evaluate reactor with no transpiration water	salt	1.5	1.7	120	I
2/16	Evaluate reactor at low effectiveness	salt	3	1.4	170	II
1/23	Evaluate reactor at medium effectiveness	salt	1.5	0.38	90	II
2/2	Evaluate reactor at high effectiveness	salt	3	0.08	160	II
2/21	Test with no heating water, hot transpiration	salt	3	0.57	225	III
3/3	Lengthen precipitation zone, no heating water	salt	1.5	2.0	100	III
7/31	Test injector in place of diamond-shaped holes	salt	3	1.8	35	III
2/28	Wash out salts at lower temperature	salt	2.7	0.71	60	III
3/14	Evaluate reactor with subcritical transpiration	salt	1.5	1.3	30	III
4/21	Evaluate reactor with red dye	red dye	5.15	0.89	52	IV
10/31	Test with red dye at higher temperature	red dye	5.15	0.75	33	IV
1/31	Measure thermal effects on pressure	water	--	--	--	Other

	Salt or Dye					Heating Water		Transpiration Water							Effluent		
Test Date (1995)	Concentration (wt%)	Flow rate (cc/sec)	Temperature after heaters (C)	Temperature entering reactor (C)	Internal reactor temperature (C)	Flow rate (cc/sec)	Temperature (C)	Top section flow rate (cc/sec)	Top section temperature (C)	Bottom section flow rate (cc/sec)	Bottom section temperature (C)	Supply pressure (psi)	Differential pressure (psi)	Cooling water flow rate (cc/sec)	Flow rate (cc/sec)	Temperature at reactor exit (C)	Run time (min)
3/16	1.5	1.7	135	235	405	3.5	625	0.0	395	0.0	390	3920	0	8	13.1	220	120
2/16	3	1.4	235	265		3.8	560	4.7	451	4.9	451	3950	130	10.7	25.5	360	170
1/23	1.5	0.38	310	355		0.88	620	4.9	440	5.1	445	4090	115	8.5	19.8	355	90
2/2	3	0.08	50	341		0.34	490	4.7	430	4.9	455	3950	106	9.2	19.2	330	160
2/21	3	0.57	160	310		0	365	4.7	470	5.0	465	4000	125	13.5	23.8	305	225
3/3	1.5	2.0	20		350	0	280	5.0	405	4.5	470	3821	78	8.9	20.4	295	100
7/31	3	1.8	25	210	435	3.4	530	6.7	410	na	na	3840	150	10	21.9	305	35
2/28	2.7	0.71	100	270		0	345	5.1	450	4.7	450	3870	110	9.5	20	325	30
2/28	0	0.71	100	170		3.3	35	5.1	445	4.7	425	3760	0	9.5	23.3	290	30
3/14	1.5	1.25	20		395	3.4	615	5.5	352	5.0	352	3960	49	6.5	21.3	275	33
3/14	1.5	1.29	20		400	3.5	617	5.0	365	5.0	365	3980	53	6.5	22.6	290	32
3/14	1.5	1.25	20		398	3.75	610	5.5	380	5.0	379	3960	57	6.5	22.9	304	30
3/14	1.5	1.35	20		402	3.63	611	5.3	365	5.3	365	3930	48	6.5	22.7	292	30
4/21	5.15	0.89		310	440	3.5	640	6.0	450	3.6	440	4000	130	16	30	310	52
10/31	5.15	0.75	25	150	520	3.4	630	3	640	2.5	610	3800	100	19	28.7	330	33
1/31	0	0.18	285	360		0	400	4.9	430	5	450	3900	130	14	24.4	310	40

Table II -- Test Compilation
The boxes are empty if no measurement was made.

A standard procedure was developed for salt deposition tests. The dye tests were more complex and required modifications to the procedure. For salt deposition tests, the pressurized salt solution enters the reactor at less than 350°C (662°F), cool enough to remain in solution. Once inside the reactor, the heating water from the diamond-shaped holes raises the solution temperature to between 400 and 420°C (752 and 788°F) causing the precipitation of a solid phase. The solubility of sodium sulfate decreases three orders of magnitude between 350 and 400°C (662 and 752°F), as shown in Figure 9 (references 4 and 11). At the reactor exit, the stream is mixed with cold water to decrease the temperature back to 350°C (662°F) thereby redissolving any salt that has not adhered to the wall. Salt deposition is monitored in three ways: electrical conductivity of the effluent, pressure changes within the reactor, and post test observation.

A roughly linear relationship exists between the concentration of an ionic species in solution and its electrical conductivity. By continuously indicating the amount of salt in the effluent stream, the electrical conductivity measurement provides real-time feedback about the extent of salt deposition, but no information about the location of deposits. The fraction of salt left in the reactor is inferred from a comparison of the effluent conductivity at the desired operating conditions with a zero-deposition baseline or calibration. This calibration is established by running the system with the salt solution at the desired pressure and flow rates before the system is heated to supercritical operating conditions. A decrease in conductivity, relative to the baseline, indicates salt deposition within the system.

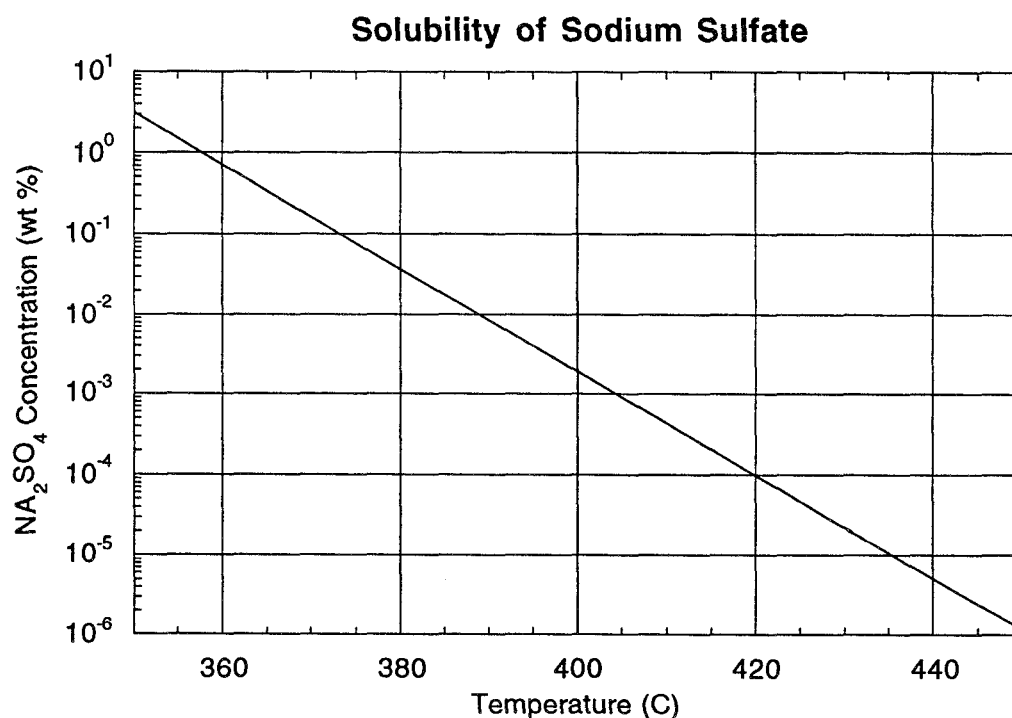


Figure 9 -- The solubility of sodium sulfate at 250 bar (3625 psi) decreases rapidly near the critical temperature of 374°C (705°F).

An increase indicates the dissolution of salt deposited earlier in the test. Such an increase can result from a decrease in temperature inside the reactor with a corresponding increase in solubility. More frequently it results from pieces of salt breaking loose and falling to the bottom of the reactor where their rapid dissolution in the subcritical water produces sharp spikes in effluent conductivity.

If salt deposits become large enough to significantly impede the flow, they are detected by an increase in the upstream pressure as the metering pumps try to maintain a constant flow rate. Differential transducers between the reactor inlet and outlet and between the wall transpiration flow inlet and the reactor outlet detect pressure changes as small as about 0.1 bar (1 to 2 psi). The use of pressure measurements to monitor salt deposition is discussed in reference 12.

The only information about the location and character of deposits comes from post test inspection. At the end of a test, the waste pump is switched from salt to water to flush dissolved salt from the system. This is done without changing the temperature so solid phase salt deposits remain in place. All pumps and heaters are then shut down almost simultaneously and a relief valve is opened to rapidly vent the pressure and drain the system before the salt dissolves. This process typically takes less than 15 seconds. Dry gas is then flowed through the reactor to remove any remaining water. After the reactor cools, usually overnight, it is opened to observe and photograph the salt deposits, using either still pictures looking in from the ends or video pictures with a boroscope inserted into the reactor.

We believe this shut-down process "freezes" the salt in place; certainly the locations of large deposits remain the same. However, there may be some change in the crystal structure. If salt is left in the reactor for several days after a test, grain growth occurs in the deliquescent salt crystals.

The procedure for the red dye tests was similar, except hydrogen peroxide was added to the heating water and the temperature was increased to enhance oxidation. The pH and electrical conductivity of the effluent were monitored on these tests, but they could not be compared with calibration data at subcritical temperature because the chemical species changed during the oxidation process. UV-visible absorption spectra, recorded on-line throughout the test, and total organic carbon (TOC) measurements were used to determine destruction efficiency. In the first test, TOC measurements and other chemical analyses were done after the test using effluent samples collected periodically throughout the test. In the second test, the TOC analyzer provided on-line sampling and analysis of the effluent stream every five minutes.

Test Without Transpiring Wall Protection - This test was run with no transpiration fluid to establish the baseline performance of an unprotected reactor. Nominal conditions were:

Hot water: 3.5 grams per second at 625°C (1157°F),
Salt (1.5 wt %): 1.7 grams per second at 235°C (455°F),
Cold water: 8 grams per second at room temperature.

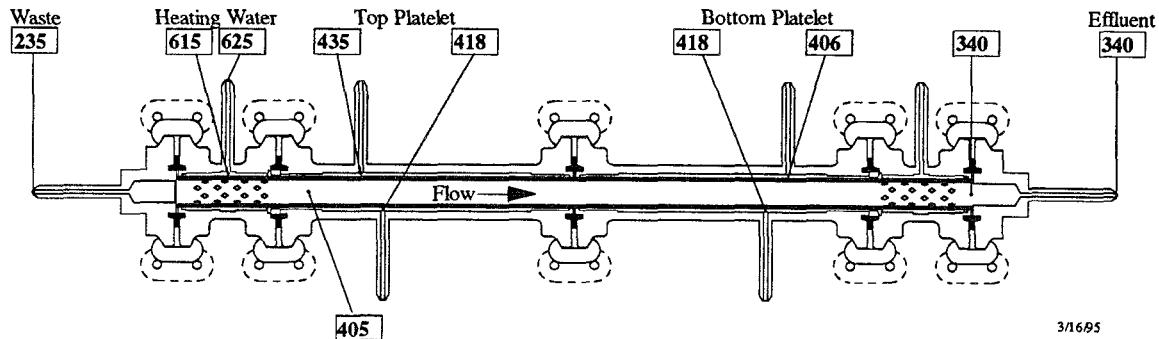


Figure 10 -- The reactor was heated with the transpiration fluid flowing. The temperatures in the reactor with the transpiration flow are shown.

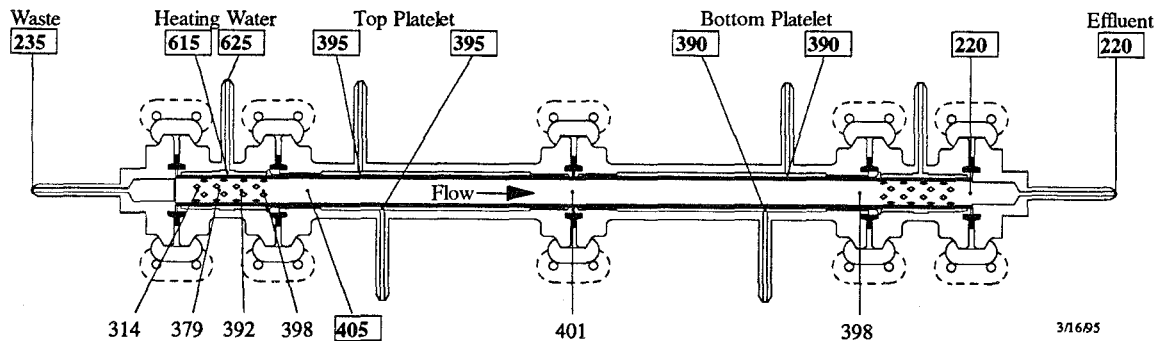


Figure 11 -- With the transpiration flow off, the system stabilized at the temperatures shown. Temperatures in boxes were measured. Others were calculated.

The test followed the normal start-up procedure with the transpiration water flowing, reaching the conditions shown in Figure 10. (Temperatures in boxes were measured; the others were calculated as described earlier.) The wall protection water was then turned off, producing the conditions shown in Figure 11.

With the wall protection water off, the salt solution was fed into the reactor for 120 minutes. Figure 12 shows the flow rates of the 1.5 weight percent salt solution and of the heating water. Flow rates were obtained by taking the derivative of the weight of the supply containers. The derivative operation amplified noise in the data so these plots were filtered and smoothed. These curves are typical of the flow data in all the tests.

Temperatures of different fluid streams throughout the test are shown in Figure 13. The internal thermocouple, located about 2.5 cm (1 inch) below the diamond-shaped heating holes, measured 400 to 405°C (752 to 761°F) at the start of the test. This was cooler than expected but was sufficient. About 30 minutes into the

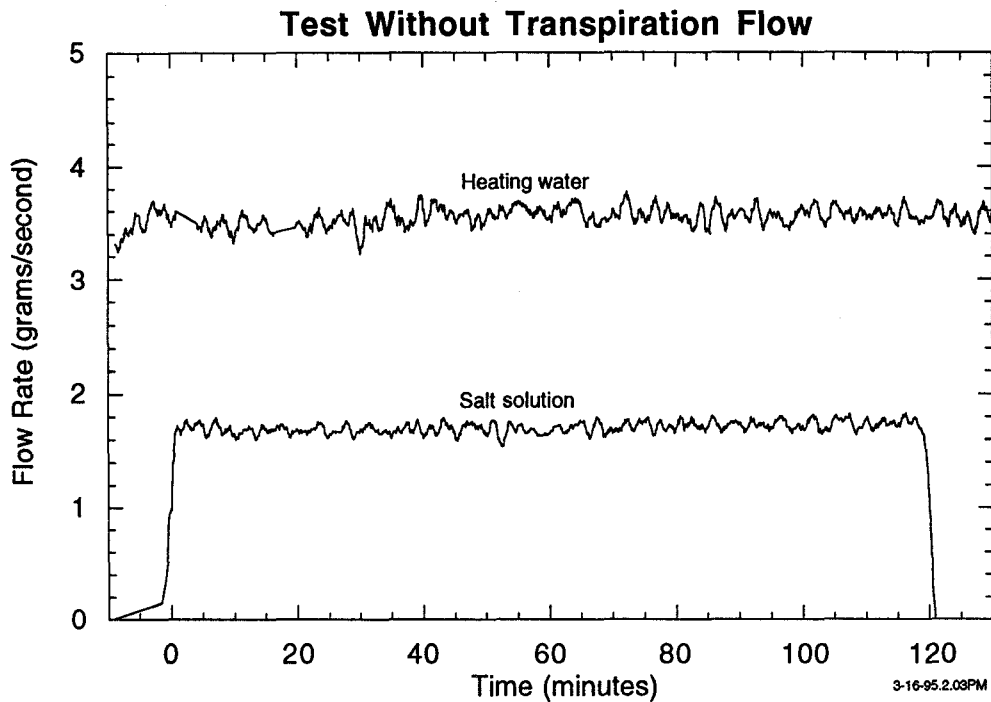


Figure 12 -- Flow rates were determined from the derivative of the weight of the supply and effluent carboys. The derivative operation amplified noise. These curves are typical of the data on all tests.

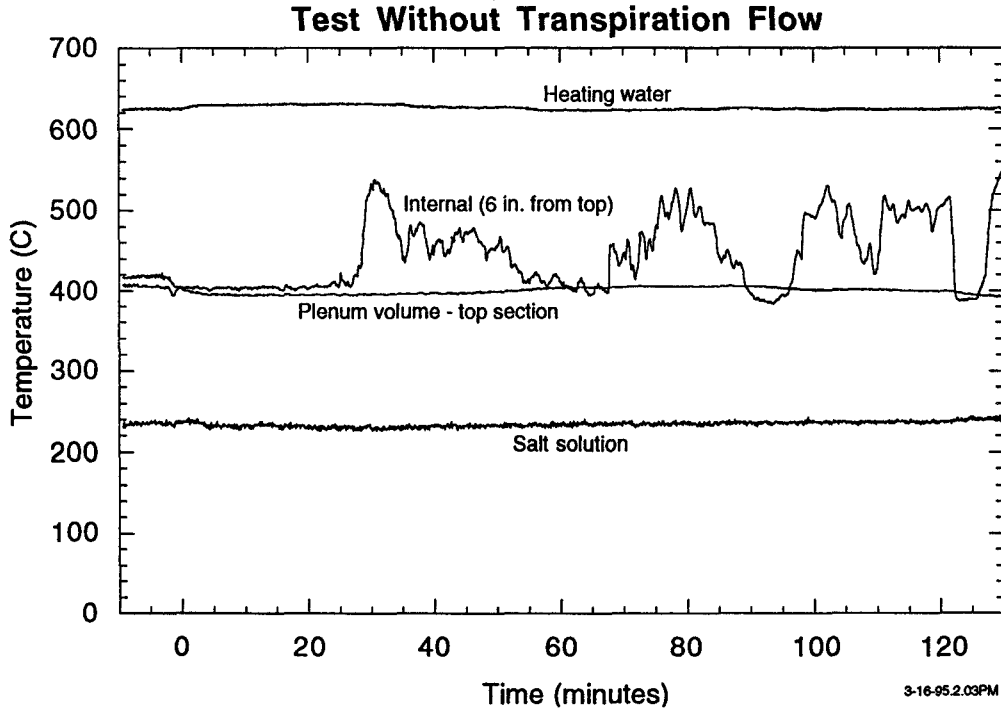


Figure 13 -- Fluid temperatures remained fairly constant except for the temperature inside the reactor. The wide fluctuations may have been caused by salt deposition on or around the thermocouple.

test it began to fluctuate widely, reaching highs of 550°C (1022°F) and lows of 380°C (716°F). This variation has not been explained but presumably it was related to salt deposition around the thermocouple. All other temperatures remained stable. The temperature in the plenum of the upper reactor section varied from 395 to 405°C (743 to 761°F). In the bottom section it decreased steadily from 390 to 380°C (734 to 716°F).

Figure 14 shows the differential pressure measured between the reactor inlet and outlet. The large pressure drop at the beginning of the plot occurred when the transpiration water was turned off. The flow of salt solution began about one minute later and the pressure gradually climbed as the salt accumulated.

The electrical conductivity of the effluent is shown in the lower curve in Figure 15. The spikes in the data resulted from pieces of salt breaking away from the wall. The curve labeled "salt out" shows the accumulated quantity of salt in the effluent. It was obtained by integrating the conductivity data, with corrections for variations in flow rate. The curve labeled "salt in" shows the accumulated quantity of salt flowing into the system. The difference between salt in and salt out is the amount that was deposited on the reactor walls.

Figure 15 shows that, without transpiration water to protect the reactor wall, about 45 percent of the salt came through. The other 55 percent was deposited

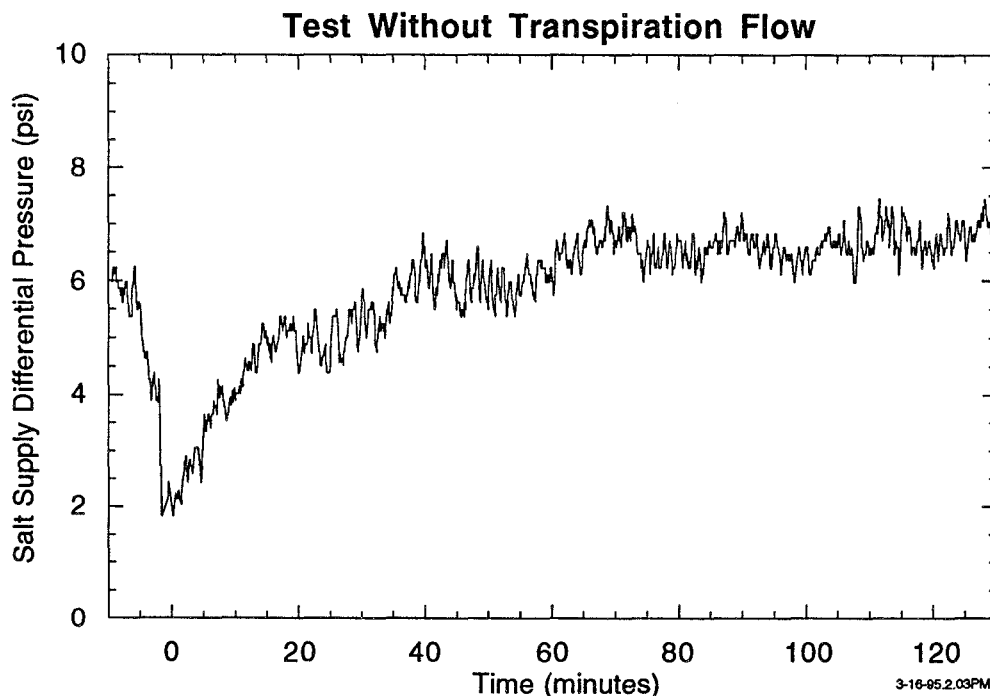


Figure 14 -- Differential pressure between the waste supply entering the reactor and the effluent down stream of the reactor. The sharp drop at the beginning resulted from reduced effluent flow when the transpiration flow was stopped. The gradual increase apparently resulted from salt build up in the reactor.

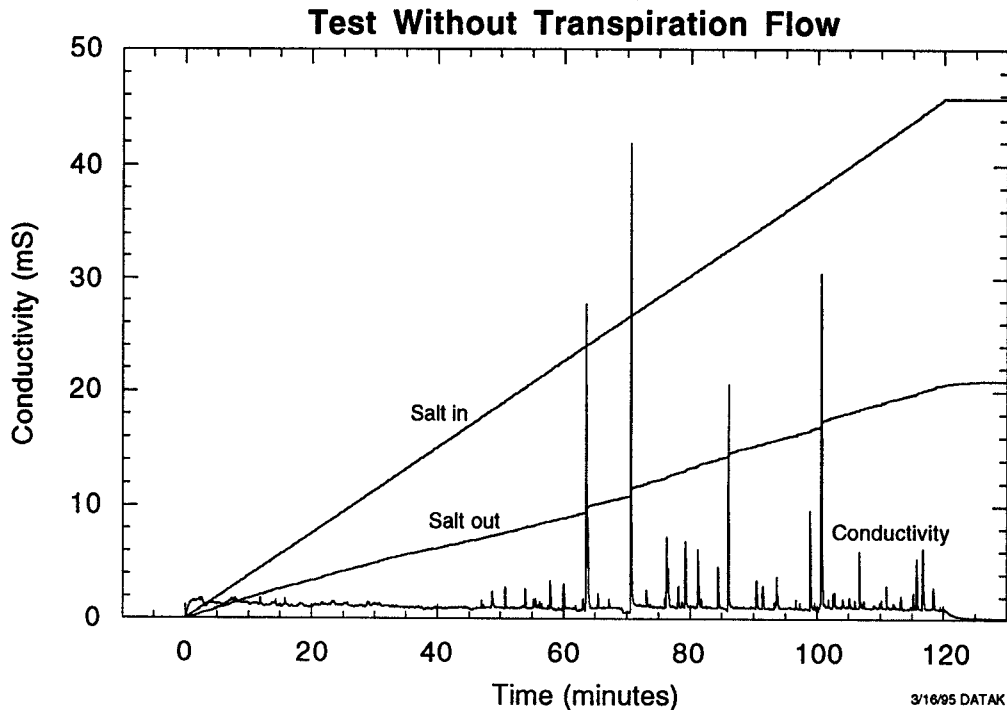


Figure 15 -- Comparison of the integrated conductivity (salt out) with the integrated supply (salt in) shows that over 1/2 the salt remained in the reactor. The large spikes resulted from pieces of salt breaking loose from the wall.

in the reactor. About 45 minutes after the salt flow began, small spikes began to appear in the conductivity. Fifteen minutes later the spikes increased in size, but they remained a small fraction of the total salt coming through the system. The largest conductivity spike, about 70 minutes into the test correlated with a small, but measurable, change in the differential pressure seen in Figure 14.

Because the fluid took a few minutes to flow through the system, there was a lag between the time that the salt was introduced to the system and the time that it appeared in the effluent. Most of this time was spent in the waste feed line upstream of the reactor. The time scale for the conductivity data on all figures has been shifted to remove this time lag so the first appearance of salt in the effluent coincides with the introduction of salt to the system. This was convenient because the conductivity and pH data were collected on a separate computer system from the other test data. The time scales on plots of other data, such as temperature and pressure, have not been shifted so coincident events appear earlier in the conductivity data.

As described earlier, the curve showing "salt in" was extrapolated from data taken with the reactor at low temperature. These data are shown in Figure 16. Since there was no salt deposition at that condition, the "salt in" had to equal the "salt out". The salt solution ran initially for 25 minutes, then after a short delay, for

another 12 minutes. Because the low temperature data from other tests were similar to that shown in Figure 16, they are not included in this report.

Figures 17, 18 and 19 show pictures of the salt as observed the day following the test. There was a lump or "thrombus" about 6 cm (2.4 inches) from the top on one side of the reactor (about 90 degrees from the hot water inlet). It was about an 2.5 cm (1 inch) long and reached out to about the middle of the reactor. It had a porous crystalline structure. Below this was a relatively clean region with just small patches of salt that looked like white paint splattered on the surface.

A second large deposit began about 15 to 18 cm (6 to 7 inches) from the top. It appeared to be more densely packed than the upper deposit. It covered the entire circumference but was much thicker on one side than the other. About 70 percent of the reactor area was blocked with just a single, off-center opening of about 1.3 cm (0.5 inch) diameter. From the top of the reactor we could not see beyond that point so we removed the top section of the reactor.

Below the point mentioned above, the entire reactor surface was covered with salt that had a surface appearance of new-fallen snow. The thickness varied considerably from point to point, but was at least 1.25 mm (50 mils) everywhere. At several points it was up to 1.3 cm (0.5 inch) thick. The thick points were not small clumps sticking out, but smooth bulges extending over several inches.

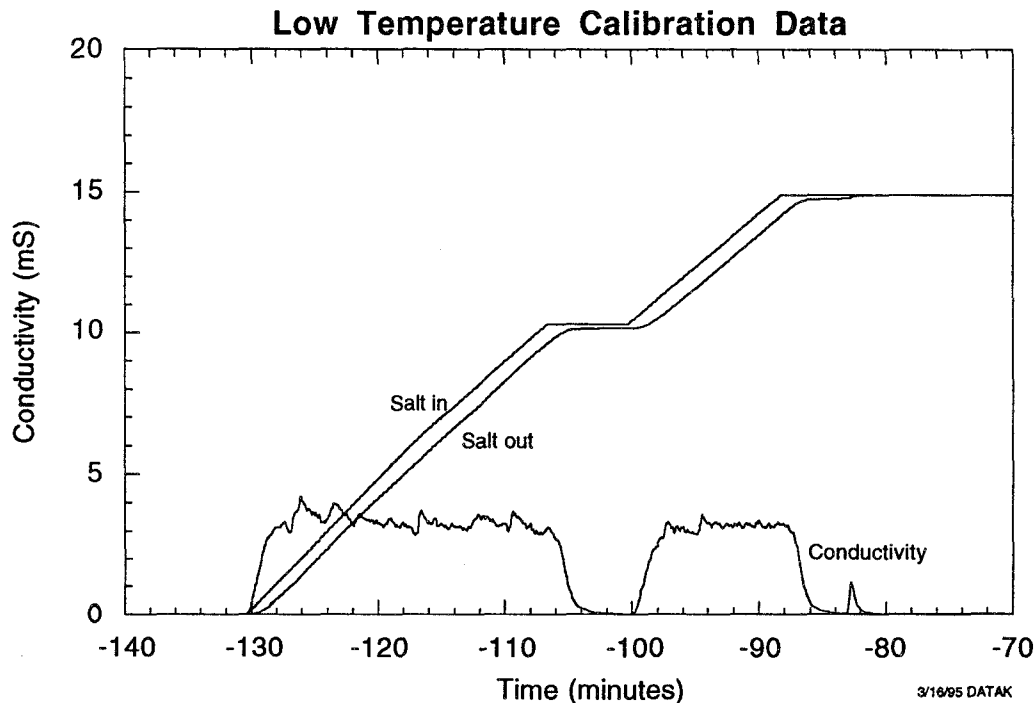
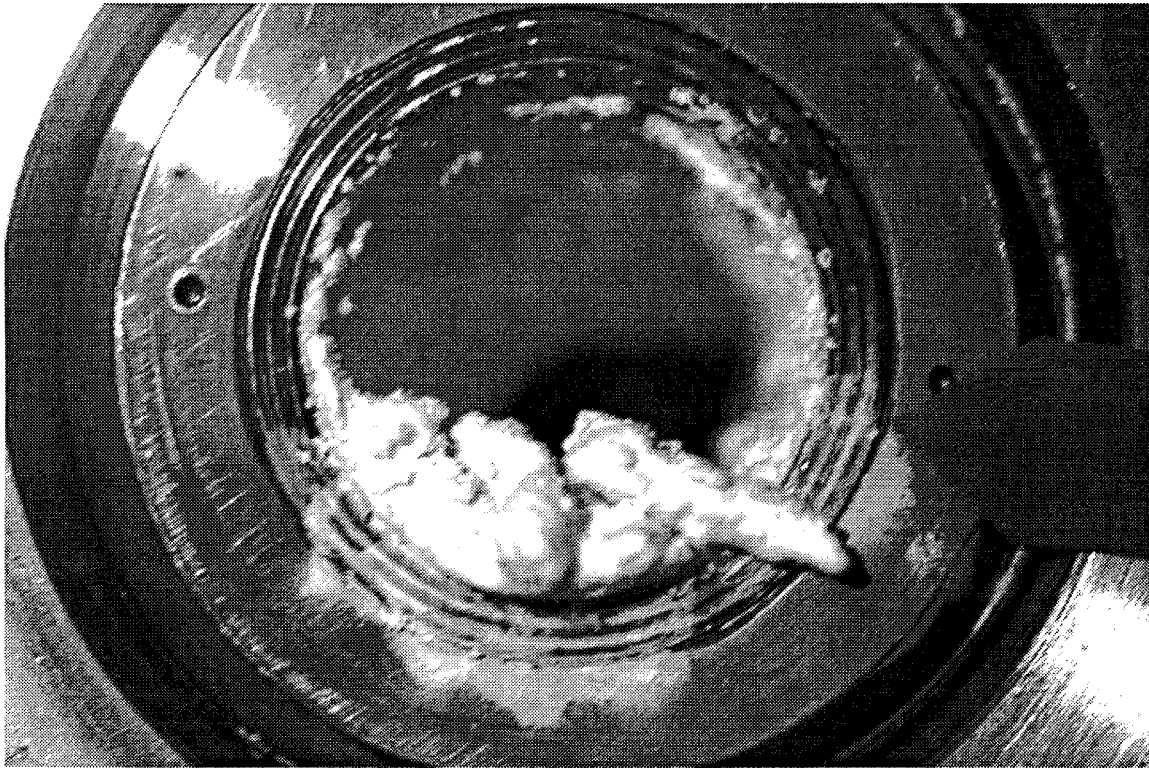
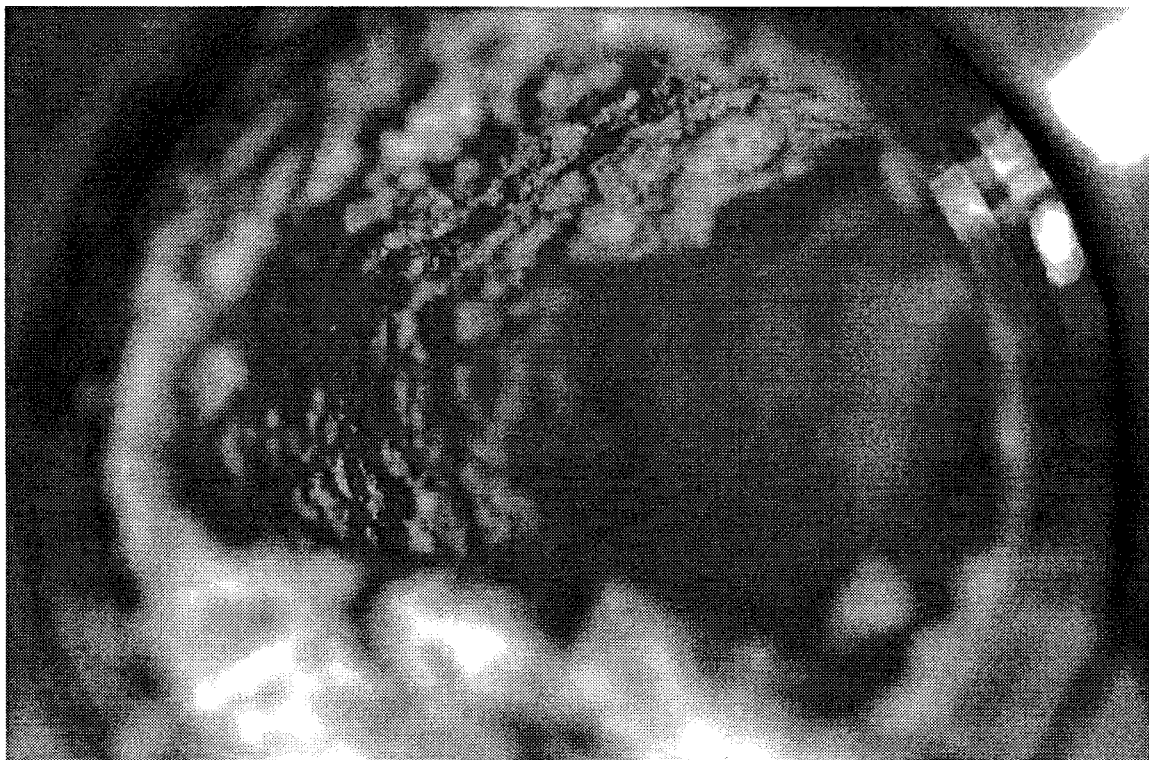


Figure 16 -- The electrical conductivity of the effluent indicates the concentration of salt. Data taken at low temperature were used to calibrate the readings by scaling the integrated flow of salt solution into the reactor to the integrated conductivity of the effluent.



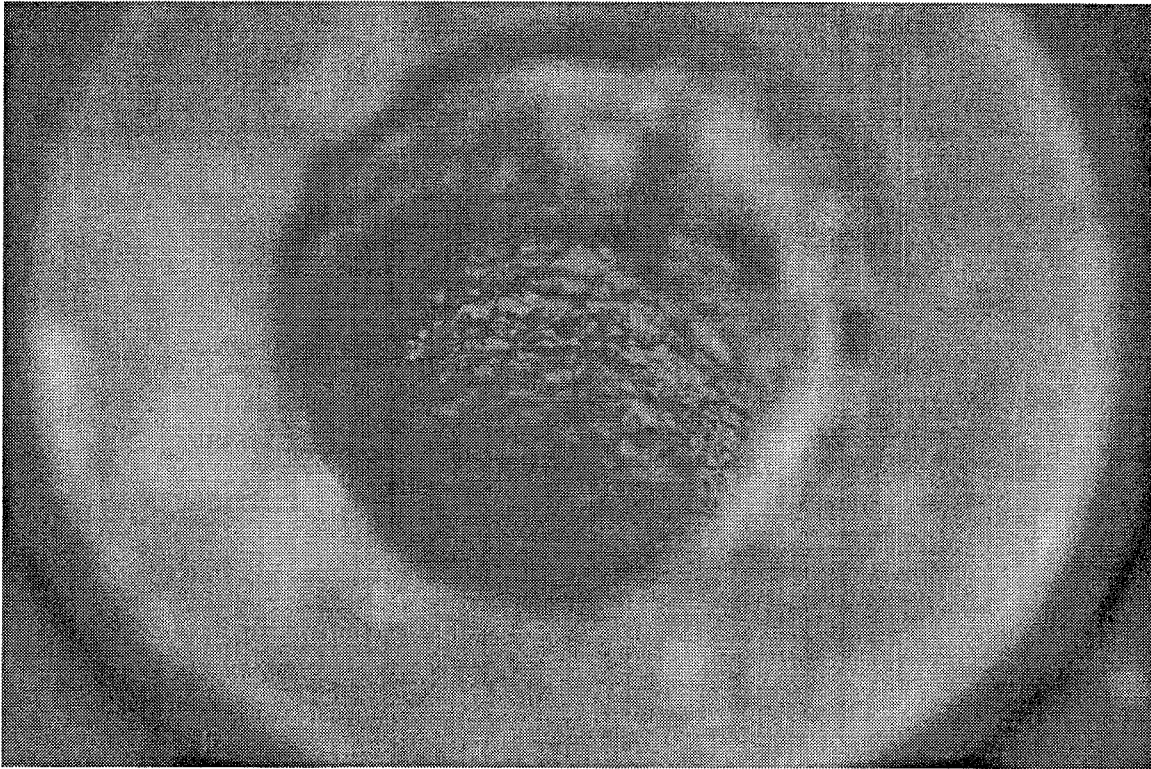
3/16/95 P1 bottom#1

Figure 17 -- Salt deposit in the upper reactor section looking from the middle joint toward the top. This test had no transpiration water.



3/16/95 P1 bottom#3

Figure 18 -- Same view as Figure 17, but focused on salt further from joint (closer to the inlet). This test had no transpiration water.



3/16/95 P2#2

Figure 19 -- Salt deposit in the lower reactor section looking from the middle joint toward the outlet. This test had no transpiration water.

Tests With Different Effectiveness Ratios - This series of three tests evaluated the ability of the transpiring wall to prevent deposition and investigated the influence of effectiveness ratio. The effectiveness ratio was varied by changing the flow rate of the waste stream. The transpiration flow was not varied because the internal metering channels in the platelet were designed for a specific flow rate. The most definitive of these tests was the last one with the lowest effectiveness ratio. The flow rates on this test were about the same as those on the test without wall protection. Nominal reactor conditions for this test were:

Platelet 1(top): 4.7 grams per second at 455°C (851°F),
 Platelet 2: 4.9 grams per second at 450°C (842°F),
 Hot water: 3.8 grams per second at 560°C (1040°F),
 Salt (3 wt %): 1.4 grams per second at 235°C (455°F),
 Cold water: 10.7 grams per second at room temperature.

With these conditions, the effectiveness ratio was 0.83. The test used a 3 weight percent solution of sodium sulfate salt and ran for 170 minutes, twice the concentration and 1.5 times the duration of the unprotected test. Figure 20 shows the conditions at the start of the test. The calculated temperature leaving the hot diamond region was 420°C (788°F).

The effluent conductivity is shown in Figure 21. Some important observations can be made from these data. During the first fifty minutes of the test, the integrated salt out curve was almost parallel to the salt in curve. This indicates that nearly all of the salt was coming through. The spikes in the conductivity began almost immediately after salt was introduced to the reactor. Recall that the unprotected test ran for 45 minutes before the salt began to break loose even though more salt accumulated. This suggests that the salt that adhered to the wall in this test was more easily dislodged.

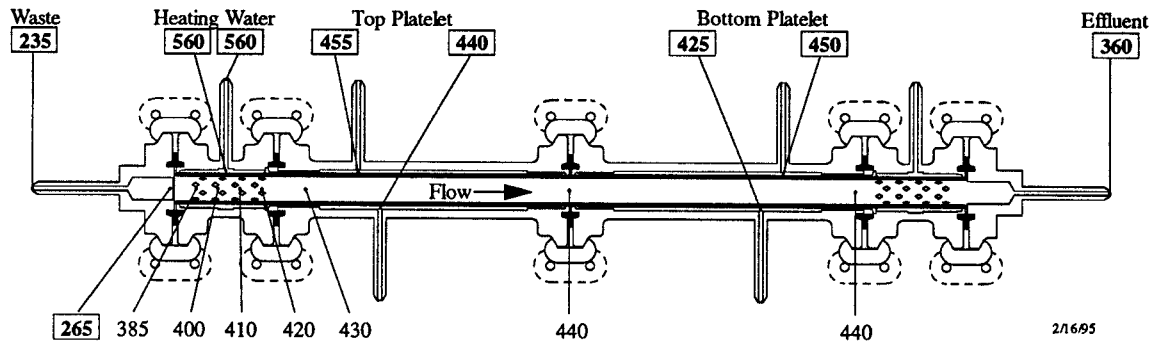


Figure 20 -- Temperatures for low effectiveness test.

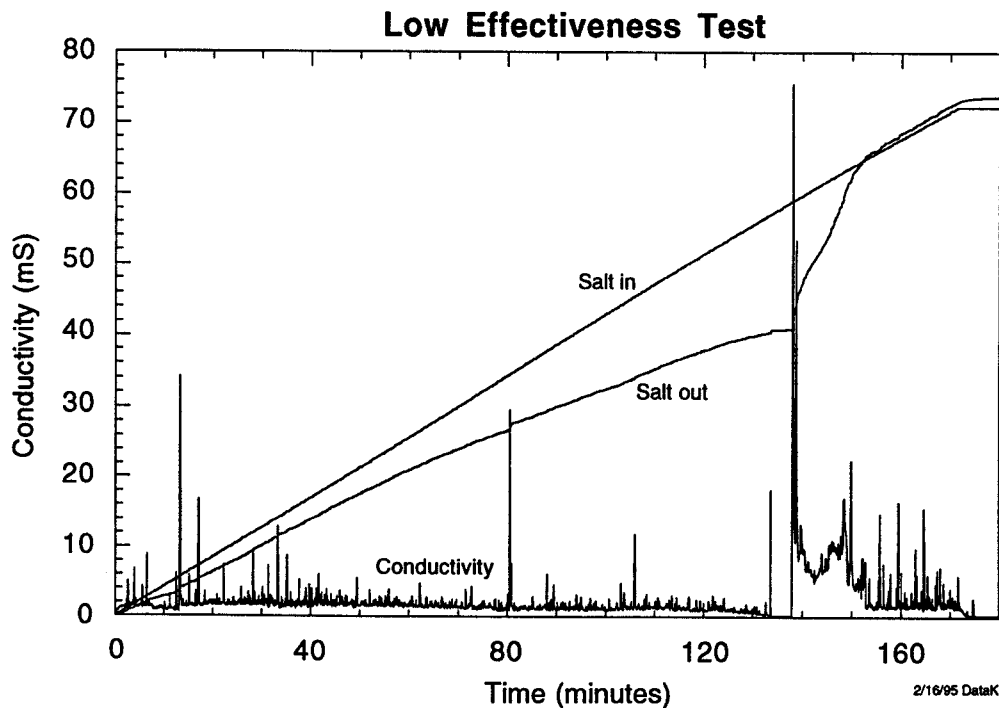


Figure 21 -- Conductivity data show a significantly greater fraction of the salt is washed through the reactor with the transpiration flow.

After about 50 minutes, the spikes became less frequent and the average conductivity began to decrease gradually. Apparently enough salt became firmly attached to provide a deposition site for more salt. The larger the deposit grew, the larger the fraction of salt it captured. After 135 minutes, essentially no salt came through the reactor. At that point the salt build up was great enough to cause an increase in the upstream pressure of about 0.7 bar (10 psi). Figure 22 shows the differential pressures between the salt solution inlet and the reactor outlet and between the transpiration water inlet and the reactor outlet. Figure 23 shows greater resolution at the time of interest.

The blockage was apparently near the top of the reactor. This is inferred from the fact that the salt inlet pressure increased with no corresponding increase in the transpiration pressure (between minutes 137 and 139). The plug broke loose suddenly as evidenced by the sudden drop in the salt inlet pressure. This was followed almost immediately by an increase in both the salt supply pressure and the transpiration supply pressure because the lump of salt blocked the 0.5 cm (3/16 inch) diameter reactor outlet before it redissolved. Most of the salt was flushed out at that point and the last twenty minutes of the test were similar to the first twenty minutes. The flow rate of the salt solution decreased slightly toward the end of the test as shown in Figure 24. This was probably due to the salt build up. Other flows remained constant.

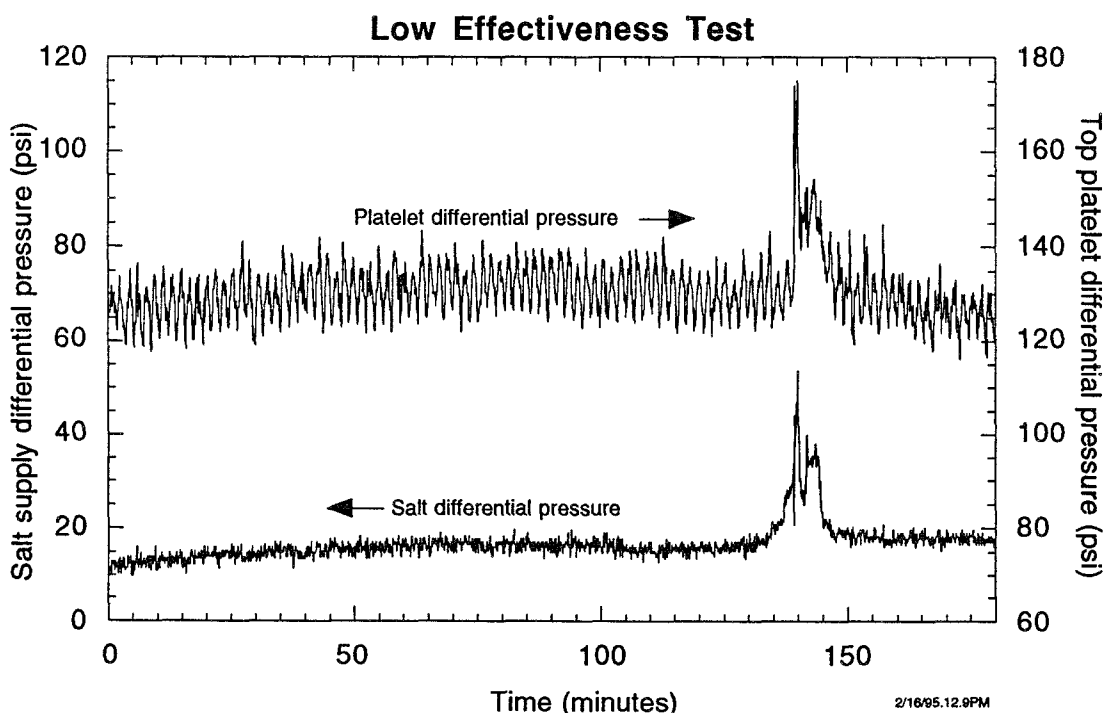


Figure 22 -- Differential pressure measurements between the salt solution entering the reactor and the down stream effluent (salt differential pressure) and between the platelet inlet and the downstream effluent show plugging due to salt deposition.

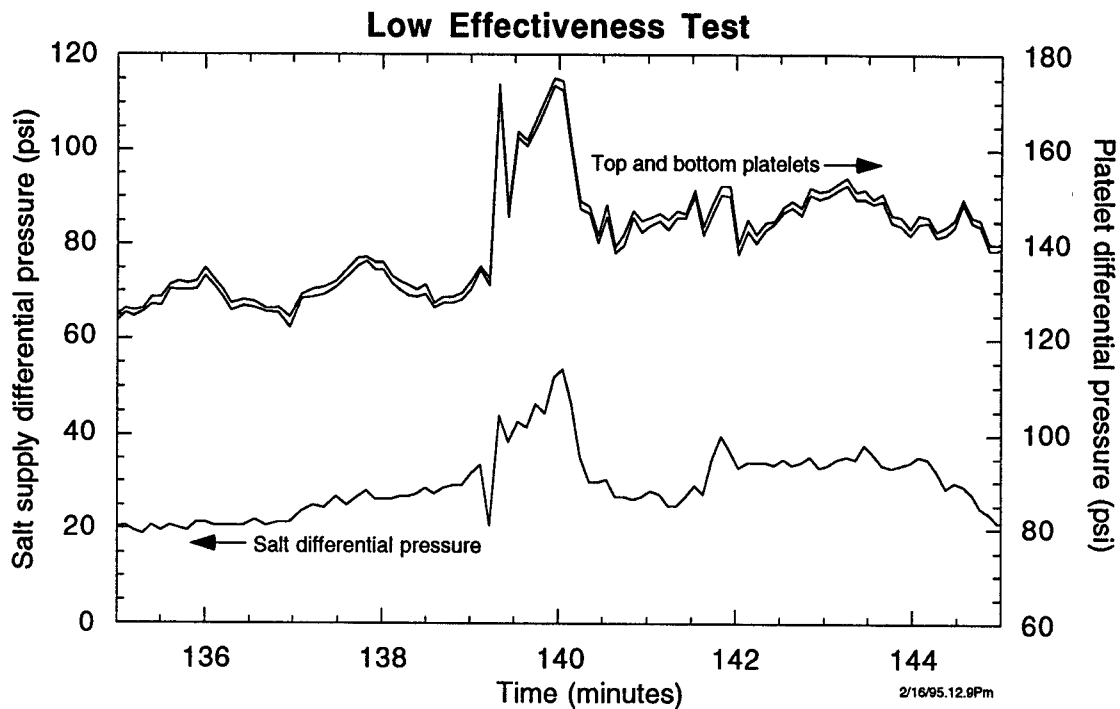


Figure 23 -- Initially only the salt supply pressure increased. After the plug broke loose, the platelet pressures increased. The salt was initially near the inlet then fell and plugged the outlet.

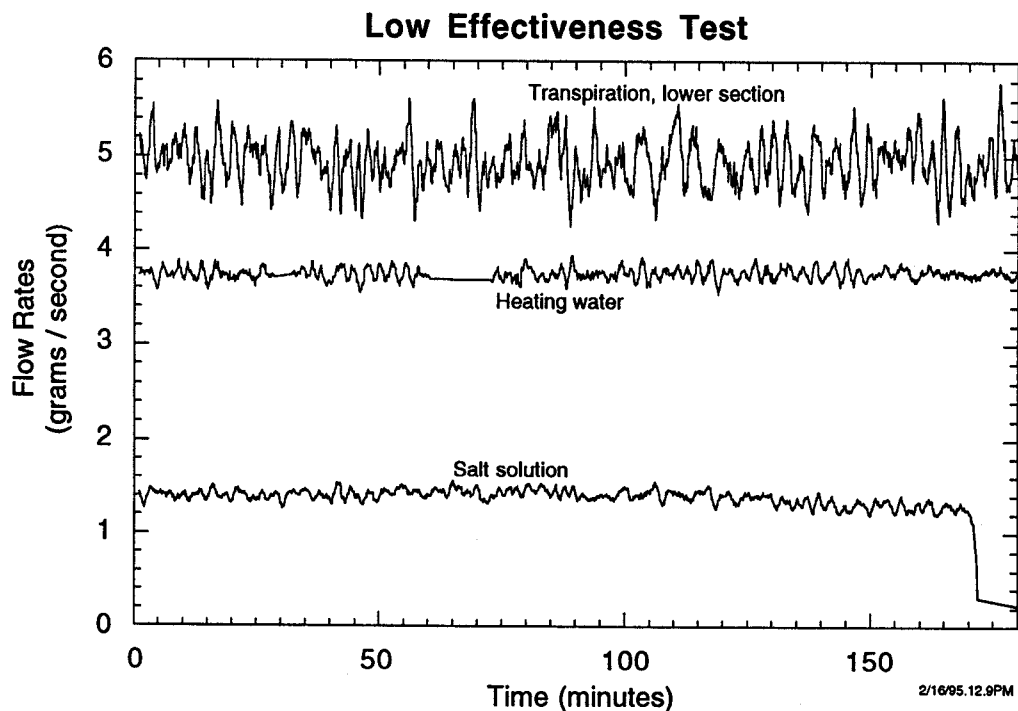


Figure 24 -- The flow of salt solution dropped slightly as the pressure increased (see Figure 22).

Comparison of the "salt in" and "salt out" curves on Figure 21 suggests almost complete closure for the salt. In fact, some salt was left in the reactor at the end of the test so the "salt out" curve should have been less than the "salt in". Closure was not expected on most tests because salt was left in the reactor for post test observation. This makes it difficult to determine the accuracy of the data. Figures 29 and 46 show the two tests in which closure was expected.

Errors in the integrated conductivity data may have resulted from three factors. First, because the large spikes in the conductivity are of short duration, the shape and size are frequently defined by just a few data points. This is apparent in Figure 25 which shows all the data points for a short segment of the test. A large portion of the total salt is included in the spikes so small errors in the shape of the spike can have a large effect. Failure to accurately measure the amplitude of the spike leads to underprediction of the amount of salt, while an error in the width or sharpness of the spike causes overprediction. Second, although corrections were made in the data for detectable variations in flow rates, the precision of the flow measurements is not sufficient to completely eliminate this source of error. Third, the conductivity meter is not temperature compensated so variations in the temperature of the effluent can cause changes in the conductivity measurement. This effect was not large because the chiller controlled the effluent temperature to within 5°C (9°F).

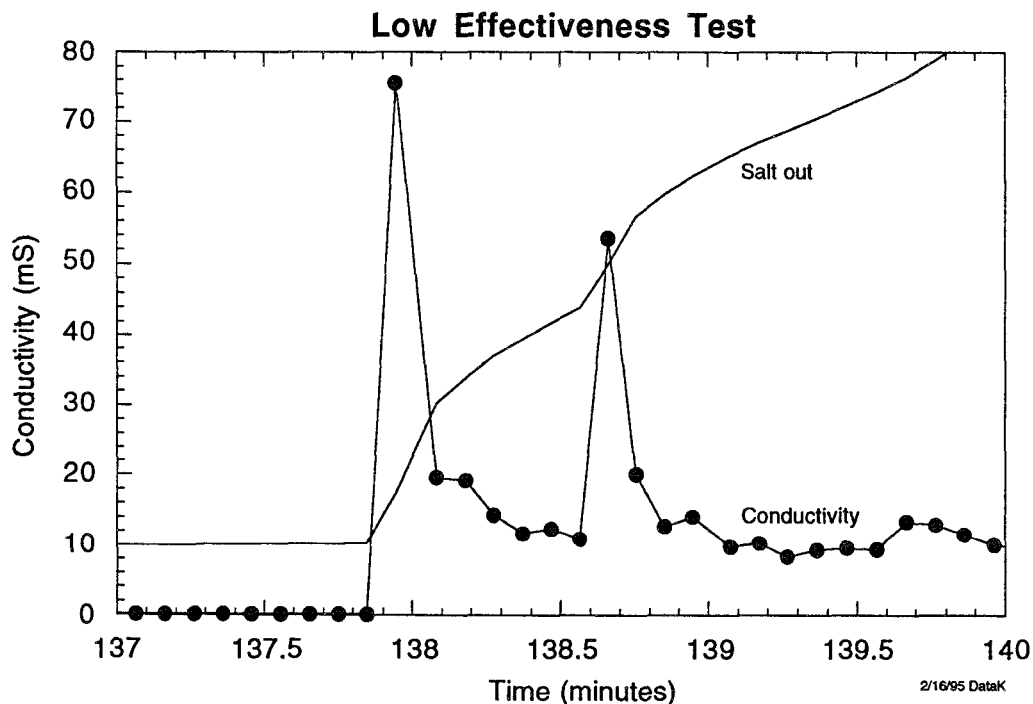
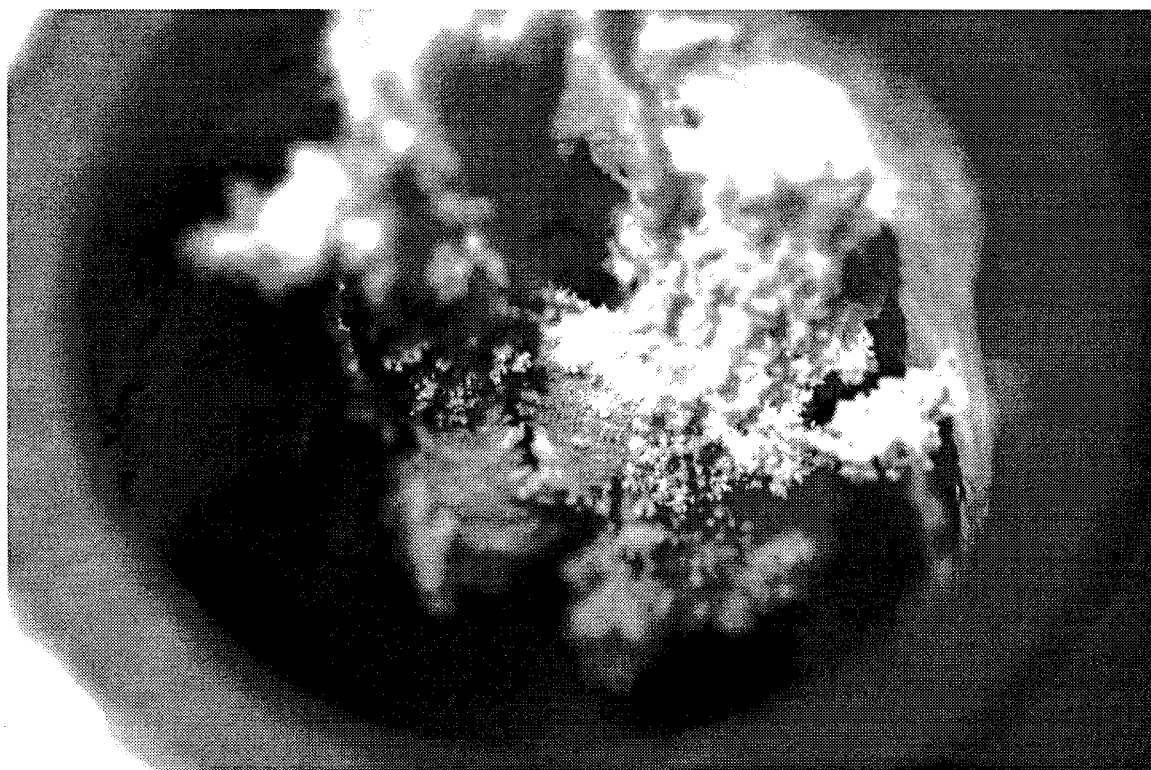


Figure 25 -- The height and width of the spikes in the conductivity measurements are not well defined.

The reactor was opened for observation the next morning. There was a large salt deposit in the region of the hot water injection holes that was caked against the wall opposite the hot water inlet. The surface of the salt was irregular with large clumps extending nearly half way across the reactor. Several of the diamond-shaped holes were completely filled with salt. There were no large deposits below the hot water injection zone, although there were small, discrete crystals scattered along the length of the reactor and some places had the appearance of a light frost forming on a window. There was an annular deposit, about 0.3 cm (1/8 inch) thick, just above the cold water injection region and a smaller one just below it. Similar deposits occurred on many tests and were probably related to turbulence from the jets of cooling water. Figures 26 and 27 show pictures of the salt near the top of the reactor and in the lower section.

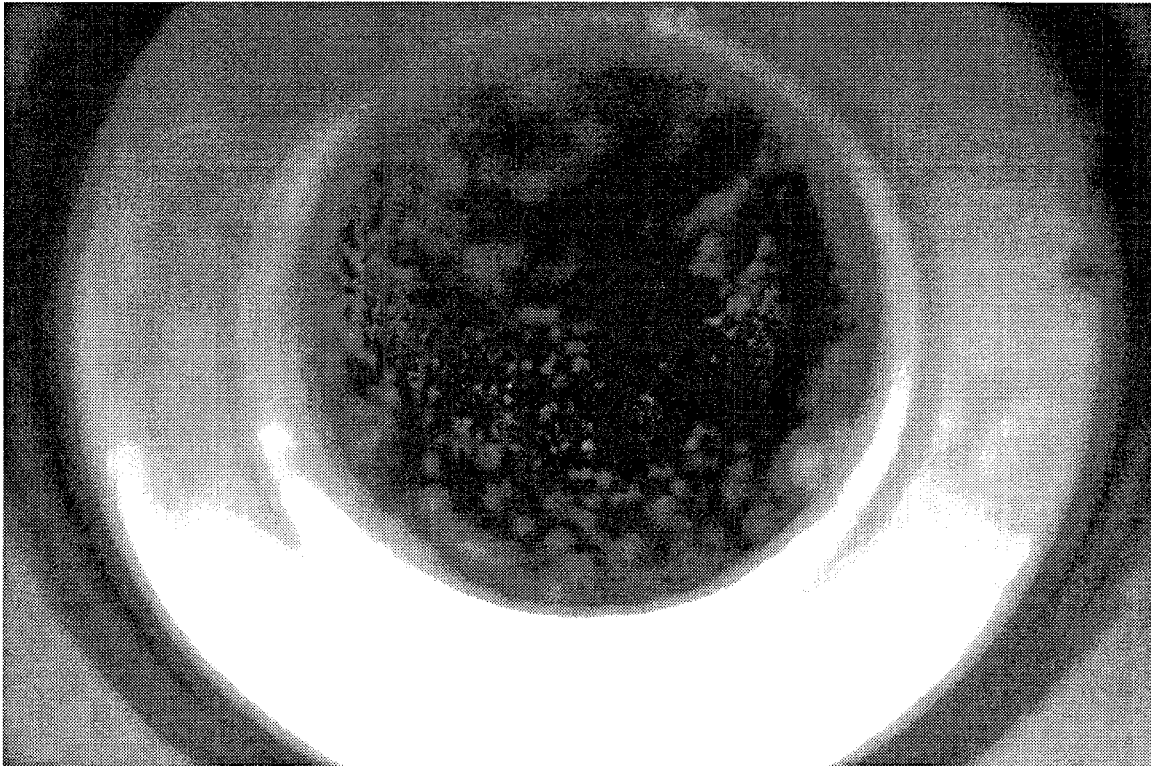
This test led to three conclusions:

- 1) Although not perfect, the transpiring wall resulted in a dramatic decrease in the salt buildup. This is evident by comparing Figure 27 with Figure 19. These pictures are both of the lower reactor section looking from the middle flange down toward the diamond-shaped cooling holes.
- 2) Even though some salt was still deposited, the transpiring wall apparently reduced the attached area of the salt. As the deposit grew radially inward, it lacked a sufficient anchor to the wall and broke away.



2/17/95 shot2

Figure 26 -- Salt deposit in the heating zone looking from the top of the reactor.



2/17/95 bt2ndjoint shot2

Figure 27 -- Small salt crystals in the lower reactor section looking from the middle joint toward the outlet.

3) The deposition was limited to the short heat-up zone at the top of the reactor. Outside that zone the transpiring wall worked entirely as expected.

The other two tests in this series used lower waste stream flow rates to increase the effectiveness ratio. Nominal conditions for one of these tests were:

Platelet 1(top): 4.9 grams per second at 445°C (833°F),
 Platelet 2: 5.1 grams per second at 445°C (833°F),
 Hot water: 0.88 grams per second at 615°C (1139°F),
 Salt (1.5 wt %): 0.38 grams per second at 310°C (590°F),
 Cold water: 8.5 grams per second at room temperature.

A 1.5 weight percent salt solution was fed into the reactor for 90 minutes. The effectiveness was 0.91. Figure 28 shows the temperatures and Figure 29 shows the conductivity measurements. Early in the test the system behaved like the 0.83 effectiveness test just described, except the large spikes in conductivity were absent. The conductivity of the effluent declined steadily until no salt was leaving the reactor. At that point the salt flow into the reactor was terminated. There was no pressure build-up so the test could have continued, but this was one of the first tests of the reactor so the approach was conservative. The salt deposits were dissolved by reducing the temperature during the shut down process so no post test observation was possible. A large increase in conductivity can be seen as the salt dissolved.

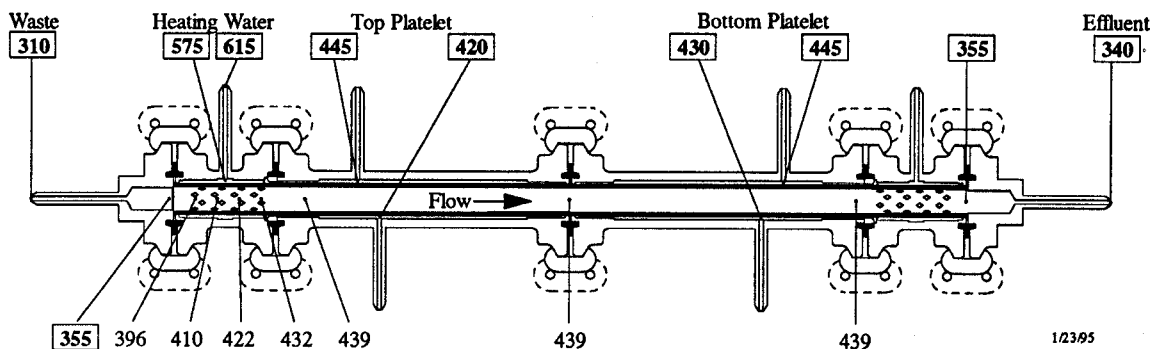


Figure 28 -- Temperatures for medium effectiveness test.

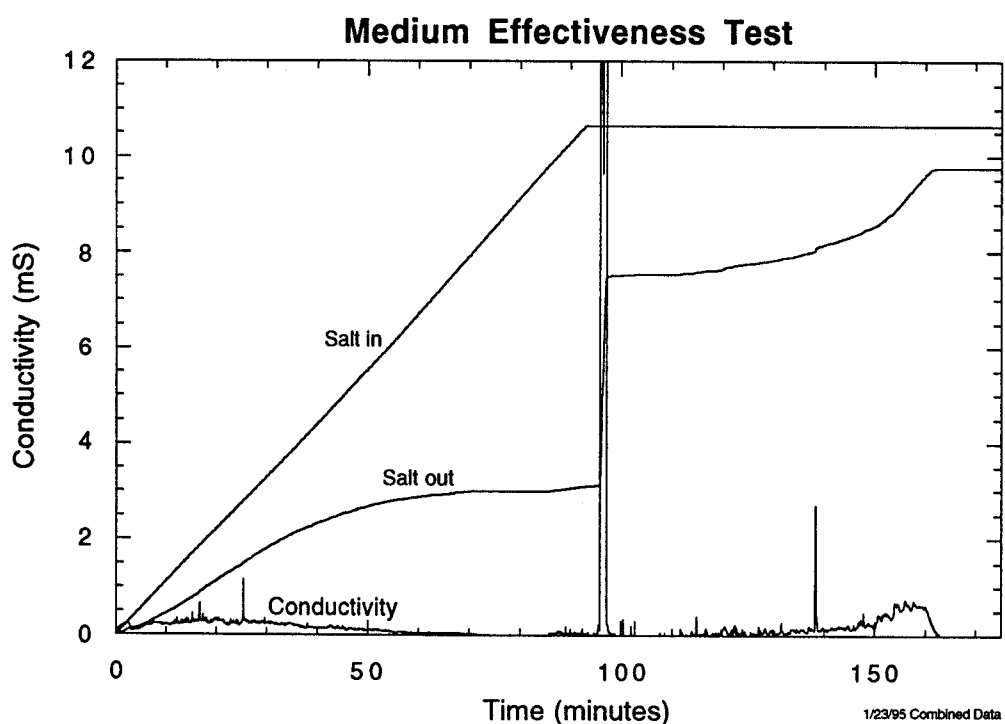


Figure 29 -- The conductivity dropped to zero meaning no salt was coming through the reactor. The large spike occurred when the temperature was reduced.

This test was inconclusive. Had the test continued, the salt may have broken loose as in the test just described. Another possibility was that the temperature of the salt solution entering the reactor was too hot, causing salt deposition around the diffuser plate. The temperature just above the diffuser was 355°C (671°F) which is near the solubility limit. The fluid near the wall could have been hotter than at the thermocouple in the center of the stream due to thermal conduction through the wall.

The third test was run with a high effectiveness ratio of 0.94 with the hope of eliminating all deposition. Nominal conditions were:

Platelet 1(top): 4.7 grams per second at 430°C (806°F),
Platelet 2: 4.9 grams per second at 455°C (851°F),
Hot water: 0.34 grams per second at 490°C (914°F),
Salt (3 wt %): 0.08 grams per second at 341°C (646°F) at top flange,
Cold water: 9.2 grams per second at room temperature.

Figure 30 shows the test conditions. With the low waste stream flow rate it was difficult to keep the inlet temperature below the saturation temperature. There was no external heating of the waste stream and the insulation on the top of the reactor was removed to keep the inlet tubing cooler. However, the temperature continued to climb during the test until the inlet temperature reached 365°C (689°F) as shown in Figure 31. At that temperature there was probably some deposition on or above the diffuser plate at the reactor inlet. The temperature of the heating water was reduced to 490°C (914°F) which brought the waste inlet temperature down to 340°C (644°F). The salt solution ran for 2 hours and 30 minutes. The test was aborted when a problem with the chiller caused the effluent temperatures to climb suddenly.

The conductivity data from this test are not shown because they are difficult to interpret. The low flow rate of salt solution resulted in a small signal-to-noise ratio and effluent temperature changes, due to problems with the chiller, further confounded the data. The salient feature in the conductivity data was the absence of any spikes from salt breaking loose. Presumably the deposits never got large enough.

Post test observations showed a large salt deposit around the hot water diamonds and some small specks dispersed fairly evenly lower down. There was a large bare spot in the diamond region roughly opposite from the injection point. The results were not significantly different from the low effectiveness test. The large deposit near the top was smaller, but the total amount of salt supplied to the reactor was much less.

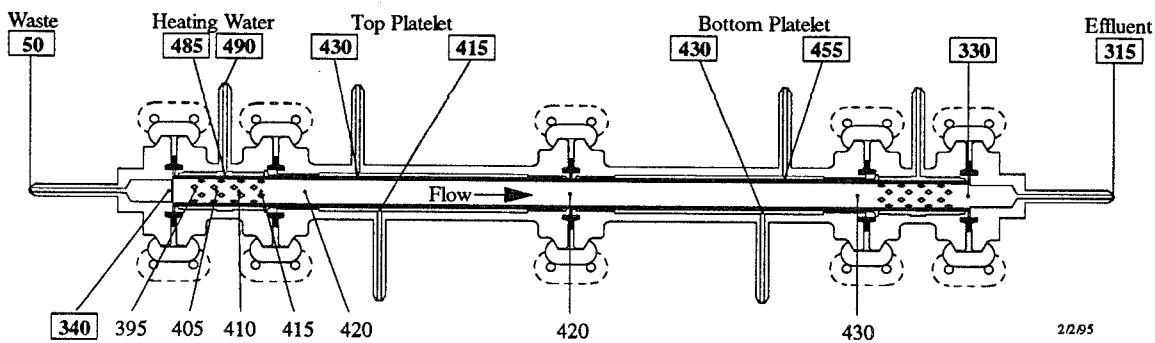


Figure 30 -- Temperatures for high effectiveness test

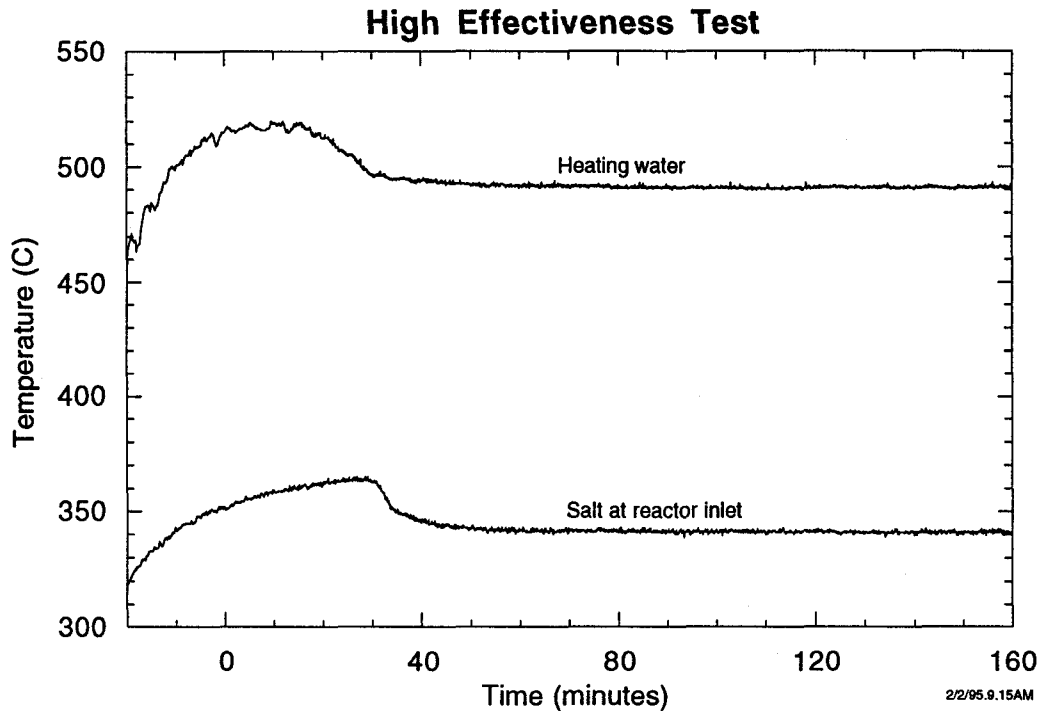


Figure 31 -- The temperature of the salt solution entering the reactor climbed to 365°C (689°F) which may have caused salt deposition in the inlet tubing.

From these tests there was no identifiable correlation between the effectiveness ratio and the amount of salt deposition. In all cases, the platelet reactor performed well, except for some deposition in the heating zone. This deposition may have overwhelmed the influence of the effectiveness ratio in the rest of the reactor where the amount of deposition was much less.

Possible Explanations - Several theories can be offered to explain the deposition in the heating zone:

- 1) The protective boundary layer was not adequately developed near the top of the reactor.
- 2) Turbulence from the hot water jets disturbed the boundary layer.
- 3) The diamond shaped holes created discontinuities in the surface that prevented a uniform boundary layer.
- 4) There was insufficient transpiration water near the top of the reactor as a result of the thermal effects discussed earlier.
- 5) The velocity of the fluid exiting the transpiration pores was too great relative to the core flow velocity.

6) The transpiring wall could not prevent deposition of salt which precipitated into the solid phase near the wall.

Numbers five and six require some explanation. For the transpiring wall to work correctly, the radial velocity of the water exiting the transpiration pores must be small compared to the velocity of the core flow through the center of the reactor so that the flow will turn and stay near the wall rather than penetrating into the core fluid. Theory five suggests that this condition may not have been satisfied near the top of the reactor where the core flow rate was small. Recall from the discussion of scaling that this reactor had a low ratio of waste flow to transpiration flow. The velocity of core flow increased as it moved down the reactor due to accumulation of heating water and transpiration water.

Regarding theory six, precipitation could occur when the cool salt solution entering the reactor mixed with either the heating water or with the transpiration water since both fluids were supercritical. Mixing with the heating water would form the solid-phase salt in the core of the reactor while mixing with the transpiration fluid would form it in the boundary layer near the wall. Although mixing with the heating water was the dominant method, some mixing of the cool salt solution with the transpiration water was inherent since the effectiveness ratio was less than one.

Theory six suggests that, once the solid-phase salt is formed in the core of the reactor, the transpiring wall is effective at preventing it from contacting and adhering to the wall further down. However, if the salt precipitates in the boundary layer, it immediately adheres to the wall. In this theory, the salt deposits near the top of the reactor consisted of salt that actually formed in the boundary layer when the waste stream mixed with the hotter transpiration water. Once the waste stream was heated, which occurred in the first few inches, there was no more precipitation in the boundary layer and no more deposition.

The next series of experiments was conducted to test these theories and investigate ways of improving the reactor performance.

Tests Without Injection Heating Water - In two tests, no injection heating water was used; heating of the waste inside the reactor resulted entirely from mixing with the transpiration water. Since the transpiration pores were designed to minimize turbulence and mixing, the heating zone, in which precipitation occurred, was expected to stretch over a greater length and probably begin further down the reactor. In the first test, the temperature of the transpiration water was increased to 470°C (878°F). Nominal operating conditions were:

Platelet 1: 4.7 grams per second at 470°C (878°F),
Platelet 2: 5.0 grams per second at 465°C (869°F),
Salt (3 wt %): 0.57 grams per second at 160°C (320°F),
Cooling water: 13.5 grams per second at room temperature.

The intent was make the flow rate of salt equal to the combined flow of the salt and heating water in the high effectiveness test discussed earlier. Figure 32 shows operating conditions assuming immediate mixing of the two fluid streams, which on this test is not a realistic assumption. Salt ran for 225 minutes. There was some variation in the flow rate as shown in Figure 33. Although the cause of the variation is unknown, it did not significantly affect the test results.

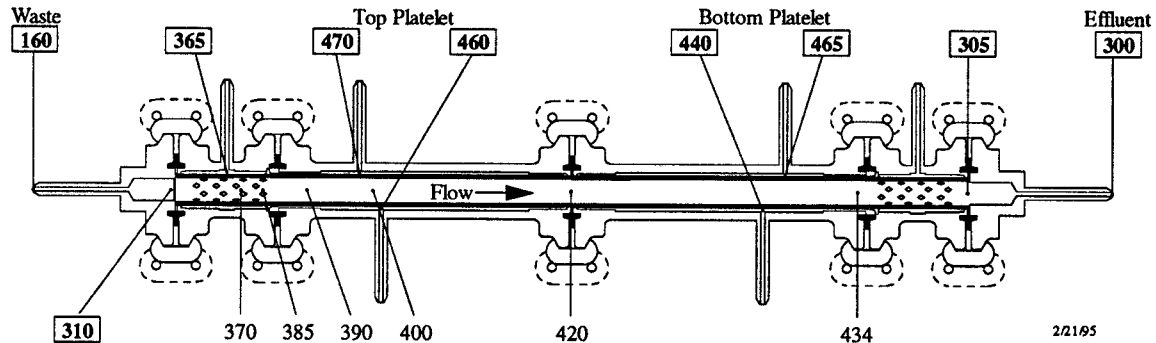


Figure 32 -- Temperatures for test without heating water.

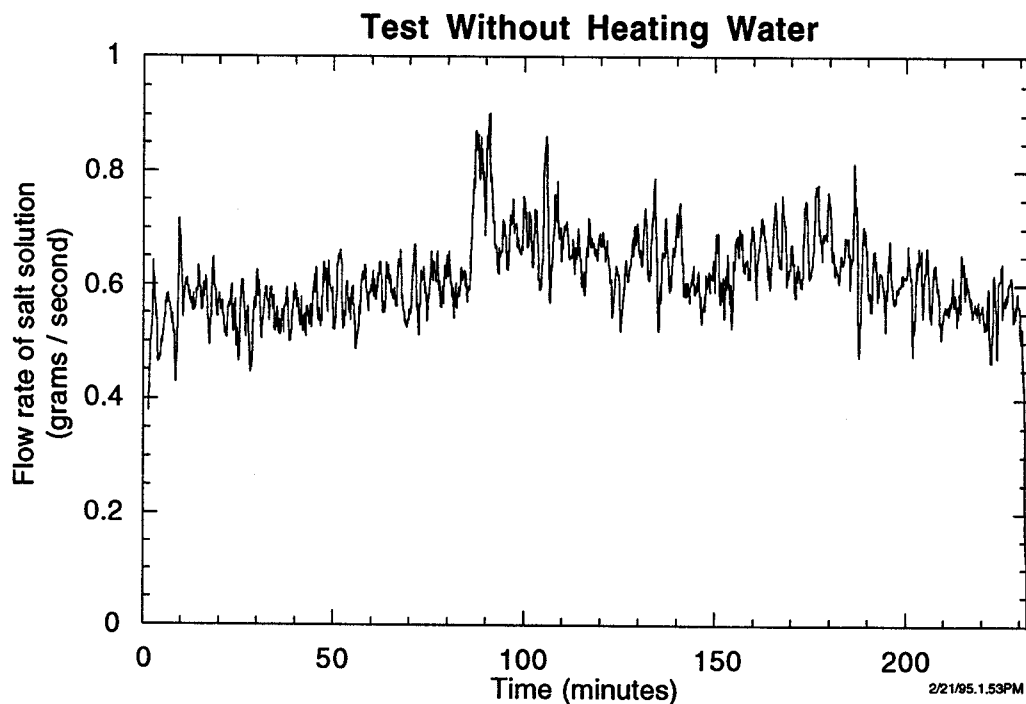


Figure 33 -- The flow rate of the salt solution varied during the test. The cause of the variation is unknown.

The conductivity data, shown in Figure 34, were similar to previous tests in that the fraction of salt that made it through the reactor decreased with time and frequent large spikes occurred. Some of the spikes were preceded by a sharp decrease in conductivity. There were small changes in the differential pressure readings but none were large enough to attribute to plugging. The spikes in conductivity were reasonably regular, but their magnitude decreased as the test continued. After about 3 hours, the spikes were no longer significant.

The effluent conductivity reading decreased during the last 30 minutes of the test. The salt flow was continued as long as possible to see if the conductivity would go to zero and if the pressure would increase due to plugging. Unfortunately, the transpiration water supply to the top platelet ran out, forcing an immediate shut down without first stopping the flow of salt. The system ran for 150 seconds with no transpiration water supply to the top reactor section. (The supply plenums in the two reactor sections were connected so shutting off one supply line reduced the flow through both sections but stopped neither of them.)

The salt deposits were observed and photographed the following day (Figures 35 and 36). The salt deposits began at about the end of the diamonds, which was about 7.5 cm (3 inches) lower than on previous tests. A single large deposit filled the entire cross-section of the platelet for a length of 7.5 to 13 cm (3 to 5 inches). The salt was not solid; there were voids and pores through which the water could flow. The deposit appeared to be delicate and fragile but in fact was quite strong. A screwdriver and hammer were needed to break a piece loose.

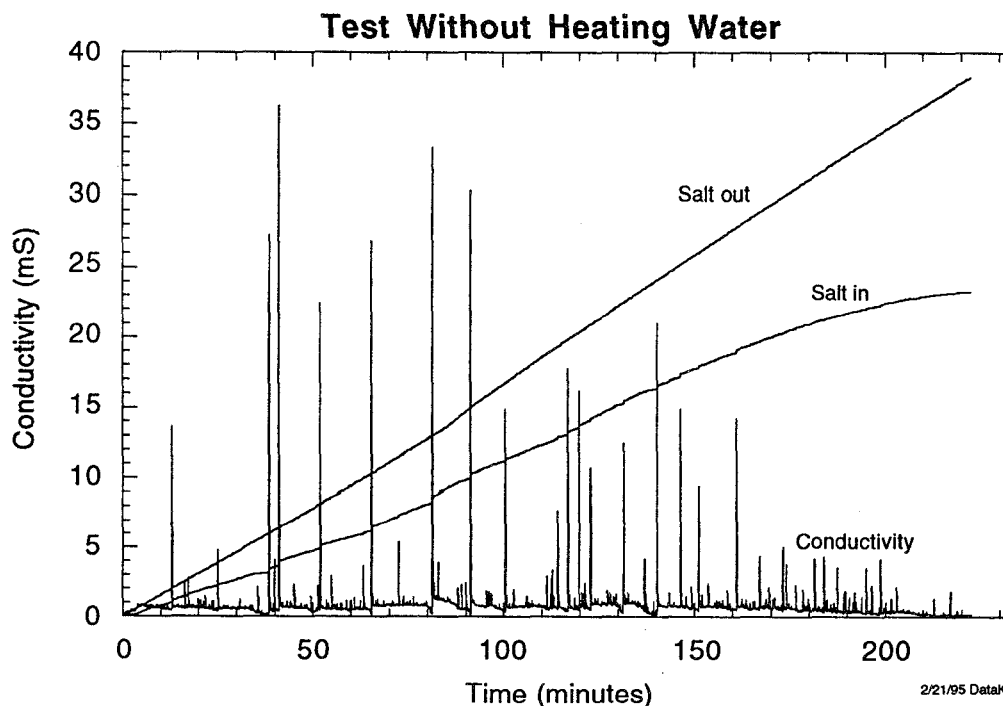
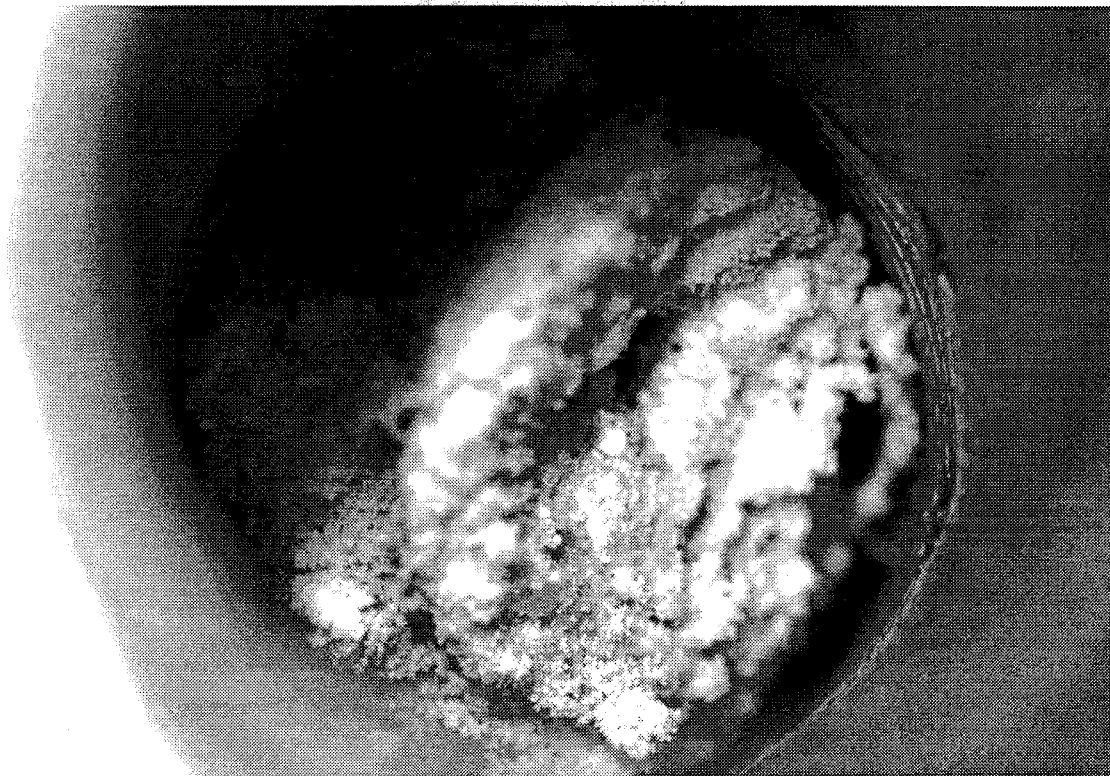
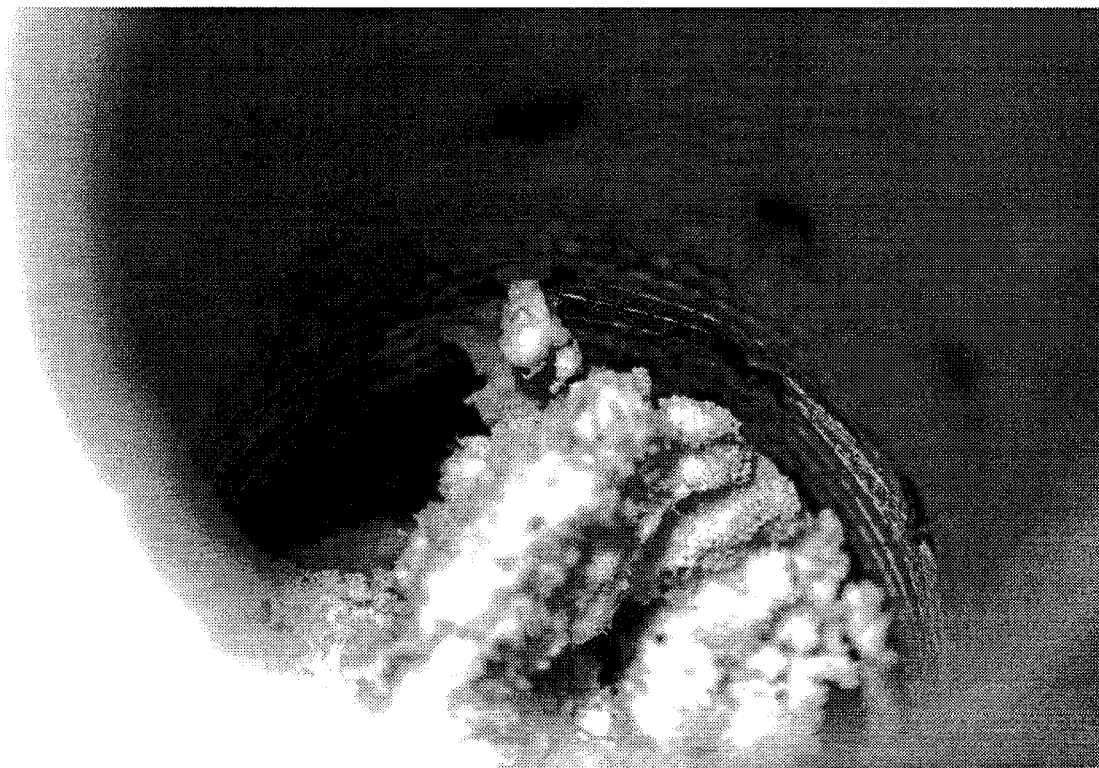


Figure 34 -- The conductivity data contained many large spikes which decreased in size as the salt deposits became more firmly attached.



2/21/95 plate8salt2

Figure 35 -- Salt deposit in the heating zone looking from the top of the reactor.



2/21/95 plate8salt3

Figure 36 -- Same view as Figure 35 at different angle to show the bare wall and diamond-shaped heating holes above the salt.

A second, smaller deposit was located further down on one side of the reactor. It was less than 1 inch long and extended about half way across the reactor. It was located near the point that the wall protection water entered the top reactor section. There were also significant deposits in the cold diamond region. Several diamonds had salt caked around them about a quarter inch thick but the diamonds were open. The rest of the wall had small specks of salt with an occasional crystal less than 0.5 cm (3/16 inch) diameter. Other than the three large deposits, the wall was probably cleaner than on the other tests.

These results tended to discredit theories 1 through 5, but were consistent with theory 6. The lower location and increased length of the deposits were consistent with the lower, longer heating zone. However, they occurred lower in the reactor where the boundary layer should have been adequately developed and where the reactor appeared to provide adequate protection on other tests (theories 1, 4 and 5). There was no heating water to create turbulence (theory 2) and the deposits were below the diamonds in an area where the boundary layer should have been uniform (theory 3).

The intent of the second test was to move the precipitation zone down into the reactor several inches by decreasing the temperature of the wall protection water in the top platelet and increasing the flow rate of the waste. Flow conditions were:

Platelet 1: 5.0 grams per second at 405°C (761°F),
 Platelet 2: 4.5 grams per second at 470°C (878°F),
 Salt (1.5 wt %): 2.0 grams per second with no heating
 Cooling water: 8.9 grams per second at room temperature.

Figure 37 shows measured and calculated conditions. The calculations again assumed immediate mixing of the waste stream with the transpiration water at each location and they assumed complete isolation of the two transpiration water streams. The salt solution ran for 100 minutes. Figure 38 shows the conductivity. A greater fraction of the salt came through the reactor as a steady flow than on the test just described. Instead of many spikes in the conductivity, there were two large spikes. One occurred at 40 minutes and one at 90 minutes. Over ten percent of the total salt was in these two lumps. Figure 39 shows temperatures during the test. The thermocouple located 2.5 cm (1 inch) below the upper

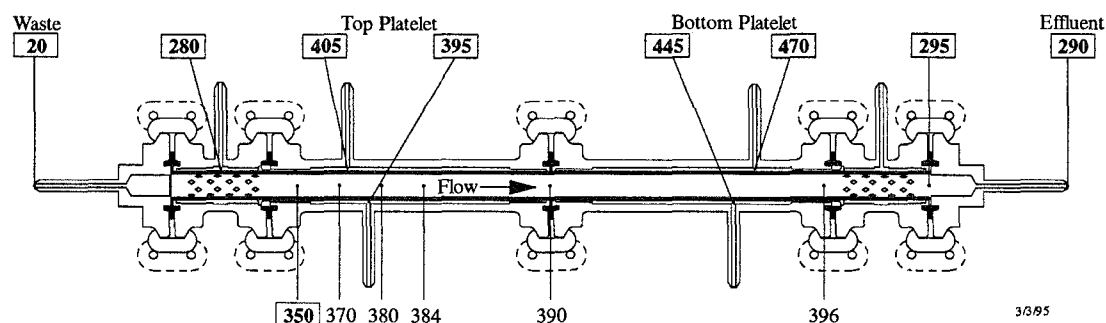


Figure 37 -- Temperatures for second test without heating water.

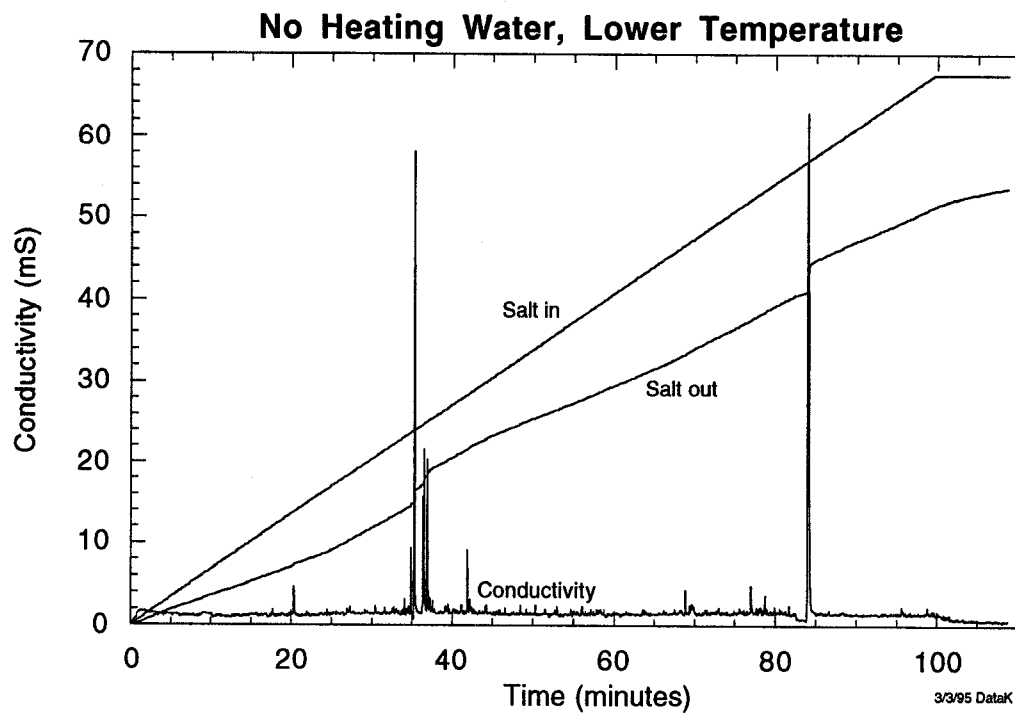


Figure 38 --The conductivity was quite steady except for two large spikes that contained about 10 percent of the total salt.

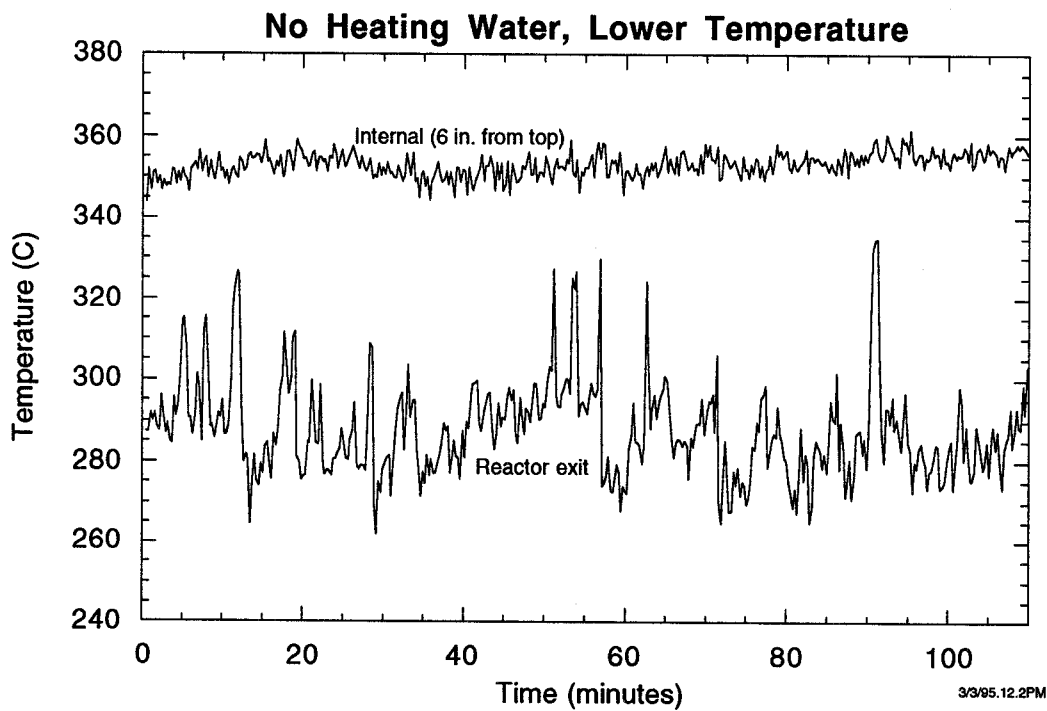
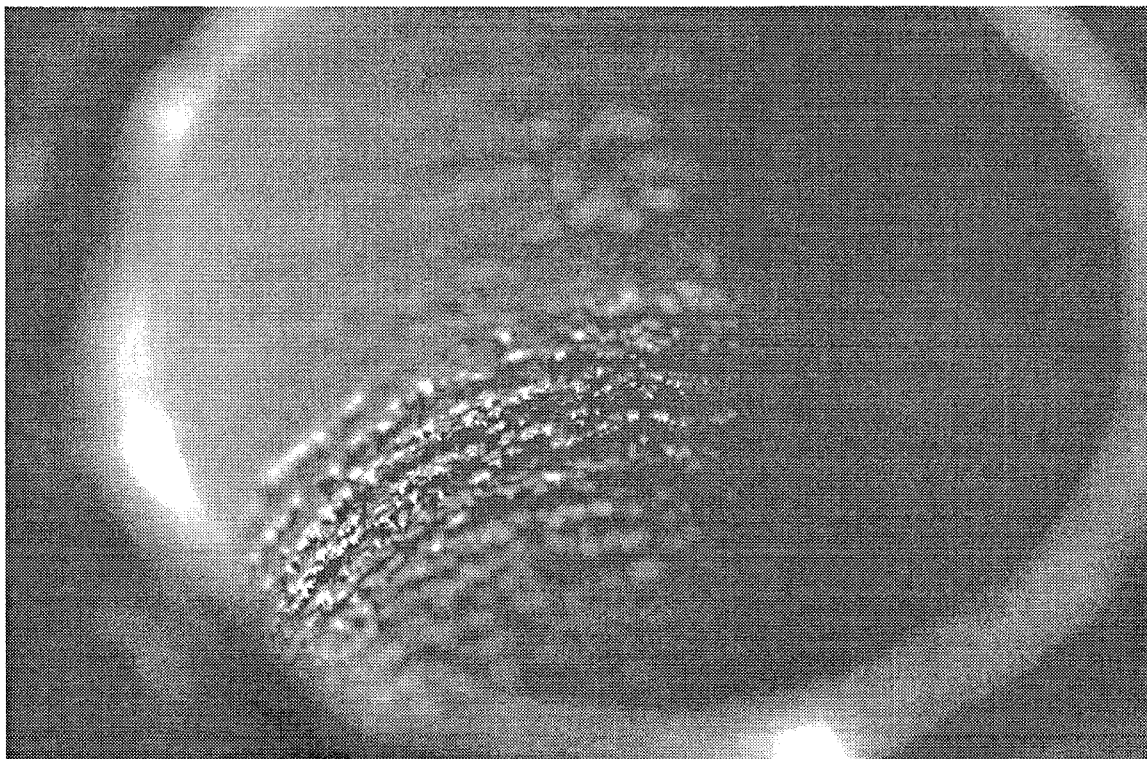


Figure 39 -- The temperature was still below the saturation temperature six inches into the reactor. The outlet temperature varied more than usual.

diamonds remained steady at 350 to 355°C (662 to 671°F) while the effluent temperature fluctuated widely. The cause of this fluctuation is not known. The reactor was shut down normally.

There were no salt deposits for the top 33 to 35 cm (13 to 14 inches) of the reactor. The last several inches of the top platelet and all of the bottom platelet down to the lower diamonds had a coating of salt 0.25 to 0.5 mm (10 to 20 mils) thick. Figure 40 shows the salt on the wall. The transition from clean wall to totally coated wall occurred in about 2.5 cm (1 inch). In the first few inches of salt, an opening was apparent in the deposit at each pore in the platelet. Further down the reactor, the location of each pore was visible from a dimple in the salt, but there was no apparent opening for the water. However, the pores must have been open during the test because the pressure drop across the platelet liner did not increase. The salt extended part way into the cold water injection region. Just upstream from the diamond-shaped cold water injection holes, the salt appeared to be a little thicker and not as uniform.

This test was also consistent with theory 6. Under these conditions the solid phase salt formed near the wall along most of the length of the reactor. No salt was deposited in the top of the reactor because the temperature was too low.



3/3/95 p2 other shot 2

Figure 40 -- The wall of the bottom reactor section was completely covered with a layer of salt.

Test With Flow Injector - Since several of the theories about salt deposition implicate the diamond-shaped holes, a simple injector was fabricated as an alternative. The injector configuration, with measured and calculated conditions, is shown in Figure 41. It consisted of a 3 mm OD (0.125 inch), 1.8 mm ID (0.070 inch) tube that extended about 13 mm (1/2 inch) below the top of the platelet. The hot water was fed through the Grayloc flange into the volume surrounding

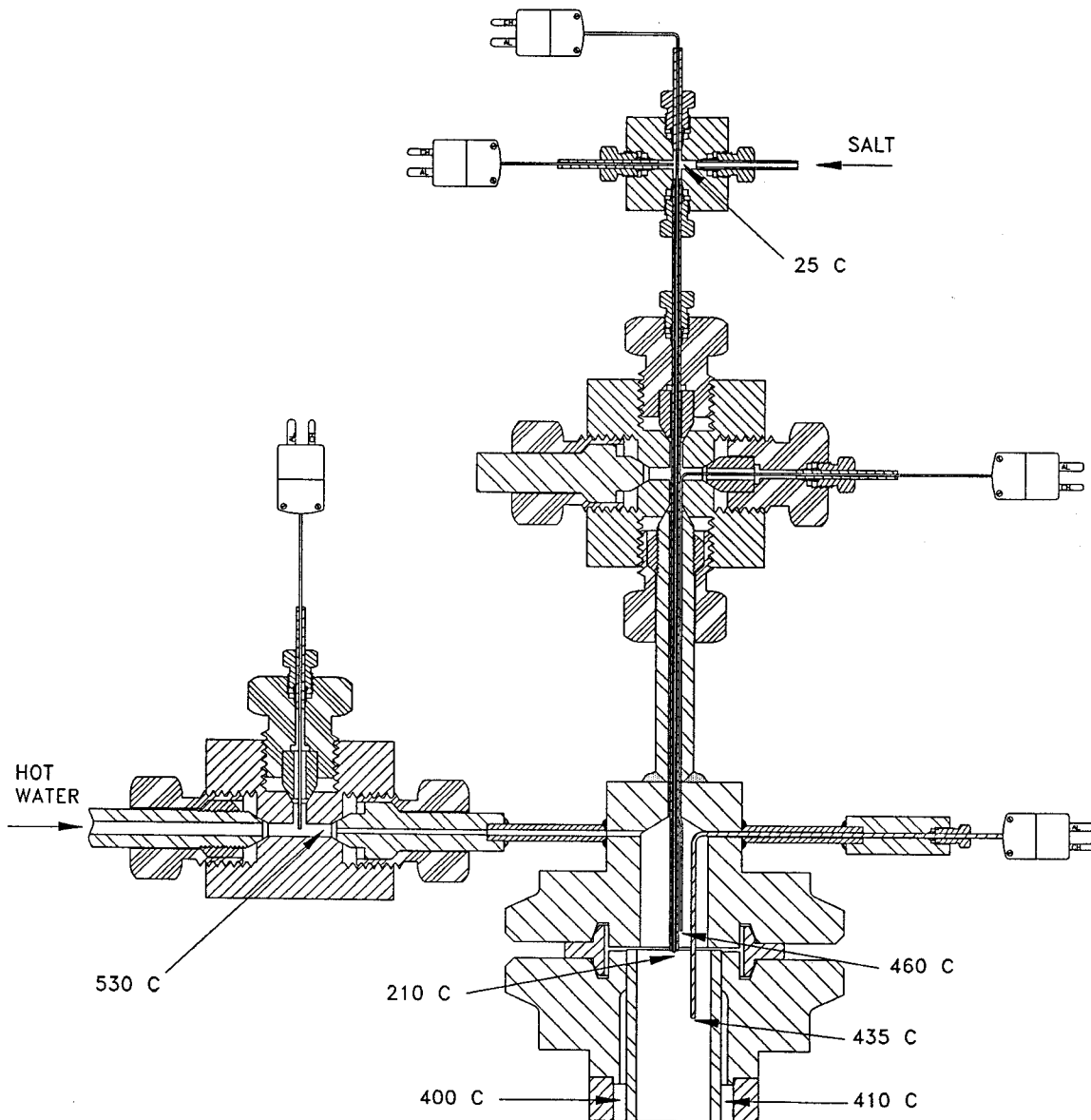


Figure 41 -- In the injector test, the salt solution entered the reactor through a 1.8 mm (70 mil) tube in the center. The heating water surrounded it.

the tube, so the hot water and waste stream entered the reactor as coaxial streams. Only one reactor section was used so there were no diamond-shaped holes at the top. Since the issue on this test was deposition in the top 13 cm (5 inches), the reduced reactor length was inconsequential.

Test conditions were:

Platelet 2: 6.7 grams per second at 410°C (770°F),
Hot water: 3.4 grams per second at 530°C (986°F),
Salt (3 wt %): 1.8 grams per second no heating,
Cold water: 10 grams per second at room temperature.

The flow rate of wall protection water was increased on this test resulting in an effectiveness ratio of 0.87. The 3 weight percent salt solution ran for 30 minutes.

Four thermocouples, shown in the schematic, recorded temperatures around the injector to monitor the streams before and after they began mixing. Data from these thermocouples are shown in Figure 42. One was an 0.8 mm (0.032 inch) thermocouple that extended through the inside of the injection tube and measured the temperature of the salt solution at the injector outlet. It reduced the flow area in the tube from 2.45 to 1.94 square millimeters (0.0038 to 0.003 square inches). The calculated velocity of the jet leaving the reactor was 100 cm per second (40 inches per second).

Although the salt solution was not heated before reaching the injector, it was heated to about 200°C (392°F) inside the injector by the surrounding heating water. Unfortunately, this thermocouple failed during the system startup shortly before the salt was introduced so the exact temperature during the test was not measured. The second thermocouple measured the temperature of the heating water before it entered the injector. The third thermocouple was in the hot water outside the tube a short distance above the mix area. Just as the salt solution was heated in the injector, the heating water was cooled about 65°C (117°F) before the streams mixed. The fourth thermocouple was about 2.5 cm (1 inch) below the injector after the two streams had begun to mix.

The conductivity looked much as it did during the first 30 minutes of the low effectiveness test discussed earlier, except a smaller fraction of the salt came through the reactor. There were large spikes from 5 to 10 times the mean value every couple minutes. This is shown in Figure 43.

The reactor was opened the next morning and inspected. There was a single salt deposit about 5 cm (2 inches) from the top of the reactor. It was about 5 cm (2 inches) long and extended around about 1/3 of the reactor wall. The thickness was about 2.5 mm (0.1 inch). The rest of the reactor surface was generally clean except for an occasional crystal of salt. This was a smaller deposit than was seen on other tests, but the test duration was less. Qualitatively it looked much the same. The conclusion was that the injector had little effect on the performance of the reactor. Tests with a better injector design are planned.

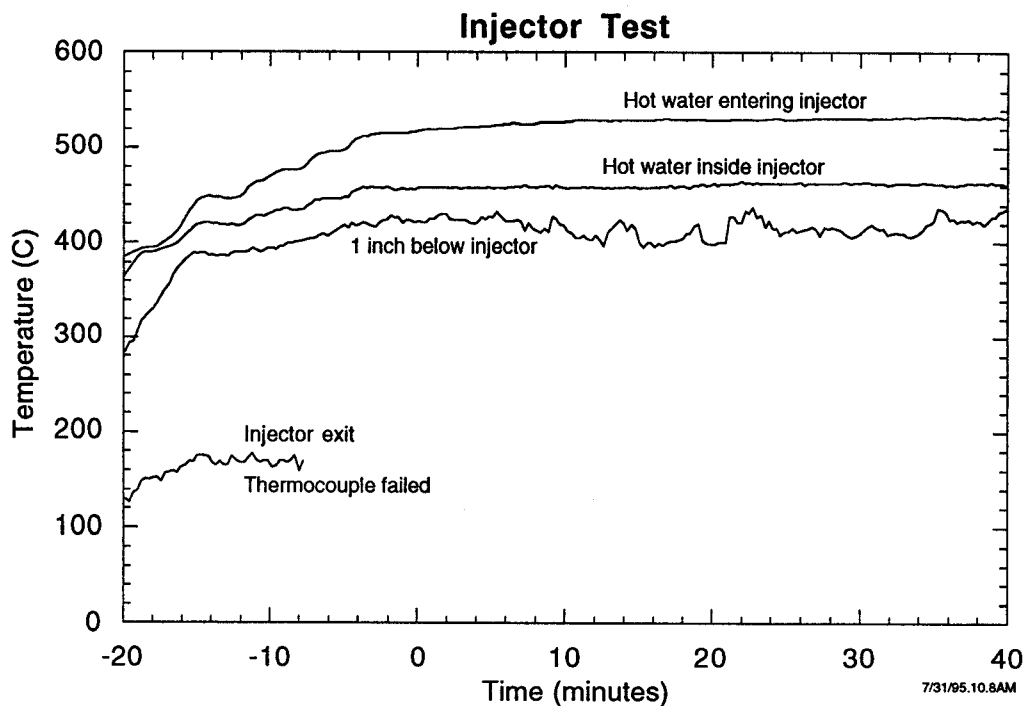


Figure 42 -- The temperature below the injector fluctuated, possibly due to salt deposition. Other temperatures remained steady

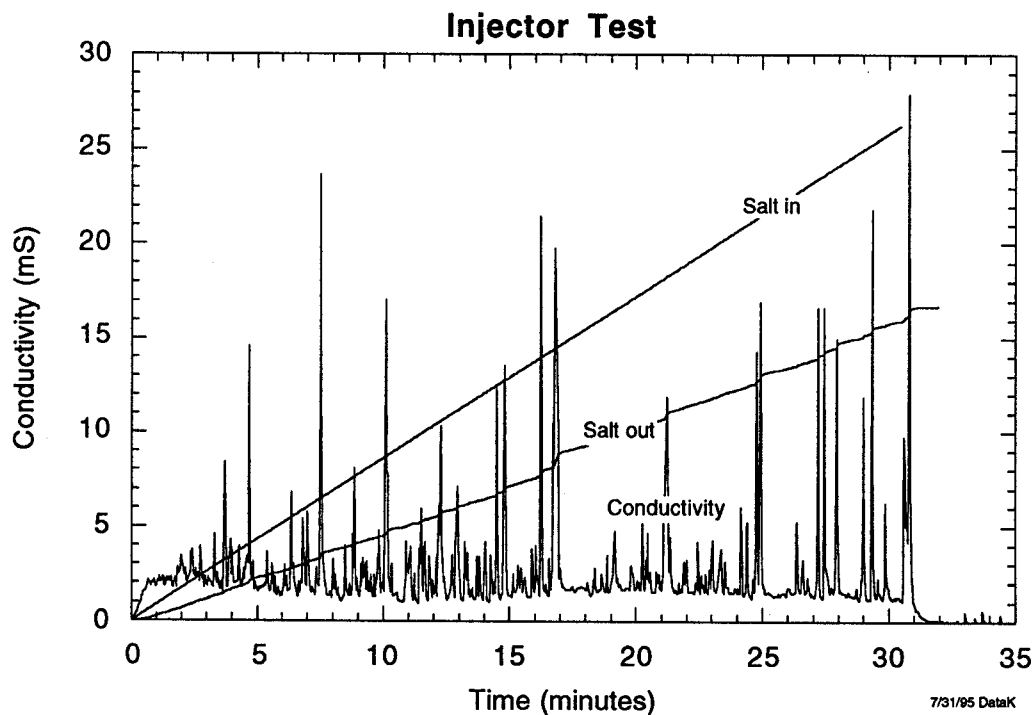


Figure 43 -- This test looks much like the first 30 minutes of the low effectiveness test discussed earlier (see Figure 21).

Test To Remove Salt Deposits - In all tests, the platelet reactor had reduced salt buildup but had not eliminated it. The next test was intended to determine if the salt could be easily and quickly removed by reducing the reactor temperature. The test was run without the injection heating water, in the same way as the tests discussed earlier. After the salt had accumulated, cold water was injected through the upper diamonds to rapidly lower the system temperature and dissolve the salt. Flow conditions were:

Platelet 1: 5.1 grams per second at 450°C (842°F),
 Platelet 2: 4.7 grams per second at 450°C (842°F),
 Salt (2.7 wt %): 0.71 grams per second at 100°C (212°F),
 Cooling water: 9.5 grams per second at room temperature,
 Rinse water (top diamonds): 3.3 grams per second cold.

Figure 44 shows measured and calculated conditions during the operational phase and Figure 45 shows them during the flush phase. The system was brought to temperature with water, then the waste stream was switched to salt. Salt was allowed to accumulate for 30 minutes, then the flow was switched back to water. After the conductivity returned to zero, cold rinse water was injected through the top diamonds. Immediately, a large pulse of salt came out followed by a second, smaller pulse less than 2 minutes later. The flow of salt then declined steadily to zero in about ten minutes. This is shown in Figure 46.

The differential pressure across the platelets dropped immediately after the cold water was introduced indicating loss of the seal between the two platelet sections. This was expected due to thermal contraction. The gasket relied on thermal expansion of the platelet at supercritical conditions to form the seal. When the cold water was turned off, the system returned to the normal operating temperature and the gasket resealed in less than two minutes.

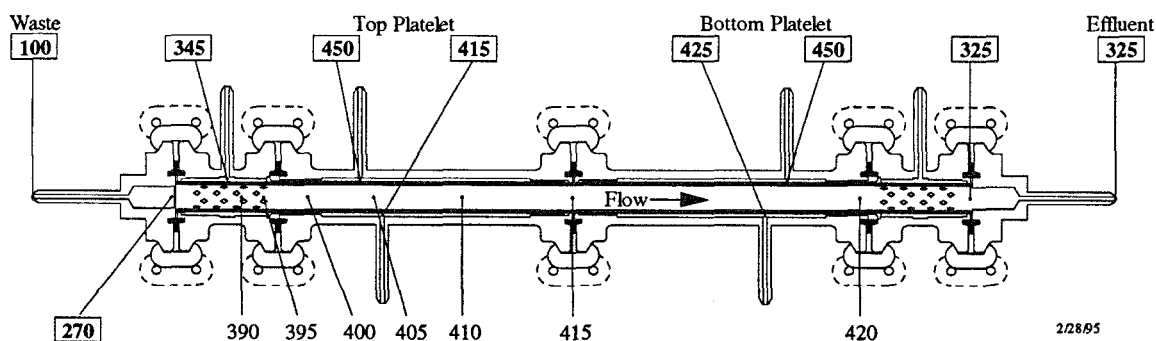


Figure 44 -- Temperature during accumulation phase of the salt removal test.

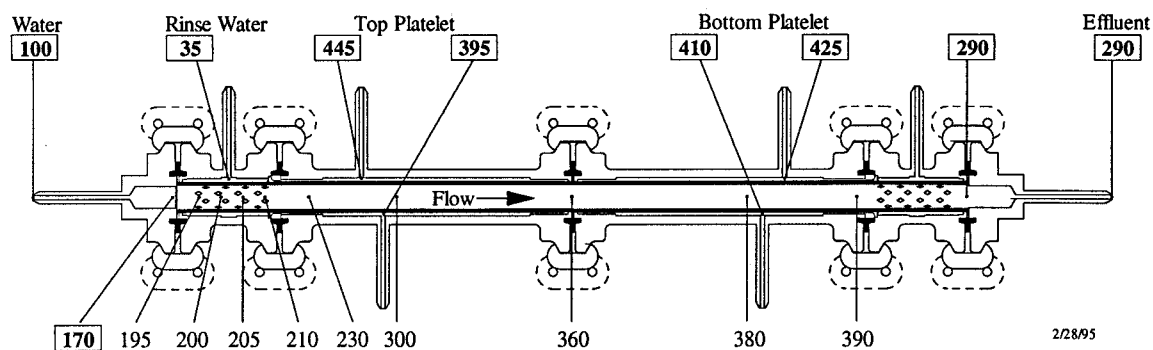


Figure 45 -- Temperature during removal phase of the salt removal test.

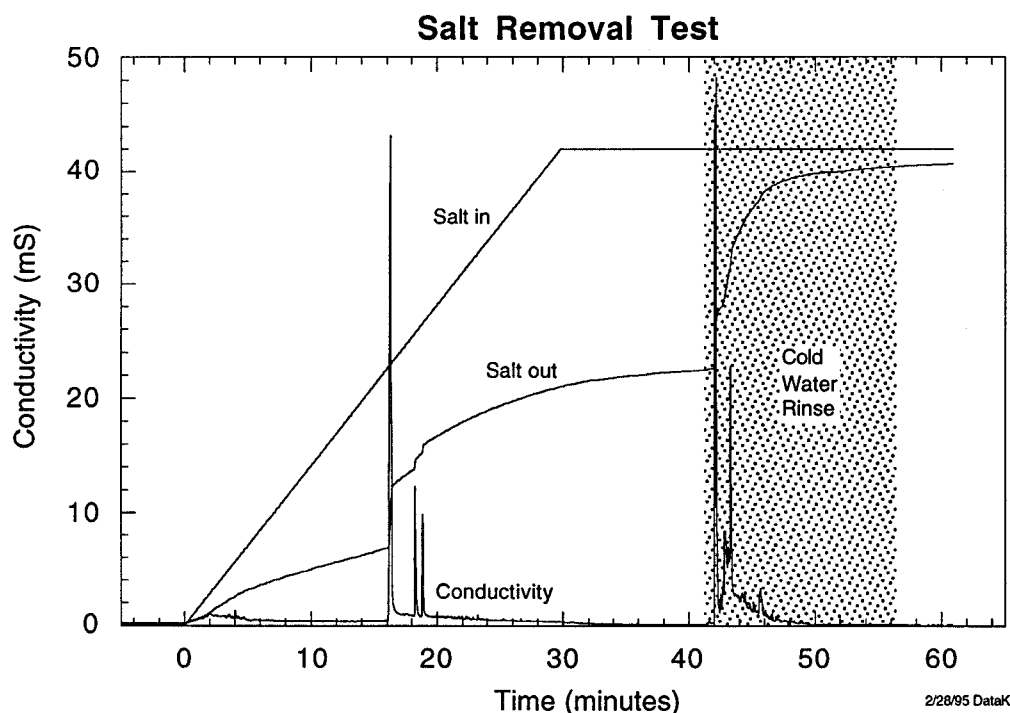


Figure 46 -- Salt accumulated for 30 minutes and was rinsed out in less than 10 minutes.

Three cycles of salt accumulation and flushing were completed. In the first two cycles, salt accumulated for 30 minutes. In the last cycle it accumulated for an hour. The results of all three cycles were the same. These tests suggest a favorable duty cycle for a prototype plant. Even if some deposition occurs, the system can be operated for several hours then rinsed in less than 10 minutes.

Test With Subcritical Transpiration Water - In theory, deposition could be eliminated by using subcritical transpiration water so any salt in the boundary layer would be soluble. There are potential drawbacks to such a system, including decreased destruction efficiency, increased energy usage, and possible concentration of acids near the wall leading to increased corrosion. Nevertheless, it was tested as an intriguing option. Successive iterations were run with the wall water at 350°C, 365°C, and 380°C (662°F, 689°F, and 716°F) for 30 minute intervals. The 365°C (689°F) condition was repeated. Test conditions were:

Platelet 1: 5.5 grams per second,
 Platelet 2: 5.0 grams per second,
 Hot water: 3.6 grams per second at 615°C (1139°F),
 Salt (1.5 wt %): 1.3 grams per second at room temperature,
 Cold water: 6.5 grams per second at room temperature.

Figure 47 shows the reactor conditions for the transpiration water at 350°C (662°F). With the cooler walls, there was some concern about the waste stream getting hot enough. A thermocouple about 2.5 cm (1 inch) below the top diamonds (15 cm or 6 inches into the reactor) measured 400°C (752°F) confirming that supercritical conditions were achieved. This temperature remained about the same even when the temperature of the transpiration water was increased.

With the transpiration water at 350°C (662°F), about 70 percent of the salt came through (see Figure 48). There was one spike in the conductivity after about 25 minutes. After 30 minutes, the waste stream was switched from salt to water until the effluent conductivity returned to zero. This should not have removed any deposits because the temperature did not decrease. The temperature of the transpiration water was increased to 365 and the salt was again switched on for 30 minutes. The conductivity, shown in Figure 49, indicated about 70 percent of the salt came through initially. However, after several minutes it increased to over 90 percent. There were no spikes.

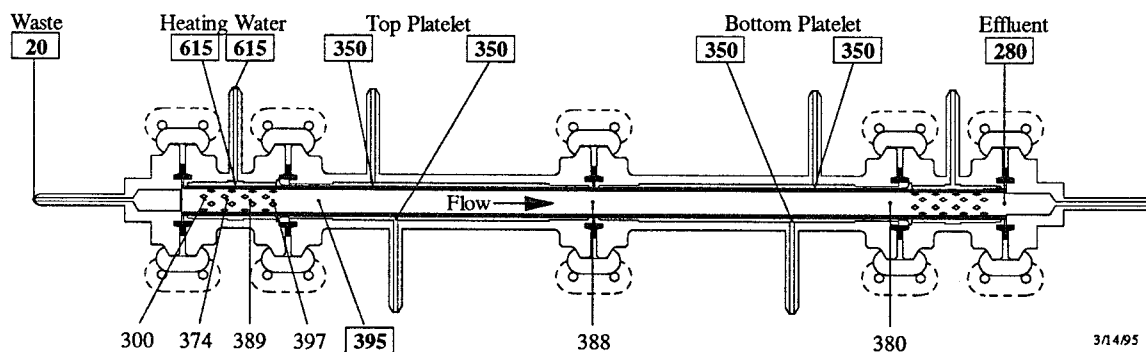


Figure 47 -- Temperatures with 350°C (662°F) Transpiration Water

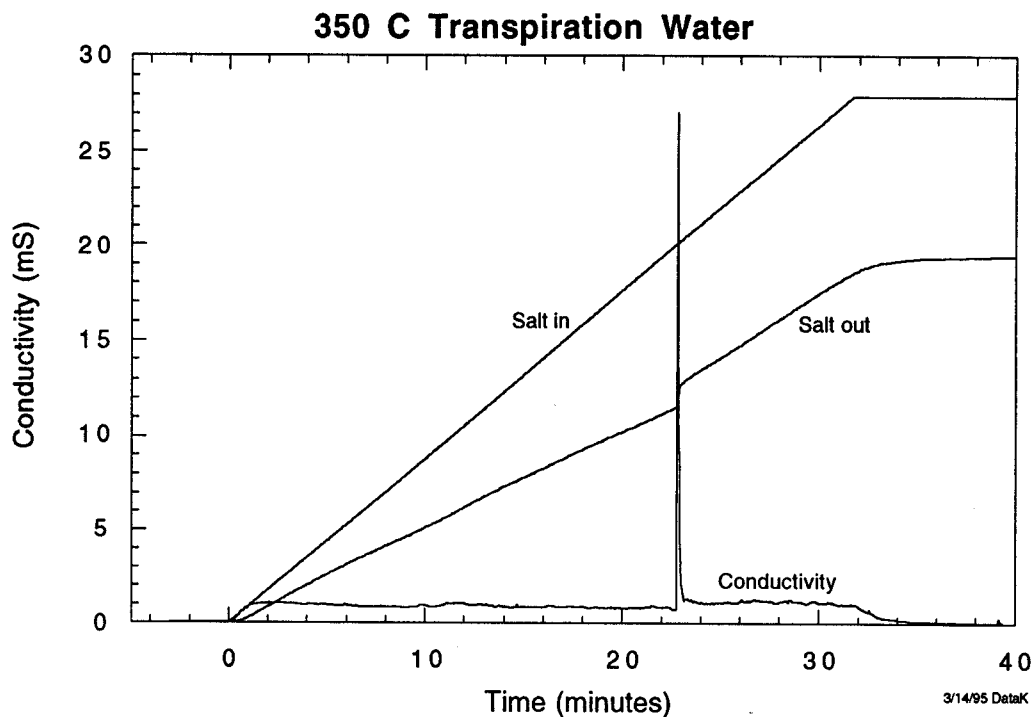


Figure 48 -- With 350°C (662°F) transpiration water, about 70 percent of the salt came through the reactor. Deposition still occurred in the heating zone.

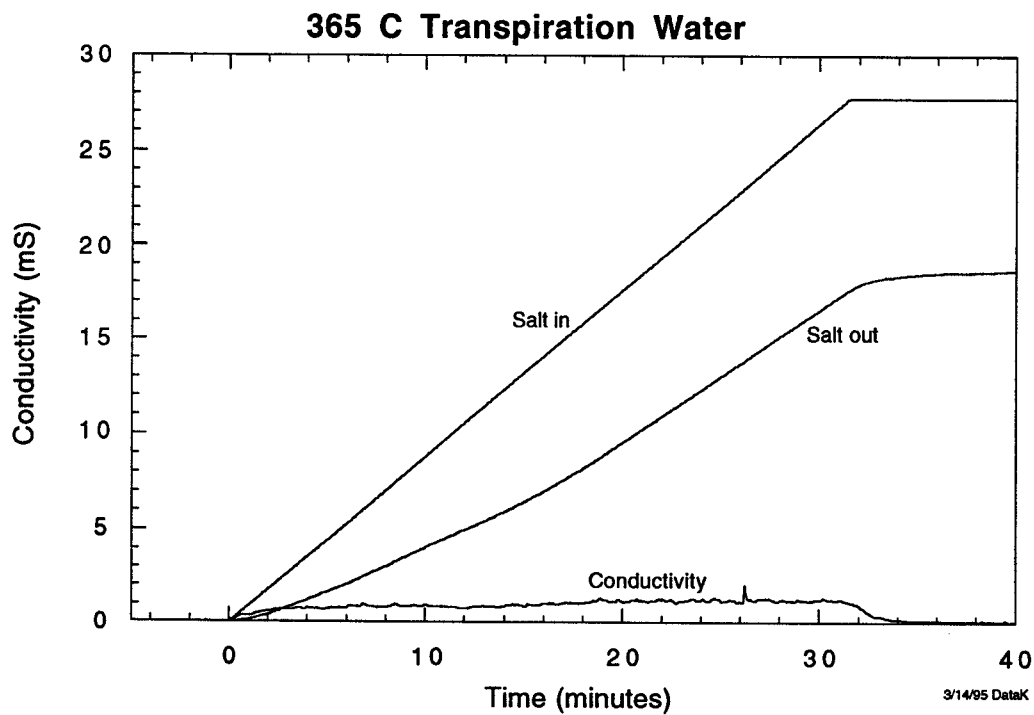


Figure 49 -- The performance improved after 16 minutes with 365°C (689°F) transpiration water. This performance could not be duplicated later.

The flow was again switched from salt to water and the temperature of the transpiration water was increased to 380°C (716°F). Again about 70 percent of the salt came through as shown in Figure 50. There were several spikes in the conductivity. Figure 51 shows that the temperature at the thermocouple below the diamonds rose from 400 to 425°C (752 to 797°F), then dropped to 380°C (716°F). All other temperatures remained stable. The thermocouple was possibly affected by salt depositing on it.

The transpiration water was cooled to 365°C (689°F) to try to repeat the earlier conditions. This time less than 1/2 of the salt came through and there were large temperature variations on the internal thermocouple. This may have been because salt deposited in the previous cycle at 380°C (716°F) was still in the reactor. The flow of hot water was stopped briefly to reduce the temperature and flush out the salt. A large increase in the conductivity indicated success. The test was repeated with wall water at 365°C (689°F). The results were essentially the same as the initial test at 350°C (662°F).

Observation the following morning revealed salt deposited along the top 10 cm (4 inches) of the reactor. The rest of the wall appeared clean other than a single streak down one side. This streak looked like a paint drip and appeared to have formed after the test from a drop of water running down the wall. The deposit near the top of the reactor implied that the transpiration water was not subcritical at that point. As with the non-uniform flow distribution described earlier, this resulted from conductive heat transfer through the structure. The transpiration water at the top of the reactor was heated while it flowed through the platelet. No good explanation has been given for the relatively good performance at 365°C (689°F) the first time.

Tests With Organic Wastes - Two tests were conducted with red dye for a final validation of the platelet reactor concept for the Army. The chemical formula for red dye was reported to be 80 percent $\text{Na}_2(\text{C}_{18}\text{H}_{13}\text{N}_3\text{O}_8\text{S}_2)$ and 20 percent $\text{Na}_3(\text{C}_{16}\text{H}_9\text{N}_4\text{O}_9\text{S}_2)$. The dye was initially mixed with water in a 10 weight percent solution. Although, it appeared to be in solution, a thick, orange sludge formed in the bottom of the quiescent storage container before the test. It could not be pumped with the equipment in the EER so it was filtered. This resulted in a solution of 5.15 weight percent, determined by dehydrating a sample. The pilot plant should not have a similar pumping problem because it will use a slurry pump and the supply tank will be continuously stirred.

The goals of the first test were: 1) to demonstrate that, in terms of deposition, a salt-containing waste was equivalent to a salt-forming waste, thereby validating tests with sodium sulfate salt and 2) to identify any unexpected issues associated with processing dye. The test used the normal reactor configuration and operating procedure. Since the reactor did not have sufficient temperature or residence time for complete destruction of the dye, demonstration of destruction efficiency was not a goal of the test.

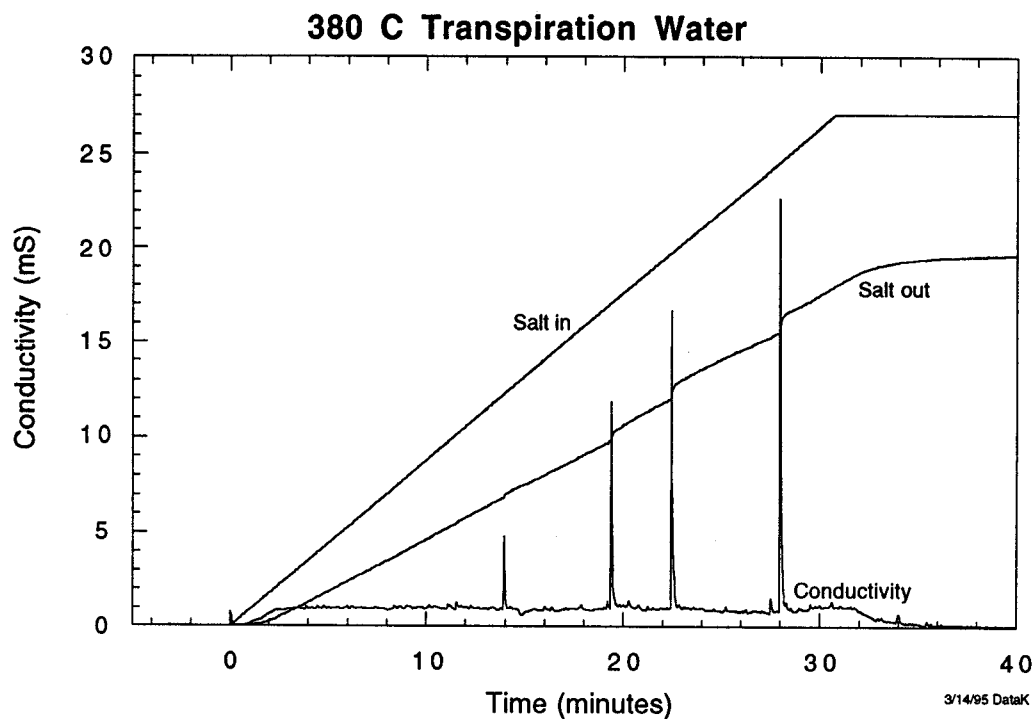


Figure 50 -- Performance was similar with 380°C (716°F) transpiration water, although there were some spikes.

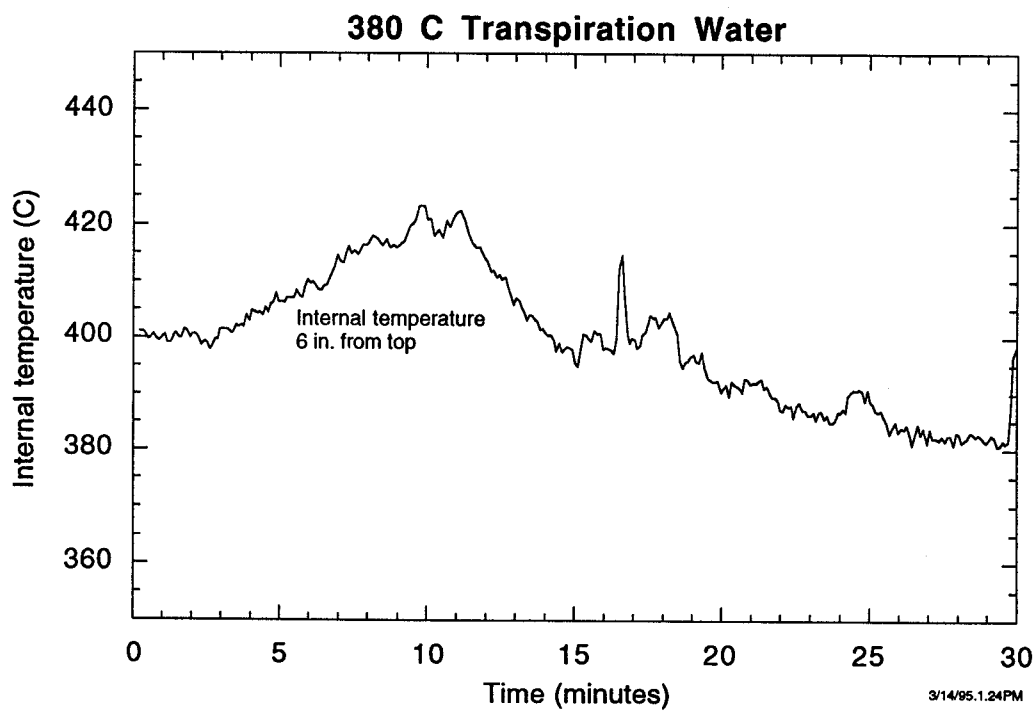


Figure 51 -- The thermocouple inside the reactor showed large temperature fluctuations with the 380°C (716°F) transpiration water.

Hydrogen peroxide was the oxidizer. It was mixed with the heating water at a concentration of 10 weight percent and injected through the diamond-shaped injection holes. The concentration and flow rates were chosen to provide 20 percent excess oxidizer with 10 weight percent dye. With the reduced dye concentration, there was over 100 percent excess oxidizer.

Test conditions were as follows:

Waste: 0.9 grams per second at 310°C (590°F) at top flange,
Hot water (with H₂O₂): 3.5 grams per second at 640°C (1184°F),
Platelet 1: 6.0 grams per second at 445°C (833°F),
Platelet 2: 3.5 grams per second at 440°C (824°F),
Cold water: 16 grams per second (estimated) at room temperature

Figure 52 shows the operating conditions. The temperature 2.5 cm (1 inch) below the diamonds was 440°C (824°F). Limited capacity of the effluent cooling system prevented operating at higher temperature.

The hydrogen peroxide ran continuously throughout the test, even during the heat up stage. Two pumps were used for the dye -- one with a flow of 0.25 grams per second and one with a flow of 0.65 grams per second. Figure 53 shows the flow rate of the dye. Once at temperature, the low flow pump was switched from water to dye while the other continued to pump water. The mixed stream had 1.4 weight percent dye concentration. After 15 minutes, the low flow pump was switched back to water and the high flow pump was switched to dye resulting in 3.7 weight percent dye in the feed. After 23 minutes, both pumps were switched to dye so the dye concentration was 5.15 weight percent. Twelve minutes later, both pumps were switched back to water to flush the dye and acids from the system before shutting down. This did not remove solid deposits in the reactor. The flow of dye can be clearly correlated with the pH of the effluent shown in Figure 54.

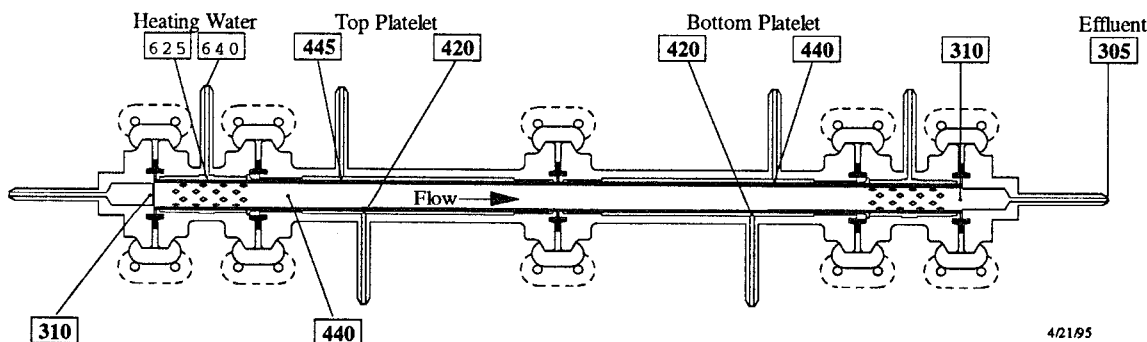


Figure 52 -- Temperatures for first red dye test.

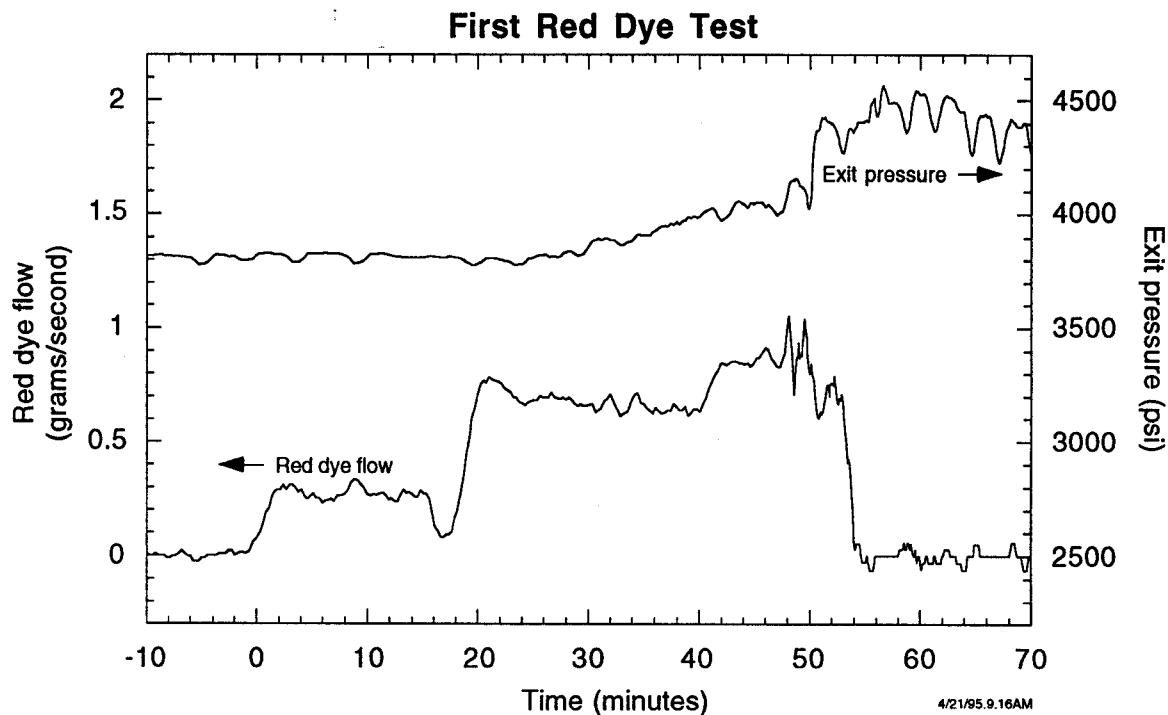


Figure 53 -- Dye concentration was increased in three steps. The system pressure increased when the downstream filter plugged with insoluble metal oxides.

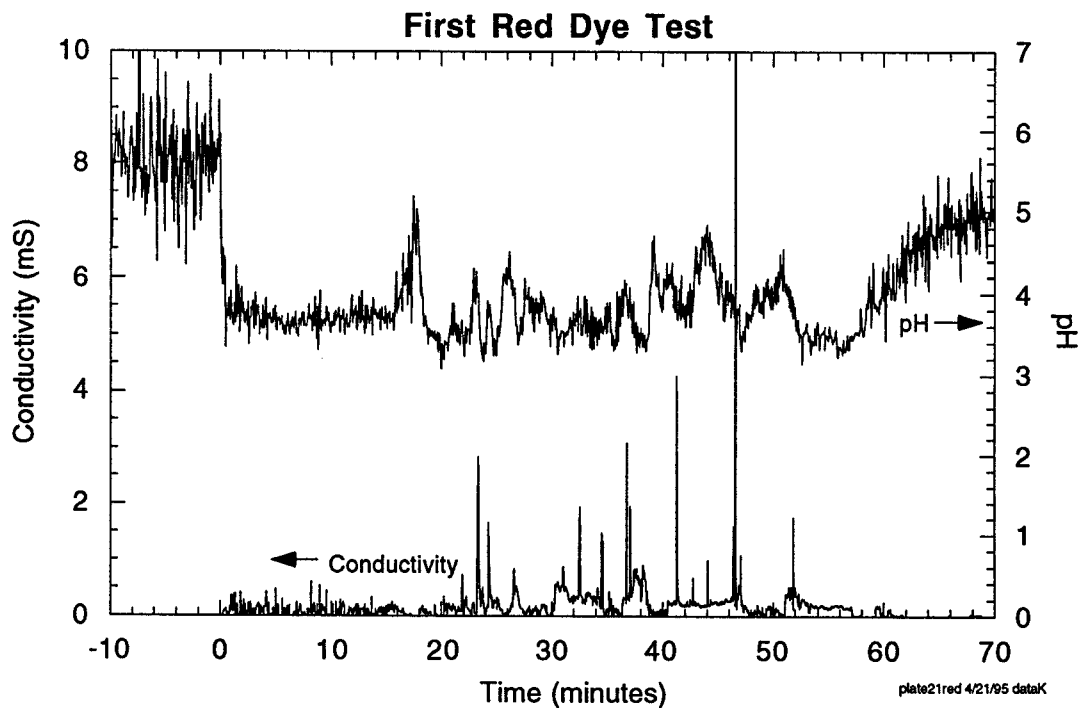


Figure 54 -- The pH and conductivity data indicate salts and acids in the effluent.

A change in the supply manifold on this test to accommodate two feed pumps resulted in a significant increase in time lag, mentioned earlier, between when the waste entered the supply line and when it actually reached the reactor. Furthermore, the delay was different for the two pumps. The smaller pump had a delay of almost ten minutes, while the larger pump was about five minutes. The time scale on Figure 54 has been shifted about 10 minutes corresponding to the small pump.

Observations and Conclusions:

1) Visually, there was no red tint in the effluent. However, TOC measurements on effluent samples indicate that less than 30 percent of the organic was oxidized. This means that the dye was broken into intermediate species, but was not fully oxidized. This was consistent with the temperature and residence time.

2) Despite the incomplete oxidation, there was sufficient energy release to raise the reactor temperature about 50°C (90°F). Figure 55 shows the internal temperature measured just below the heating section. Accounting for the lag time in the supply manifold, the steps in temperature correspond with increases in dye concentration. A caveat to this observation is that variations in this thermocouple reading have been observed on other tests that had salt with no organic waste due simply to salt deposition.

3) Salt deposition was observed in the hot water injection area comparable in magnitude and location to previous tests. Figures 56 and 57 show the salt. The salt was gray, not white, indicating the presence of impurities. The location of the deposits near the top of the reactor indicates that the salt formed early in the oxidation process. This was validated using a salt solution instead of an organic for the feed in the earlier deposition studies.

4) When the dye flow was increased from 0.25 to 0.65 grams per second, the total system pressure, which started at 265.5 bar (3850 psi), began to rise gradually. When it reached 303.4 bar (4400 psi) the test was stopped. The pressure stopped climbing when the flow was switched back to water, but it did not return to the previous level. The pressure increase was not related to salt deposition because the source was downstream of the reactor. This is evident from the reactor exit pressure shown in Figure 53. The pressure rise led to a decrease in flow rates as shown in Figure 58.

There is a filter in the effluent line just upstream of the pressure regulator valve. After the test, a large amount of dark gray material was found on the filter, which apparently caused the increase in pressure. Analysis showed that the material consisted of insoluble metal oxides from corrosion of the stainless steel platelet. There was no organic content. A small amount of these oxides also appeared as sediment in the effluent samples.

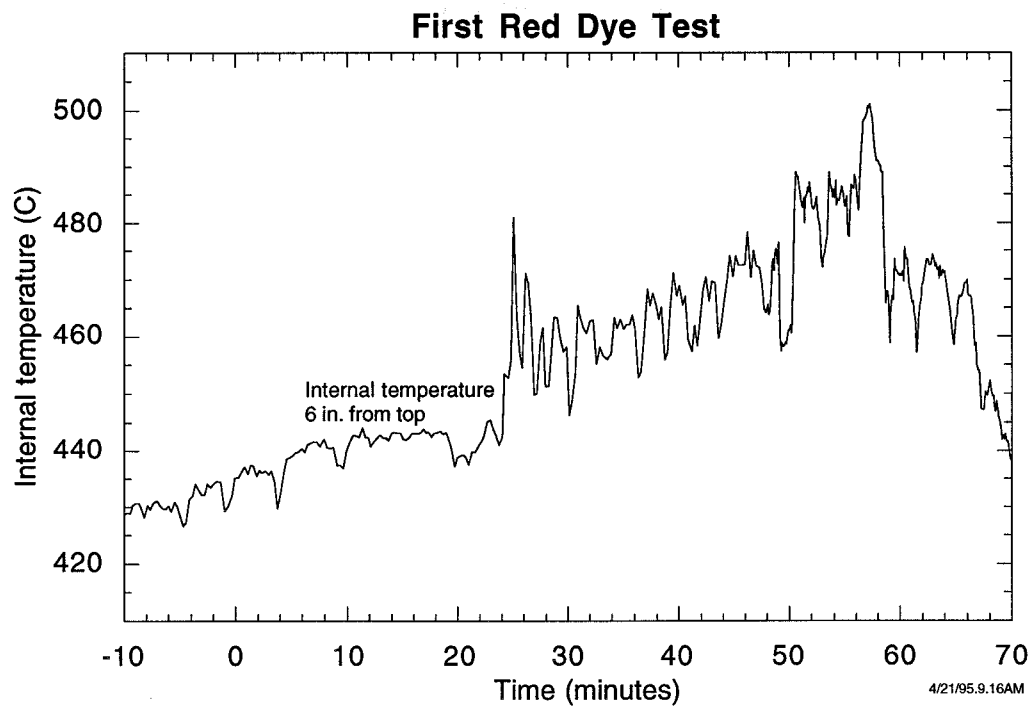
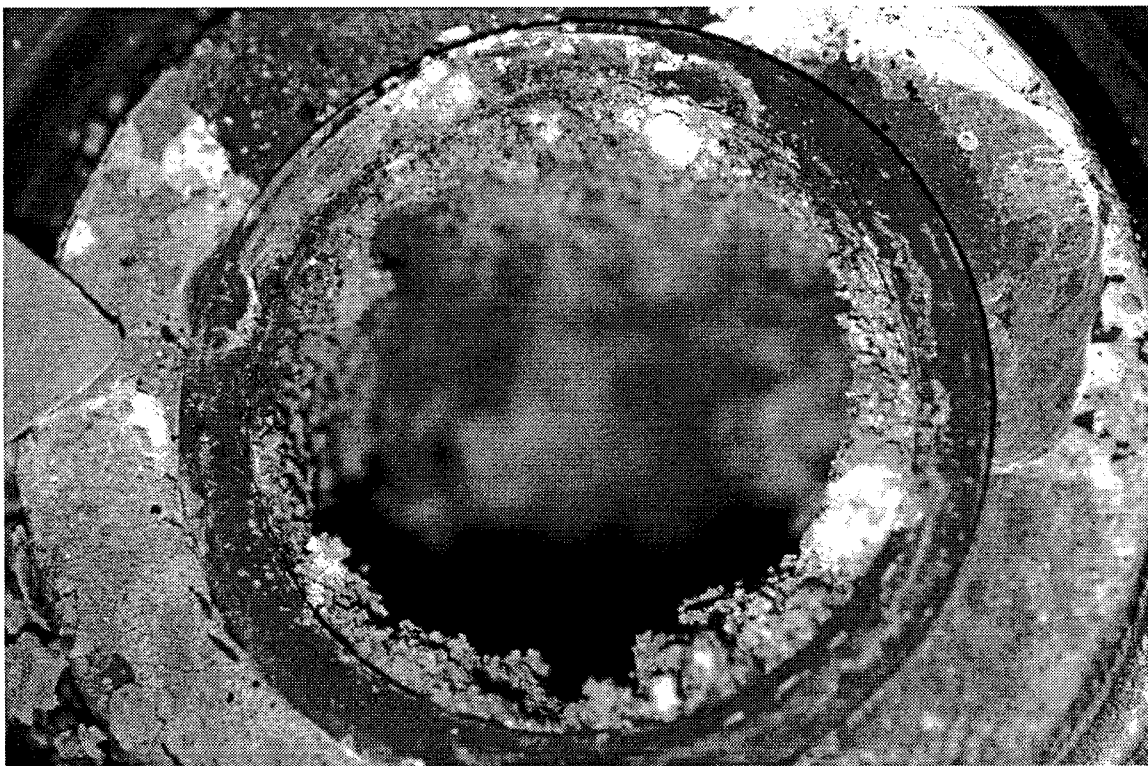
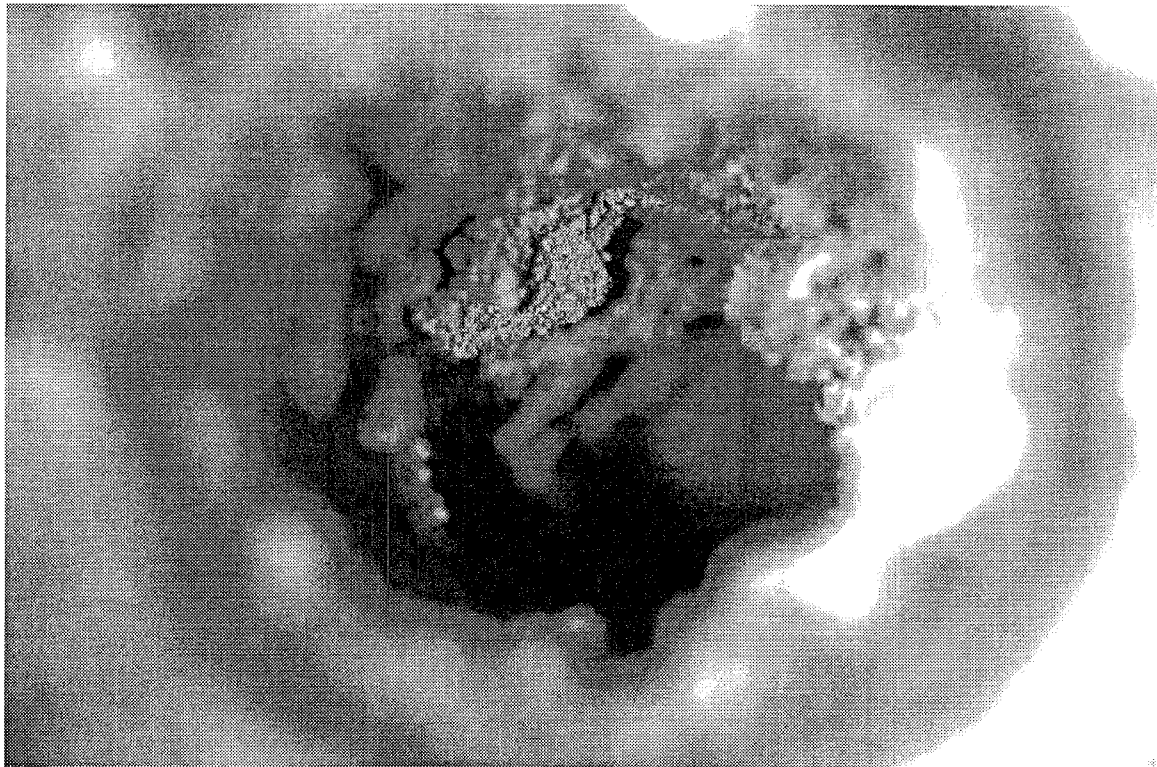


Figure 55 -- The increase in the internal reactor temperature appears to be from the exothermic reaction of the dye.



4/25/95 P1 top#2

Figure 56 -- Salt deposit in the heating zone looking from the top of the reactor.



4/25/95 P1top#4

Figure 57 -- Same view as Figure 56, but focused a few inches into the reactor.

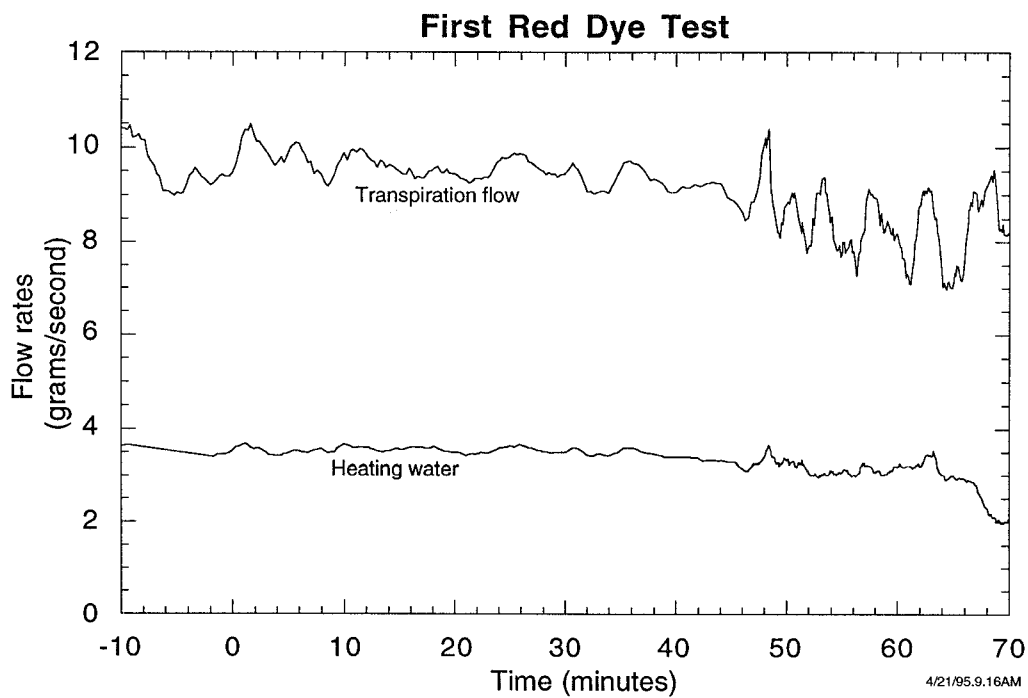


Figure 58 -- Flow rates decreased as the pressure increased.

5) Pressure measurements showed plugging near the reactor inlet. This is shown in Figure 59. The differential pressure jumped quickly to 31 bar (450 psi) about five minutes after the flow of dye was increased to 0.65 grams per second. It then fluctuated rapidly between 0 and 34.5 bar (0 and 500 psi). When the flow was switched back to water, the differential pressure returned to zero. There were several large spikes in the differential pressure that somewhat coincided with spikes in the conductivity shown in Figure 54. However, the conductivity spikes were small compared to other tests while the pressure spikes were huge. There was no increase in the platelet wall differential pressures. The small spikes in conductivity and the lack of unusually large salt deposits after the test were inconsistent with the high pressure. This suggested that the plugging may have occurred in the small holes in the diffuser plate and not in the reactor. The temperature just above the plate was 310°C (590°F) which is well below the saturation temperature. However, the temperature immediately below the plate was hotter than usual because the higher temperature of the heating water -- 625°C (1157°F) -- and the exothermic oxidation of the dye. Consequently, the fluid may have exceeded the saturation temperature and precipitation of solid phase salt may have occurred in the diffuser.

6) The concentration of dissolved metals in the effluent was low. Corrosion of the Inconel reactor housing or the inlet and outlet tubing would produce soluble chromium and nickel in the effluent.

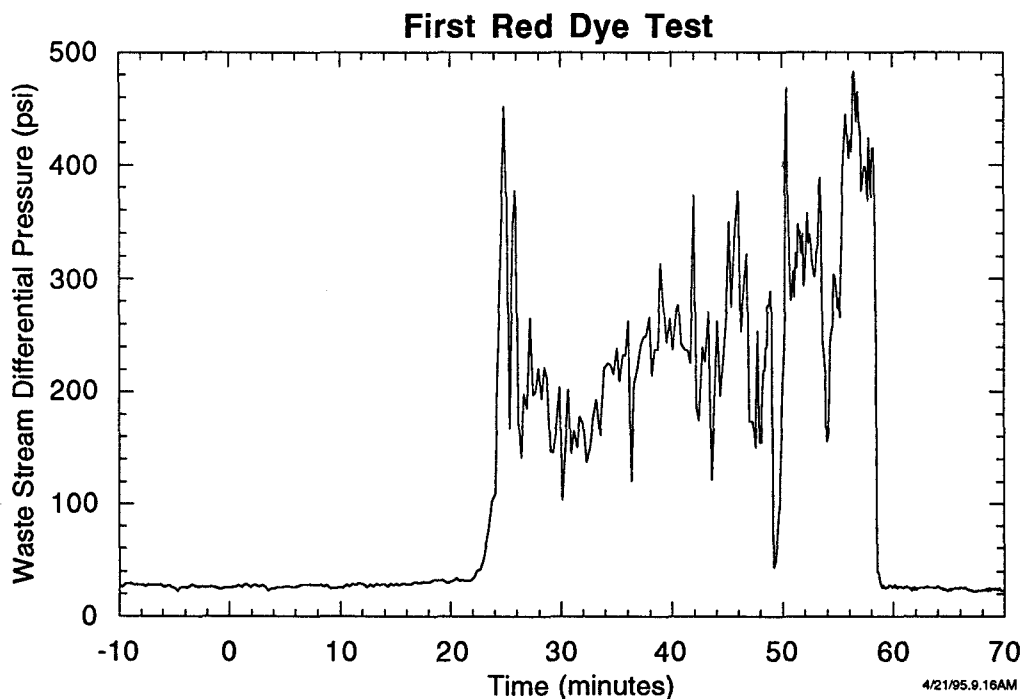


Figure 59 -- The differential pressure measurement shows severe plugging at the reactor inlet, possibly in the pores of the diffuser.

On the second test with red dye, the intent was to demonstrate that the transpiring wall did not affect destruction efficiency. Two aspects of destruction are important. The first is destruction of the dye by converting it to another organic compound. The second is complete oxidation of all organic compounds. Destruction of the dye was determined from UV-visible absorption which detects the red color. TOC analysis was used to determine the completeness of the oxidation process. To achieve a higher temperature and residence time, the transpiration flow through the platelet wall was reduced to about 1/2 the normal flow and its temperature was increased. This resulted in a calculated residence time for the dye of 8 to 9 seconds at 500°C to 520°C (932°F to 968°F), but it reduced the effectiveness ratio to about 0.70. The concentration of the dye was 5.15 weight percent. Five weight percent hydrogen peroxide mixed with the heating water provided 45 percent excess oxygen.

The simple injector described earlier was used except both reactor sections were included. Consequently the diamond-shaped holes were present at the top of the reactor but there was no flow through them. Figure 60 shows test conditions. The waste stream was not heated before entering the injector, but reached 150°C (302°F) in the injector due to the surrounding heating water. The temperature about 2.5 cm (1 inch) below the injector was 500°C (932°F). The temperature of the wall protection water was higher than on any other test. This was possible because of the reduced flow rate, but it also resulted in larger temperature gradients around the circumference of the plenum volume. The difference in temperature between the inlet side and the opposite side was a 135°C (243°F) in the top section and 155°C (279°F) in the lower section. Test conditions were:

- Waste: 0.75 grams per second at 150°C (302°F) at end of injector,
- Hot water (with H₂O₂): 3.4 grams per second at 630°C (1166°F),
- Platelet 1: 3 grams per second at 640°C (1184°F),
- Platelet 2: 2.5 grams per second at 605°C (1121°F),
- Cold water: 19 grams per second at room temperature.

Water was used in the heat-up stage for both the waste and the heating water. Once the system was at temperature, the two streams were switched to the dye and hydrogen peroxide solutions, respectively. Dye ran for a little over 33 minutes. As before, the test duration was limited by pressure buildup in the system from clogging of the filter in the effluent line (see Figure 61). Clogging began immediately after the dye was introduced. The pressure climbed steadily from 262 to 310 bar (3800 to 4500 psi) when the flow of dye was stopped. There was no increase in differential pressures as was seen on the previous red dye test, presumably because there was no diffuser.

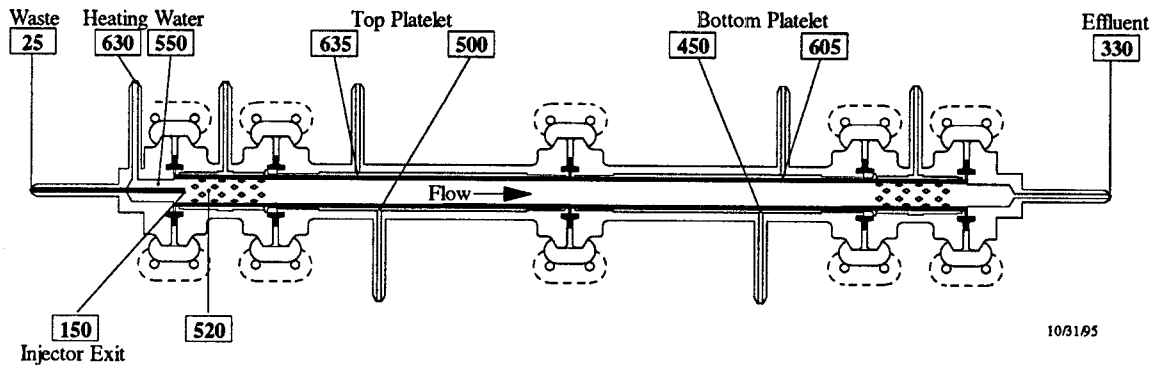


Figure 60 -- Temperatures for second red dye test.

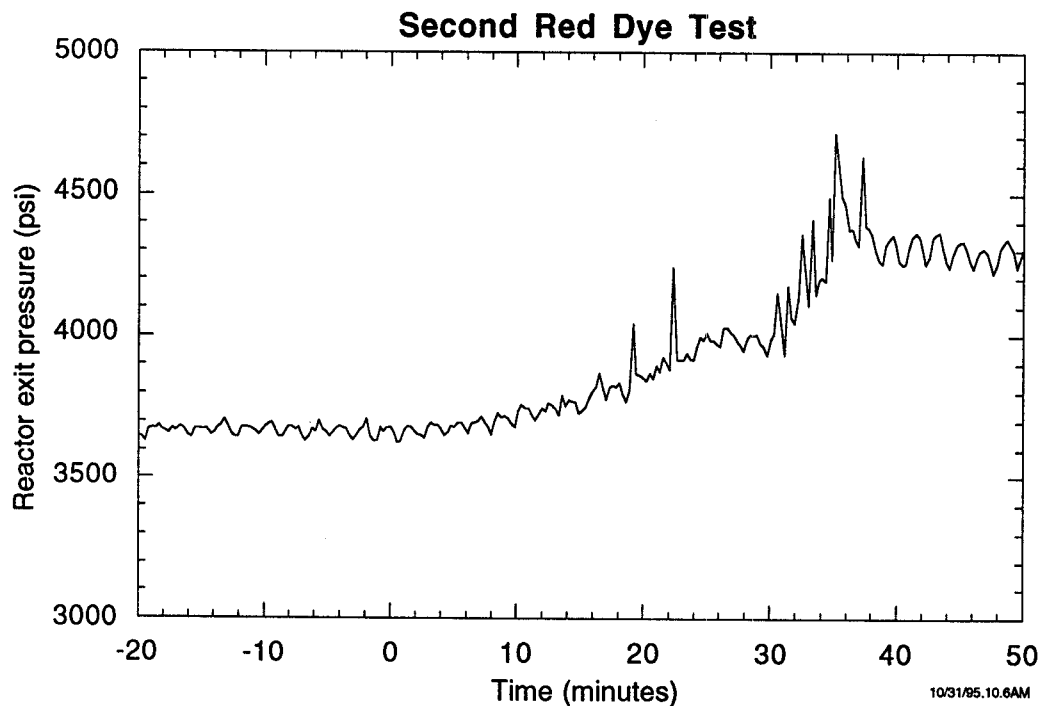


Figure 61 -- The system pressure again increased due to plugging of the down stream filter with insoluble metal oxides.

As the pressure increased, the flow rate of dye and transpiration water decreased. This complicated interpretation of the test data. Figure 62 shows flow rates.

The TOC analyzer was placed on-line for this test to provide almost real-time feedback. In this mode, small samples of the effluent were automatically collected and analyzed as the experiment progressed. Alternate samples were used to measure total carbon and inorganic carbon with the difference being TOC. The combined analysis took about five minutes. Due to the short duration of the test, the TOC level did not stabilize. However, the measured TOC shown in Figure 63 was between 75 and 100 ppm. The calculated TOC of the waste was 900 to 950 ppm resulting in destruction efficiency around 90 percent. The absorption spectra of the effluent showed no detectable red color.

Post test visual observation of the reactor showed a dense salt deposit (compared to previous tests) beginning 6.4 cm (2.5 inches) from the top of the platelet. The deposit was about 2.5 cm (1 inch) long and consisted of needle-like crystals pointed radially inward. Deposits on all other tests had a much more amorphous structure. The salt was gray in color. Above and below the salt, the platelet wall was black with a slightly raised texture. It was not clear if there was any salt on the wall or if this was entirely from corrosion. The salt was washed out of the reactor a few days later producing a murky gray effluent. After the washout, several cubic centimeters of metal oxide were removed from the volume just below the reactor where the diameter steps down to 5 mm (3/16 inch). The raised texture on the surface of the platelet disappeared but thin deposits of oxides remained, especially in the region where the salt deposit had been.

This test led to the following conclusions:

- 1) The dye was 100 percent destroyed. Total organic destruction was at least 90 percent. These results are consistent with data from Rice (reference 10) for the temperature and time, demonstrating that the transpiring wall was not detrimental to destruction of the waste. More accurate estimates of destruction efficiency are difficult because the system did not have time to stabilize, the flow rates varied during the test, and the EER is not configured for precise measurements of this kind.
- 2) Substantial corrosion of the platelet occurred. It is hard to determine how relevant this is because the transpiration flow was reduced and because the platelet in the test reactor is made of stainless steel. In the prototype plant reactor, it will be made of Inconel 600 with a platinum face plate and it will operate with an estimated effectiveness ratio of 0.99 compared with 0.70 on this test.
- 3) Salt deposition was more concentrated (smaller region and higher density) than on previous tests. This may correlate with more rapid heating due to the higher temperatures of both the transpiration water and the heating water.
- 4) Metal oxides that were deposited with the salt did not wash away when the salt was removed, but remained on the wall.

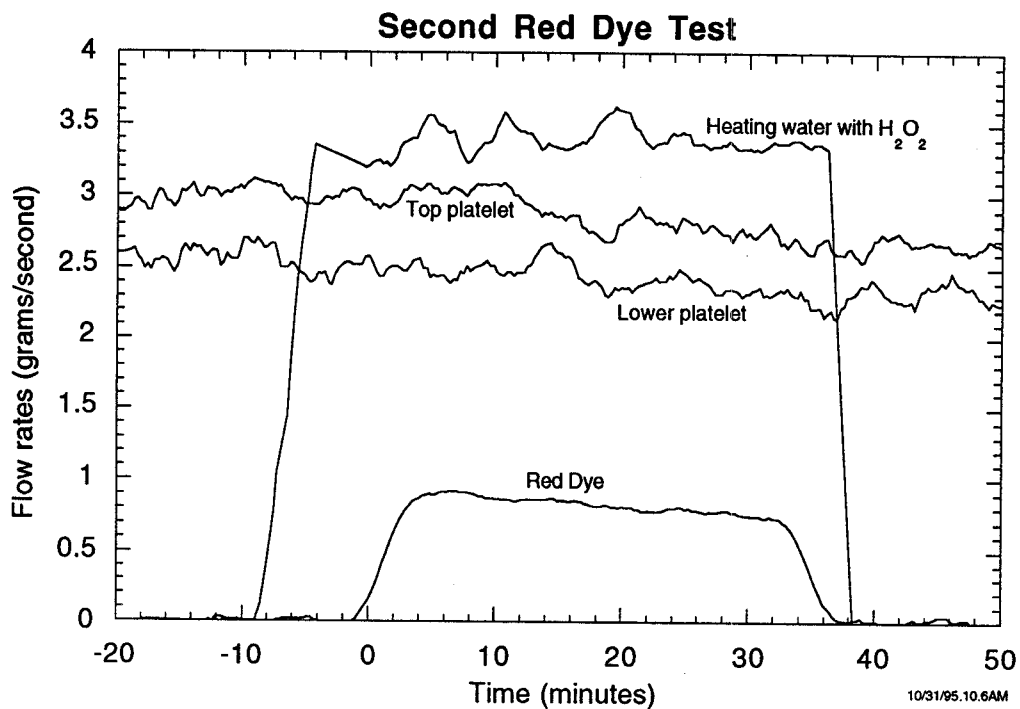


Figure 62 -- Flow rates decreased as the pressure increased making it difficult to calculate the destruction efficiency

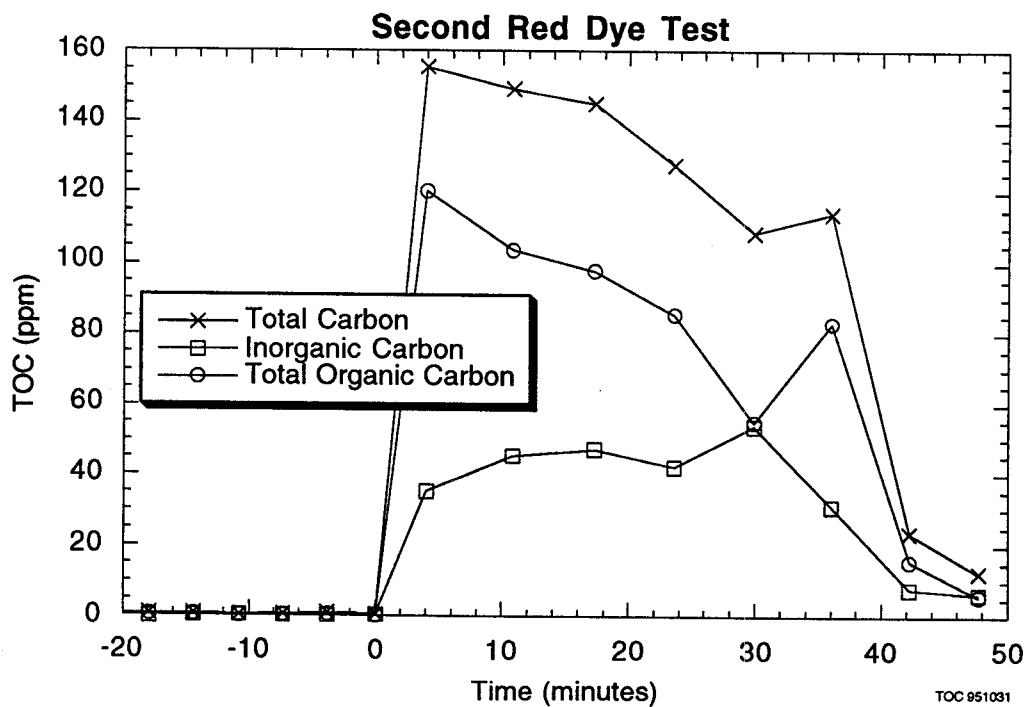


Figure 63 -- The effluent contained between 75 and 100 ppm Total Organic Carbon so the destruction efficiency was about 90 percent.

Implications for the Prototype Plant

The most significant conclusion from these tests is that the transpiring wall reactor dramatically reduces the deposition of sticky salts thereby allowing extended operation. Although these tests were limited to about three hours duration, no test was terminated due to salt build up and the expected operational duration is longer. Two phenomena observed on these tests appeared to contribute to the extended operational capability.

First, the transpiring wall nearly eliminates salt deposition on most of the reactor surface. If salt deposition could be eliminated in the first few inches of the reactor, it could run almost indefinitely. The prototype plant will have several advantages in this regard. With the larger diameter, it will have the geometrical advantages of less wall surface area relative to flow area and greater distance between most of the reactor volume and the wall. Furthermore, the wastes will be supplied through an injector that should cause the solid phase salt to form near the center of the reactor and there will be no diamond-shaped injection holes to disturb the boundary layer.

Second, even though some deposition occurred, the size of the deposits seemed to be self limiting. When they became too large, they broke away from the wall. Presumably the strength of a salt deposit and its ability to remain attached to the wall are functions of its aspect ratio. The transpiring wall limited the deposits to a short section of the wall, which apparently caused them to break away more easily. This effect should also be more pronounced with a larger diameter reactor.

The tests with the steepest temperature gradients in the heating zone were observed to have the shortest deposits. Since shorter deposits appear to break loose more readily, this suggests that a design goal should be to heat the waste rapidly once it enters the reactor.

Despite improvements from the transpiring wall, salt deposition was not eliminated on any of the tests. Even with the advantages of the injector and the larger diameter mentioned above, the prototype plant should be designed to accommodate some salt buildup. Salt deposits were removed in less than 10 minutes by reducing the reactor temperature to less 350°C (662°F). In that condition, the salt was quickly dissolved and washed through the system. Temperature was reduced either by adding cold water or shutting off the flow of heating water. No negative effects from the thermal shock were observed on either the platelets or the Grayloc flanges. The prototype plant design should provide for periodic low temperature flushing.

This recommendation applies to soluble salts only. Insoluble deposits, specifically metal oxides, were not washed away, even when they were mixed with the salts. Consequently, deposits of insoluble salts or oxides must be avoided. This may be a problem if the waste contains calcium which forms insoluble salts. The prototype plant should not have trouble with insoluble metal

oxides like those observed on the red dye test for three reasons. First, the Inconel platelet with platinum liner will be much more resistive to corrosion than the stainless steel platelet. Second, the effectiveness ratio of the transpiring wall will be much higher, which should help inhibit corrosion. Third, the nickel, chromium and molybdenum oxides that form from Inconel are soluble at much higher concentrations than the iron oxides from the stainless steel.

The corrosion protection aspect of the transpiring wall reactor has not been studied. However, corrosion tests are planned as the next phase of testing. The tests with red dye demonstrated that the stainless steel platelet is not appropriate for corrosion tests. Consequently, Aerojet has fabricated a new reaction section with an Inconel 600 platelet that will be used for these tests.

Another conclusion is that no significant problems were discovered with the operation of the platelet reactor. No change in destruction efficiency or reaction chemistry was observed. There was no evidence of plugging within the channels or pores of the platelets. Pressure pulsations from the pumps were naturally damped once the system reached supercritical temperature. This is shown in Figure 64.

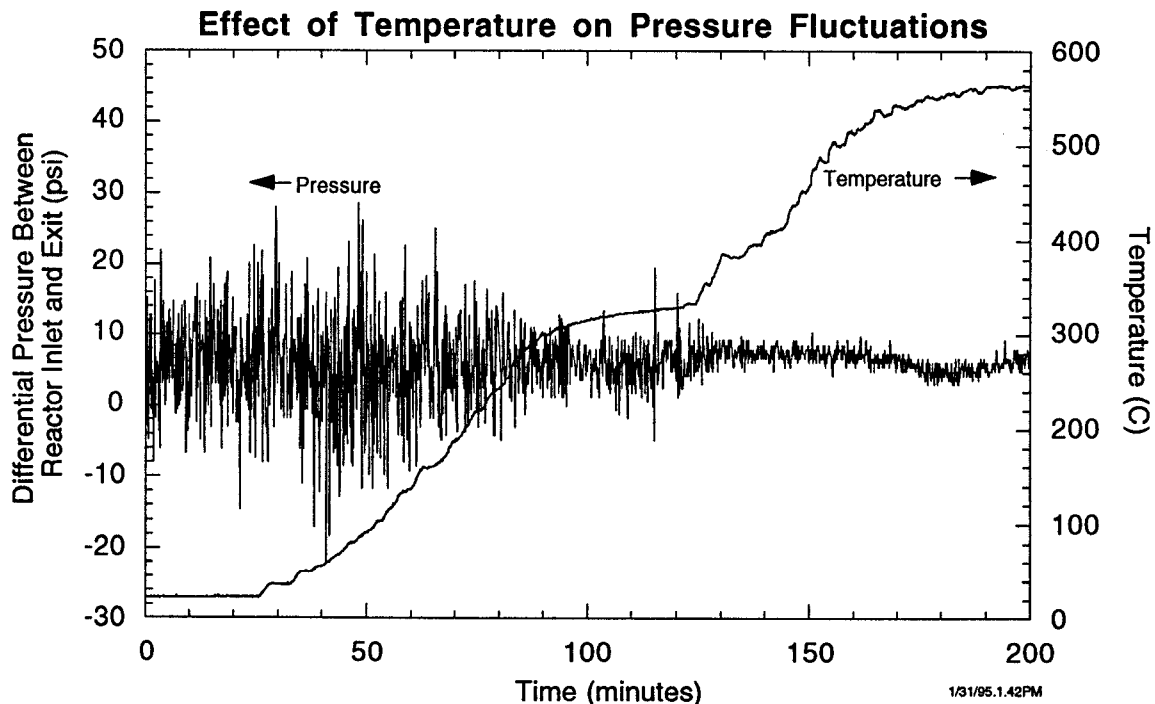


Figure 64 -- As the fluids approached supercritical temperature, pressure oscillations from the pumps were naturally damped.

From an operational perspective, the most significant lesson from the test program was the significance of density changes in the fluid during emergency shutdowns. With a loss of pressure, the water flashes to steam. In the supercritical regions such as the reactor, the density decreases by an order of magnitude. In subcritical regions such as heat exchangers and cooling tanks, it decreases by two orders of magnitude. This has a major effect on flow resistance and heat transfer that must be considered in shutdown and accident procedures. These considerations include the size and location of pressure relief devices, the design of heat exchangers, and the automatic shutdown of pumps and heaters.

Summary

Testing of the 1/4 scale transpiring wall reactor with sodium sulfate salt and red dye has demonstrated the benefit of a transpiring wall liner using platelet technology for inhibiting salt deposition in a supercritical water oxidation reactor. No major technical nor operational problems were discovered. The test results were sufficiently positive for the Army to proceed with the full scale design of the prototype plant. Further testing of the transpiring wall reactor is planned.

References

1. "Supercritical Water Oxidation of Colored Smoke, Dye, and Pyrotechnic Compounds", WFO proposal 83920103, ARDEC / DOE - Sandia
2. "Testing and Application of a Transpiring Wall Platelet Reactor for Supercritical Water Oxidation of Hazardous Waste", K. S. Ahluwalia et al, Presented at the First International Workshop on Supercritical Water Oxidation, Sponsored by DOE, Office of Technology Development, February 6-9, 1995.
3. "Identification of Technical Constraints for Treatment of DOE Mixed Waste by Supercritical Water Oxidation", C. M. Barnes et al, Oct., 1993, Idaho National Engineering Laboratory, EG&G, Idaho, Inc., Idaho Falls, Idaho, EGG-WTD-10768.
4. "Experimental Techniques to Determine Salt Formation and Deposition in Supercritical Water Oxidation Reactors", J. P. C. Chan et al, ASME, HTD-Vol. 296, Fire, Combustion, and Hazardous Waste Processing, Book No. G00913 - 1994.
5. "Corrosion In Supercritical Water Oxidation Systems: Workshop Summary", R. M. Latanision and R. W. Shaw, MIT-EL 93-006, September 1993.
6. "Platelet Actively Cooled Thermal Management Devices", H. H. Mueggenburg et al, Presented at the 28th Joint AIAA/SAE/ASME/ASEE Propulsion Conference and Exhibit at Nashville, TN, July 6-8, 1992.

7. "Development of Components for Waste Management Systems Using Aerospace Technology", D. Rousar et al, Presented at the 46th International Astronautical Congress at Oslo, Norway, October 2-6, 1995, Published by the American Institute of Aeronautics and Astronautics.
8. U.S. Patent No. 5,387,398, February 7, 1995, "Supercritical Water Oxidation Transpiration Reactor." Aerojet - General Corp.
9. "Transpiring Wall Supercritical Water Oxidation Test Reactor Design Report", B. L. Haroldsen et al, SAND96-8213, January 1996
10. "Supercritical Water Oxidation of Colored Smoke, Dye, and Pyrotechnic Compositions", S. F. Rice et al, SAND94-8209, January 1994.
11. "Experimental Methods for Studying Salt Nucleation and Growth from Supercritical Water", F. J. Armellini and J. W. Tester, The Journal of Supercritical Fluids, Vol 4, No. 4, 1991
12. "Salt Deposition Studies in a Supercritical Water Oxidation Reactor", S. F. Rice et al, SAND94-8201, October, 1993

UNLIMITED RELEASE
INITIAL DISTRIBUTION:

Phil Dell'Orco
Los Alamos National Laboratory
Mail Stop C920
Los Alamos, NM 87545

Jim Hurley
Armstrong Lab/EQC
Suite 2
Tyndall Air Force Base, FL 32403-5323

Richard Kirts
Naval Civil Engineering Laboratory
560 Laboratory Dr.
Port Hueneme, CA 93043-4328

Ray Goldstein
U.S. Army Armament Research Development
and Engineering Center
SMCAR-AES-P, Bldg 321
Picatinny Arsenal, NJ 07806-5000

Crane Robinson (10)
Armament Research, Development & Engineering
Center
SMCAR-AES-P, Building 321
Picatinny Arsenal, NJ 07806-5000

Mr. Dan Burch
Ordnance Engineering
Sea Department, Code 4022
Naval Surface Warfare Center
Crane, Indiana 47522

Alan Caplan
US Army EDEC
SCBRD-EN (Demil)
Bldg E4405, Room 216
Aberdeen Proving Ground, MD 21010-5401

Jerry Hanks
USADACS
Attn: SIOAC-TD
Savanna IL 61074-9639

James Q. Wheeler
Chief, Demil Technology Office
U.S. Army Defense Ammunition Center
and School
Attn: SMCAC-TD
Savanna, IL 61074-9639

Ed Ansell
Demil Technology Office
U.S. Army Defense Ammunition Center
and School
Attn: SMCAC-TD
Savanna, IL 61074-9639

Curtis Anderson
Chief, Energetics Systems Process Division
U.S. Army Armament Research
and Development & Engineering Center
SMCAR-AES-P, Bldg 321
Picatinny Arsenal, NJ 07806-5000

Dr. Alanna Mitchell
Walcoff
2001 North Beauregard Street, Suite 800
Alexandria, Virginia 22311

Jaffer Mohiuddin
Office of Technology Development
US Department of Energy
Trevion II, 12800 Middlebrook
Germantown, MD 20874

Dr. Peter Schmidt
Program Officer
Physical Sciences Division & Materials Division
800 N. Quincy St.
Arlington, VA 22217-5660

Dr. Regina E. Dugan
Science & Technology Division
Institute for Defense Analyses
1801 North Beauregard Street
Alexandria, VA 22311-1772

Commander
Pine Bluff Arsenal
Attn: SIOPB-ETD Maggie Barry
Pine Bluff, Arkansas 71602-9500

Commander
Pine Bluff Arsenal
Attn: SIOPB-ETD Jim Haley
Pine Bluff, Arkansas 71602-9500

Commander
Pine Bluff Arsenal
Attn: SIOPB-ETD Loy Aikman
Pine Bluff, Arkansas 71602-9500

Frank A. De Rosa
Glitsch Technology Corporation
1055 Parsippany Boulevard
Parsippany, NJ 07054

Michael Modell
President & CEO
Modell Environmental Corporation
300 Fifth Avenue
Waltham, MA 02154

Mark M. Bianco, P.E.
Foster Wheeler Environmental Corporation
8 Peach Tree Hill Road
Livingston, New Jersey 07039

Prof. Earnest Gloyna
College of Engineering
University of Texas
Austin, TX 78712

Prof. Phillip A. Savage
Department of Chemical Engineering
3034 Dow Building
University of Michigan
Ann Arbor, MI 48109-2136

Prof. Jefferson W. Tester
Massachusetts Institute of Technology
Energy Laboratory
Room E40-455
77 Massachusetts Avenue
Cambridge, MA 02139

E. L. Daman
Foster Wheeler Development Corporation
12 Peach Tree Hill Road
Livingston, NJ 07039

K. S. Ahluwalia (10)
Foster Wheeler Development Corporation
12 Peach Tree Hill Road
Livingston, NJ 07039

Gopal Gupta
Foster Wheeler Development Corporation
12 Peach Tree Hill Road
Livingston, NJ 07039

Dr. David A. Hazlebeck
General Atomics
M/S 15-100D
350 General Atomics Court
San Diego, CA 92121-1194

Dr. Jeffrey Marqusee
ESTCP Program Manager
Office of the Under Secretary of Defense
Acquisition and Technology
3000 Defense Pentagon
Washington, DC 20301-3000

Dr. M. F. Young
GenCorp Aerojet
P.O. Box 13222
Sacramento, CA 95813-6000

Len Shoenman
GenCorp Aerojet
P.O. Box 13222
Sacramento, CA 95813-6000

Daniel Greisen
GenCorp Aerojet
P.O. Box 13222
Sacramento, CA 95813-6000

Don Rousar
GenCorp Aerojet
P.O. Box 13222
Sacramento, CA 95813-6000

Harry Mueggenburg
GenCorp Aerojet
P.O. Box 13222
Sacramento, CA 95813-6000

John Beller
EG&G Idaho, Inc.
P.O. Box 1625
Idaho Falls, ID 83415-3710

Tom Charlton
EG&G Idaho, Inc.
P.O. Box 1625
Idaho Falls, ID 83415-3710

MS0861	T. Hitchcock 9103
MS0756	G. C. Allen, 6607
MS1143	J. F. Rice, 6600
MS9001	T. O. Hunter, 8000
	Attn: E. E. Ives, 5200
	J. B. Wright, 2200
	M. E. John, 8100
	L. A. West, 8200
	W. J. McLean, 8300
	T. M. Dyer, 8700
MS9007	R. C. Wayne, 8400
MS9101	W. C. Peila, 8411
MS9101	J. P. Damico, 8411
MS9108	E. T. Cull, 8415
MS9108	L. G. Hoffa, 8415
MS9105	B. G. Brown, 8414
MS9102	A. L. Hull, 8416
MS9106	P. R. Bryson, 8417
MS9105	J. C. Swearengen, 8419
MS9105	K. L. Tschritter, 8419
MS9105	T. T. Bramlette, 8422
MS9105	D.Y. Ariizumi, 8412
MS9105	J. P. Chan, 8412
MS9105	H. H. Hirano, 8412
MS9105	T. N. Raber, 8412
MS9105	W. C. Replogle, 8412
MS9105	M. C. Stoddard, 8412 (10)
MS9105	C. A. LaJeunesse, 8412
MS9105	B. L. Haroldsen, 8412 (10)
MS9105	D. V. Zanini, 8412
MS9042	B. Nilson, 8345
MS9042	S. Griffiths, 8345
MS9052	S. F. Rice, 8361
MS9404	B. E. Mills, 8713
MS9404	J. F. C. Wang, 8713
MS9141	S. Johnston, 8103
MS9052	R. Hanush, 8361
MS9053	R. Steeper, 8352
MS9052	D. Hardesty, 8361
MS9103	K. Wally, 8111
MS9052	J. Aiken, 8361
MS9101	L. M. Mara, 8411
MS9221	D. A. Wright, 8421
MS9221	J. J. Bartel, 8418
MS9221	P. T. Larson, 8418
MS9021	Technical Communications Department, 8815, for OSTI (10)
MS9021	Technical Communications Department, 8815/Technical Library, MS0899, 4414
MS0899	Technical Library, 4414 (4)
MS9018	Central Technical Files, 8950-2 (3)